ON THE IDENTIFICATION AND HAPTIC DISPLAY OF FRICTION

A DISSERTATION

SUBMITTED TO THE DEPARTMENT OF MECHANICAL ENGINEERING

AND THE COMMITTEE ON GRADUATE STUDIES

OF STANFORD UNIVERSITY

IN PARTIAL FULFILLMENT OF THE REQUIREMENTS

FOR THE DEGREE OF

DOCTOR OF PHILOSOPHY

Christopher Richard

August 2000

© Copyright 2000 by Christopher Richard
All Rights Reserved

Abstract

Although friction is an important phenomenon and greatly affects the way in which individuals interact with the world, friction is all but absent from force-feedback computer simulations of reality. Haptic interfaces are mechanisms that allow one to interact with a computer through the sense of touch. Past research has shown that haptic interfaces can be used both to identify the properties of an environment and to simulate its feel to a human user. Much of this work has been limited to environments dominated by stiffness. This thesis expands the state-of-the-art of the haptic rendering of friction for the purposes of generating higher fidelity virtual experiences and improving human performance in manipulation tasks. This work discusses the use of a haptic interface to: a) explore and model the frictional and inertial properties of real environments, b) provide a realistic haptic simulation of these properties to a user, and c) examine human perception of simulated friction.

I present a method for probing a system with unknown friction and inertia with a haptic interface. Experimental results show that the method is an effective means of characterizing the system's dynamic properties. Next, I present an algorithm to haptically display the identified friction and inertia. By considering how changing parameters of the model affect both the stability and fidelity of the haptic rendering, I provide guidelines for selecting parameters to avoid a set of undesirable sustained oscillations termed limit cycles. Lastly, to learn about human perception of friction, I describe and present results from a series of human subject tests. The results indicate that a moderate amount of friction, either real or simulated, tends to improve human performance in a targeting task. Very sticky friction, however, degrades performance. I also show that humans are able to discern subtle differences in kinetic friction more readily than differences in static friction.

Acknowledgments

Through my years at Stanford, many kind, generous and helpful people made my experience one that I will never forget. First, I would like to thank my advisor Professor Mark Cutkosky for his guidance, encouragement and support throughout my time here. Next, I am a grateful to Dr. Karon MacLean, formerly of Interval Research Corporation, and now a professor at the University of British Columbia. I am thankful to Dr. MacLean, not only for serving on my reading committee, but for all of the advice and direction she provided in every phase of my research program. Special thanks are due to Professors Oussama Khatib, Sheri Sheppard, Jerry Harris and Dr. Herb Rauch for reading drafts, asking helpful and insightful questions, and making valuable suggestions. Matt Hage and Michael Keonig providing invaluable assistance in designing and conducting the human subject testing portions of this work.

Funding for this research was provided in part by Interval Research Corporation and the National Consortium for Graduate Degrees for Minorities in Engineering and Science Inc. (GEM). Additional funding and support was provided by the student affairs section of the School of Engineering with the help of Dr. Noe Lozano.

I am thankful to all of the residents of the Center for Design Research and particularly to my cohorts in the Dextrous Manipulation Lab: Allison Okamura, Michael Costa, Michael Turner and Niels Smaby. They made the lab both academically enriching and a fun place to work. I wish them all the best in their future endeavors. I would also like to extend best wishes to the lab's current round of aspiring academics: Jorge Cham, Weston Griffin, Sean Bailey, Jonathan Clark, Wendy Cheng, and Will Provancher.

ACKNOWLEDGMENTS

I spent many late nights and early mornings working on assignments with my friends Aaron West and Mark Perez with whom I attended both U.C. Davis and Stanford. They provided many words of motivation and encouragement as did other good friends: Alton Phillips, Dr. Alan Bowling, Eric Hayes, Dr. Ian Sobieski, and Dr. Ade Mabogunje. I am thankful for all of the wonderful people I met via Stanford's Black Graduate Students' Association and through the Abundant Life Christian Fellowship.

There are many other friends, family members and loved ones that made the completion of this dissertation possible. They are too numerous to mention. Above all, however, I give thanks to God for blessing me with the opportunity to pursue a graduate degree at Stanford University and to see it to completion.

Table of Contents

Abstract . . . . . **iv**
Acknowledgments . . . . . **v**
Table of Contents . . . . . **vii**
List of Figures . . . . . **x**
List of Tables . . . . . **xiii**
1. Introduction **1**
1.1. What are haptic interfaces? 2
1.2. Motivation 3
1.3. Thesis Overview 5
1.4. Thesis Contributions 6
2. Modeling Friction **8**
2.1. Introduction 8
2.2. Brief Historical Overview 9
2.3. Microscopic Perspective 10
2.3.1. Asperity interaction 10
2.3.2. Boundary lubrication 12
2.3.3. Lubrication effects 12
2.3.4. Stick-Slip Vibration and Relaxation Oscillations 13
2.4. Macroscopic Models 13
2.4.1. Basic Coulomb models 13
2.4.2. The “Classic” Model 15
2.4.3. Karnopp 15
2.4.4. Bristle 16
2.4.5. Dahl 18
2.4.6. Armstrong’s integrated model 19
2.4.7. Exponential Models 20
2.5. Models for Haptic Friction 21
3. Friction Identification **23**
3.1. Introduction 23
3.2. Previous Work 24
3.2.1. Environment and Device Identification 24
3.2.2. Friction Identification 25
3.3. Model Selection 26

3.3.1. Modified Karnopp Model 27
3.3.2. Modified Dahl Model 28
3.4. Experimental Apparatus 29
3.5. Identification Procedure 30
3.5.1. Modeling the force/motion interaction 31
3.5.2. Move the system over the range of velocities of interest 31
3.5.3. Record force/motion variables included in the model 32
3.5.4. Solve for unknown parameters 33
3.5.4.1. Fitting the Karnopp model to the data 33
3.5.4.2. Fitting the Dahl model to the data 36
3.6. Results 37
3.7. Discussion and Conclusions 41
4. Haptic Friction Rendering 46
4.1. Introduction 46
4.2. Previous Approaches 47
4.2.1. The Bristle Model 47
4.2.2. The Dahl Model 48
4.2.3. The Karnopp Model 49
4.2.4. Other methods 51
4.3. System description 52
4.3.1. Algorithm for implementing Karnopp Friction 52
4.4. Computer simulation of friction rendering 54
4.4.1. Simulating the human 55
4.4.2. Simulating the Haptic Device Motion 56
4.4.3. Simulating the Haptic Device Sensors 57
4.4.4. Determining the friction 57
4.5. Effects of model parameters in three regimes 57
4.5.1. Pre-sliding displacement 57
4.5.1.1. Upper limit on Kp 58
4.5.1.2. System Damping 60
4.5.1.3. Lower Limit on Kp 61
4.5.2. Stick-slip and sliding 62
4.5.3. Free Motion 64
4.5.4. Simulation Results 67
4.6. The Virtual Coupling 69
4.6.1. The design of the virtual coupling 71
4.6.2. Interpretation of the virtual coupling analysis 73
4.7. Conclusions 76
5. Perception and Psychophysics 78
5.1. Introduction 78
5.2. Experimental Apparatus 79
5.3. Experiment Descriptions 80
5.3.1. Fitts-Type Targeting Task 80
5.3.2. Forced Choice Tests 83
5.3.2.1. Basics of discrimination 85

5.3.2.2. Weber's Law 85
5.3.2.3. Standard Methods for Measuring the JND 86
5.3.2.4. Method of limits 86
5.3.2.5. Method of adjustment 87
5.3.2.6. Method of constant stimuli 87
5.3.2.7. Modified method of constant stimuli 88
5.4. Results 91
5.4.1. Forced Choice Test Results 91
5.4.2. Forced Choice Test Results 97
5.5. Discussion and Conclusions 100
5.5.1. Friction effects in a targeting task 100
5.5.2. Just Noticeable Difference 101
6. Conclusions 103
6.1. Thesis Summary 103
6.1.1. Friction Modeling and Identification 103
6.1.2. Haptic Friction Rendering 104
6.1.3. Human Perception of Friction 104
6.2. Recommendations for Future Work 105
References 106

List of Figures

Figure 1-1. Overview of haptic friction identification and rendering. 4
Figure 2-1. Part-to-part contact occurs at surface asperities. Adapted from Armstrong et al. (1994) 11
Figure 2-2. Various representations of friction. a) Viscous damping, b) the Coulomb model, c) Coulomb plus viscous, d) Coulomb with stiction. 14
Figure 2-3. The “classic” stick-slip friction model. 15
Figure 2-4. The Karnopp friction model 16
Figure 2-5. Bristle Model, (a) N randomly located bristle bonds, (b) a single bond. Adapted from Haessig and Friedland (1990). 17
Figure 2-6. Parameters and shape of the Dahl model. 19
Figure 2-7. The effect of various model parameters on the Majd and Simaan model. a) The effect of ‘n’. b) The effect of wc. c) The effect of s.. 21
Figure 3-1. Parameters of the modified Karnopp model..... 28
Figure 3-2. Experimental Apparatus for Identification..... 30
Figure 3-3. Typical velocity, acceleration, and force data..... 32
Figure 3-4. Example of how velocity is split into positive and negative components 34
Figure 3-5. Aluminum sliding on brass. a) Measured force versus velocity. b) Force adjusted by inertia with Karnopp fit overlaid. c) Force adjusted by inertia with Dahl fit overlaid. 38
Figure 3-6. Aluminum sliding on Teflon. a) Measured force versus velocity. b) Force adjusted by inertia with Karnopp fit overlaid. c) Force adjusted by inertia with Dahl fit overlaid. 39
Figure 3-7. Aluminum sliding on rubber. a) Measured force versus velocity. b) Force adjusted by inertia with Karnopp fit overlaid. c) Force adjusted by inertia with Dahl fit overlaid. 40
Figure 3-8. Typical measured force and Karnopp model predicted force versus velocity (aluminum on rubber) over four cycles of motion. 42
Figure 3-9. Typical measured force and Dahl model predicted force versus velocity (aluminum on rubber) over four cycles of motion. 43
Figure 4-1. Block Diagram of the Haptic System..... 53

Figure 4-2. Block diagram of a digital regulator 58
Figure 4-3. Step responses for various gains Kp 61
Figure 4-4. Effect of virtual damping, Kd, on system response 62
Figure 4-5. Examples of quantized and nonquantized velocity signal. 63
Figure 4-6. Applied Force, Fa, and Friction Force, Ff, plotted against time (Kp = 120). 64
Figure 4-7. Friction force versus velocity (Kp = 120). If Kp is too low, then v > DV even in the stuck region. 65
Figure 4-8. Effect of DV on the duration of the stick-slip regime. 66
Figure 4-9. Detail of stick-slip regime 67
Figure 4-10. A haptic rendering of the Karnopp Model with tuned parameters. The oscillations in the central portion of the figure are due to Kp. (See the upper curve in Figure 4-8) 68
Figure 4-11. The virtual coupling (block diagram adapted from Adams and Hannaford (2000)) 69
Figure 4-12. Schematic of a sliding block with friction rendered a)without a virtual coupling and b) with a virtual coupling. 70
Figure 4-13. Surface representing amplitude (velocity) of the limit cycle as a function of vitural coupling stiffness, K, and damping B. 74
Figure 4-14. Cross section of the limit cycle surface for K=10,000 N/m (upper plot) and B= 995Ns/m (lower plot) 75
Figure 4-15. Force velocity plots of real fricton and simulated friction. These results are for Aluminum sliding on Teflon. The inertia of the system is 1kg and the friction force is roughly 2N. 76
Figure 5-1. Experimental Apparatus for Perception Experiments 80
Figure 5-2. Screen seen by subjects during the Fitts test. 82
Figure 5-3. Hypothetical results of a difference threshold experiment 89
Figure 5-4. Possible effects of friction on subject performance 92
Figure 5-5. Subjects' performance relative to their baseline case for index of difficulty #1 (upper) Number of Errors versus Time (lower) Average Error Magnitude versus Time. 93
Figure 5-6. Subjects' performance relative to their baseline case for index of difficulty #4 (upper) Number of Errors versus Time (lower) Average Error Magnitude versus Time. 94
Figure 5-7. Subjects' performance relative to their baseline case for index of difficulty #1 (upper) Number of Errors versus Time (lower) Average Error Magnitude versus Time. 95
Figure 5-8. Subject's trajectory on a the baseline case. The subject was able to acquire the target 7 times in 800ms. 97
Figure 5-9. Subject's trajectory on a High Stiction case--note the difficulty positioning the cursor within the target bounds 98

Figure 5-10. Psychometric curve fit to subject responses during Batch 1. Estimated JND = 0.78 N..... 100
Figure 5-11. Psychometric curve fit to subject responses during Batch 2. Estimated JND = 3.14 N..... 101
Figure 5-12. Psychometric curve fit to subject responses during Batch 3. Estimated JND = 0.36 N..... 102

List of Tables

Table 3-1. Experimental Apparatus Parameters 29
Table 3-2. Standard Deviations of the Measurement Errors..... 33
Table 3-3. Friction estimates for aluminum sliding on brass, Teflon and rubber using Fuller's method (Equation 3.6). The parameters correspond to the modified version of Karnopp's model (Equation 3.1). 41
Table 3-4. Friction estimates for aluminum sliding on brass, Teflon and rubber using nonlinear least squares regression. The parameter s is tuned manually. The parameters correspond to the modified version of Dahl's model (Figure 3.2). 41
Table 4-1. Algorithm for rendering Karnopp Friction. 53
Table 5-1. Indices of difficulty for Fitts test 84
Table 5-2. Frictional resistances used for the Fitts test..... 84
Table 5-3. Friction rendering parameters for the reference stimulus..... 90
Table 5-4. Parameter differences for Batch 1 90
Table 5-5. Parameter differences for Batch 2 90
Table 5-6. Parameter differences for Batch 3 91
Table 5-7. Number of subjects (out of 20) that performed better and worse based on task completion time. Tests with highest index of difficulty are highlighted.....98
Table 5-8. Number of subjects (out of 20) that performed better and worse based on the number of errors committed. Tests with highest index of difficulty are highlighted. 99
Table 5-9. Number of subjects (out of 20) that performed better and worse based on average error magnitude. Tests with highest index of difficulty are highlighted. 99

To Mom, Melanie and Ma.

Chapter 1

Introduction

Friction is essential to even the most basic of human activities. Without friction, shoes would not grip the ground and walking would be difficult. Without friction, fingers would not be able to grasp and turning the pages of this dissertation would be difficult. We depend on the friction between the pulleys and belts in machines to transmit power. We depend on the friction between the pads and discs of automobile brakes to stop our cars when we press the brake pedal. The examples of beneficial friction are innumerable. Equally innumerable, however, are the negative effects of friction. The nature of friction is to dissipate energy. The friction between the moving parts inside a car's engine and between the wheels and axles means that one must use more fuel to reach one's final destination. When two solids rub against one another, the friction at the interface results in heat and wear. As mechanisms wear under the sometimes-destructive nature of friction, billions of dollars are spent annually to maintain and replace critical components. The presence of friction and its effect on our lives is abundantly clear.

Nevertheless, friction is all but absent from force-feedback computer simulations of reality. Haptic interfaces are the mechanisms that allow one to interact with a computer through the sense of touch. They give users a sense of being immersed in virtual worlds. These interfaces have grown in complexity and performance in recent years, but friction simulation has remained somewhat primitive. This dissertation expands haptic rendering of friction for the purposes of generating higher fidelity virtual experiences (i.e. virtual

experiences that are closer to the feel of real friction) and improving human performance. This dissertation shows how to 1) use a haptic interface to explore an environment to estimate its frictional properties, 2) use the same interface to generate realistic renderings of friction based on models acquired from real data, 3) use a haptic interface to evaluate human perception and task performance in the presence or absence of friction.

1.1. What are haptic interfaces?

In the last decade haptic interfaces and haptic rendering have become increasingly popular subjects of research. Derived from the Greek term haptesthai, the second edition of the online Oxford English Dictionary (http://www.oed.com) defines the word haptic as "Of, pertaining to, or relating to the sense of touch or tactile sensations." A haptic interface is a mechanical device equipped with motors or other such actuators and sensors that allows a person to experience kinesthetic (force) and/or tactile (touch) sensations. Typically computer controlled, haptic interfaces provide a force-feedback link to virtual reality. A force-feedback joystick used in a video game is one popular example of a haptic interface. Such a joystick allows a game player to experience the aerodynamic force on an airplane control yoke, or to feel the recoil of a fired missile, or to wrestle with the vibrating suspension of a high performance race car. In addition to allowing people to interact with a virtual environment, they allow people to experience the forces of a real environment as well. Haptic interfaces are also commonly used to control a remote manipulator. In such an arrangement, referred to as tele-operation, the motions of the haptic interface determine the motion of the remote manipulator while the forces experienced by the manipulator are relayed back to the haptic interface and are subsequently felt by the operator. Skilled operators can guide remote robots into hazardous situations where vision feedback is either unavailable or insufficient and perform their task by feeling what the robot feels.

Besides the obvious entertainment applications, haptic interfaces have an abundance of practical applications. In virtual reality simulation, they can be used for virtual training. Doctors can practice and perfect delicate surgical procedures via haptic simulation without

having to endanger the lives of humans or animals. Similarly, pilots and drivers can learn the nuances of a particular aircraft or vehicle without ever leaving the classroom.

Virtual instruments and controls are other promising applications for haptic interfaces. It is not difficult to imagine vehicles where the control interfaces are all haptic devices. Like fly by wire technology in airplanes, drive by wire technology in a car would have no mechanical connecting between the steering wheel and the suspension. A haptic interface could replace the traditional steering wheel giving the driver a virtual “feel” for the road providing force clues to help the drivers performance.

Engineers and designers could one day benefit from the application of haptics to computer aided design and virtual prototyping. In such a scenario, a designer could design a mechanism with a solid modeler and then manipulate the virtual mechanism with a haptic interface. Such interaction would allow the designer to quickly iterate between mechanism parameters to design the one that feels best.

1.2. Motivation

Simulating the feel of real friction with a haptic interface is a natural extension of previous haptic rendering studies. Gillespie (1996) carefully modeled the dynamics of a grand piano to generate a haptic rendering of the grand piano’s feel on a specially designed haptic piano keyboard. MacLean (1996) introduced the notion of a haptic camera, a system that could take a haptic snapshot of an environment and subsequently reproduced the environment’s haptic properties. MacLean demonstrated the feasibility of the haptic camera by using a haptic device to characterize the dynamics of a toggle switch and then using the same device to simulate the switch’s feel. The work presented here extends the idea of the haptic camera and the haptic piano. In previous work, the dynamics of the environments in question were dominated by stiffness and inertia. The environment identification could be done by directly measuring the physical parameters of the environment and/or by quasi-static motion of the haptic interface. In this work we take a haptic snapshot of environments with

significant friction. As friction is a dynamic property, the identification must also be conducted dynamically.

The dynamic and nonlinear nature of friction also introduce new challenges in the area of haptic rendering or haptic display.

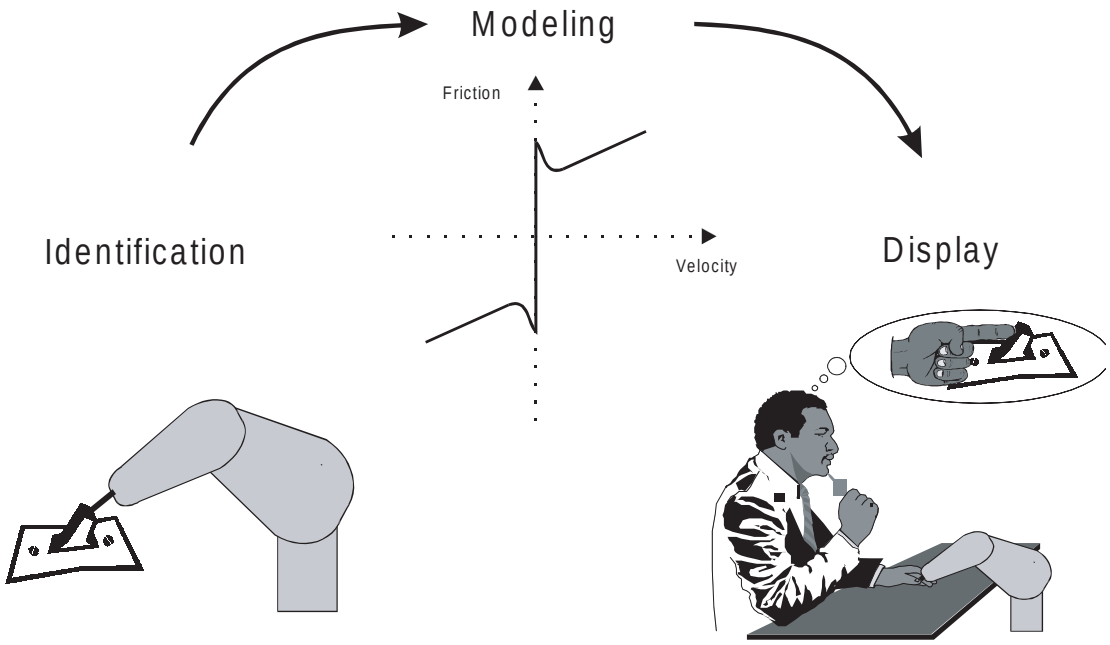

Figure 1-1. Overview of haptic friction identification and rendering.

Figure 1-1gives an overview of the main steps in the process of identifying and rendering friction on a haptic interface. First we measure the friction in real environments by manipulating the environments directly. Next, we determine the parameters of a friction model that will match the collected data. Last, we create a realistic simulation of the friction that a user can experience as if he or she were manipulating the original environment directly.

It is important to display friction for at least two reasons. The first is realism. To provide realistic haptic renderings of any environment, a rendering of friction is essential. In the absence of friction, the virtual world is akin to a world where everything is made of ice.

Adding viscous damping, the oft used substitute for dry friction is helpful, but it does not provide a realistic sensation when objects are manipulated.

A second reason to display haptic friction is to improve human comfort and task performance. Some tasks simply seem easier with a small amount of friction. At the very least, friction plays a role in the quality of the experience. Consider the different levels of quality felt when writing with various pens and pencils on various grades of paper. There is no doubt that the level and quality of the friction play an important part. Turning the tuning knob on an old analog radio also gives a distinctive feel. Friction in the system helps us position the dial and helps the dial stay in place once we have found the frequency we desire.

1.3. Thesis Overview

Chapter 2 is a concerned with friction models. After a brief historical overview, the chapter describes the basic mechanism for dry friction. The chapter concludes with descriptions of several of the more commonly used friction models. The models presented in Chapter 2 are commonly used for dynamic simulation of systems with friction.

Chapter 3 deals with the experimental identification of friction. The chapter opens with a literature review of robotic environment identification. Next, an algorithm for estimating the friction and inertia of a system is outlined. Experimental results are presented for a block of aluminum sliding over three different surfaces: brass, Teflon, and aluminum. Also, two friction models, the Karnopp model and the Dahl model, are compared.

The haptic rendering of friction is the subject for Chapter 4. An algorithm that results in a realistic haptic simulation of friction is presented. We will look at how changing parameters in the friction model affect the fidelity of the simulation. We will also look the stability of the haptic rendering and suggest ways to avoid undesirable sustained oscillations referred to as limit cycles.

Chapter 5 explores the effects of friction on human performance in a targeting task and human perception of friction. We will see how the presence of friction, either real or simulated aids or degrades the speed and accuracy of subjects as they attempt to acquire targets a various levels of difficulty. We will also look as the level of friction that humans are able to perceive.

Chapter 6 concludes the thesis. It presents a summary of the observations and highlights some areas for future research in friction and haptics.

1.4. Thesis Contributions

The three most significant contributions of this thesis are:

1) The formulation and demonstration of a method to use a haptic interface to explore a system and subsequently return an estimate of the system's friction and inertia.

2) The development and analysis of an algorithm to use a haptic interface to generate realistic renderings of friction.

3) The evaluation of human perception of friction and how human performance in a targeting task is affected by the addition of various types of friction.

This dissertation provides a background into the basic mechanisms of friction. It provides a summary of the some of the commonly used models for friction simulation and identification. The reader will learn how the models differ, and which ones are best suited for haptics. We use these models in conjunction with data collected from an environment to estimate the friction and inertia of the environment. Next, this work demonstrates how one can use a haptic interface to generate high-fidelity renderings of friction. The stability of a haptic friction rendering is studied and we set some bounds on the selection of model parameters to ensure the quality of the rendering. In addition to stability, this work provides insight into the issue of limit cycles and how to avoid them in a haptic friction rendering. I show that friction does affect a human's task performance in challenging targeting tasks.

Moderate amounts of both real and simulated friction improved subjects' task completion time and reduced their error rates. However, very sticky friction results in slower performance with more errors. Finally, by conducting psychophysical tests I show that humans can discern between small levels of simulated friction. The results indicate that humans are more adept at discerning differences in kinetic friction than differences in static friction.

Chapter 2

Modeling Friction

This chapter examines the basic mechanism that causes friction between sliding surfaces. After a brief historical overview of the study of friction, the microscopic aspects of friction are presented. Next the macroscopic friction models that are commonly used for identification and simulation are described. The chapter concludes with a discussion about which models are best suited for haptics applications.

2.1. Introduction

The study of friction is encompassed by a much broader field of study termed tribology. Tribology, based on the Greek root tribos meaning to rub, literally means the study of rubbing. In addition to refining models of friction, tribologists study a wide range of subjects such as how materials wear and how lubricants can be used to reduce both friction and wear.

This thesis is concerned primarily with dry friction. Friction refers to the resistive force that is present when there is relative motion between two bodies in contact. Dry friction refers to the resistance due to the motion of bodies with solid to solid contact. Lubrication is not a factor. Fluid friction, on the other hand, concerns the resistance between adjacent layers of a fluid as the fluid flows.

2.2. Brief Historical Overview

Friction has presented challenges to humankind for thousands of years. People have tried to understand friction and reduce its negative effects. As early as 1880 B.C., in a painting of ancient Egyptians transporting a massive colossus on a sled, a man at the front of the sled pours lubricant on the ground to ease the load (Dowson 1998). Although these ancient Egyptians may not have understood the physics behind friction, it is clear that they understood that lubrication can lower frictional resistance.

The most basic laws of friction date back to the work of Leonardo DaVinc, prior to 1500. DaVinci postulated that friction obeyed two laws. First, that friction is directly proportional to the applied load. Second, that friction is independent of the apparent area of contact. DaVinci also introduced the concept of a coefficient of friction relating level of observed friction to the weight of a sliding object. The observations of DaVinci remained undiscovered for years, as his notes went unpublished. In 1699, the French physicist Guillaume Amontons independently rediscovered what DaVinci had found earlier. The two laws of friction mentioned above are therefore commonly referred to as Amontons' laws of friction. In 1748, the Swiss mathematician Leonhard Euler contributed to the knowledge of friction with the submission of two papers to the Academy of Sciences. Euler's work was the first to draw distinction between the static coefficient of friction and the smaller dynamic coefficient of friction. Euler is also credited with introducing the commonly used symbol μ to denote the coefficient of friction.

In 1785, Charles Augustin Coulomb published the most comprehensive study of friction up until that time. Coulomb verified and extended the groundwork that had been established by Amontons and others. Among Coulomb's contributions in his lengthy treatise is the notion of rising static friction. Coulomb found that the level of static friction would increase from an initial value to some larger value while the system was at rest. In other words the level of static friction is a function of the time of repose or dwell time. Coulomb also found that under dry sliding conditions the kinetic friction was independent of velocity for both metal-on-metal and for wood-on-wood contacts. For wood-on-metal, he found

that the kinetic friction increased at higher speeds. Despite Coulomb's published results, a third law of friction is usually attributed to him. The third law states that in the absence of lubrication kinetic friction is independent of sliding velocity. The third law, like the first two, is empirical, and does not hold in all situations. All three laws, however, work quite well for describing the friction in metal-on-metal contacts.

Perhaps the most significant portion of Coulomb's work deals with the cause of friction. Coulomb believed, like others before him, that friction is due to the interaction of surface features on all materials known as "asperities." He felt that the deformation of the surface asperities could not be neglected in an explanation of friction between surfaces.

2.3. Microscopic Perspective

From a microscopic perspective, friction is in fact caused by the interaction of surface asperities. Crystalline surfaces, which may appear to be quite smooth, are actually somewhat rough. The rough surface features, the asperities, interact with each other when two surfaces are brought into contact (Figure 2-1). The only true contact between the two surfaces occurs at the asperity junctions. This situation was aptly described by tribologist F.P. Bowden in a 1950 BBC radio broadcast where he compares the topology of solids to the mountainous topology of earth. According to Bowden, "…putting two solids together is rather like turning Switzerland upside down and standing it on Austria – the area of intimate contact will be small."

2.3.1. Asperity interaction

When the surfaces are in contract, the friction force is the force necessary to deform the asperities and (according to some tribologists) to overcome the interfacial adhesion. The friction is proportional to the shear strength of the asperity junction or the weaker of the bulk materials (Armstrong-Helouvry et al. 1994; Blau 1996). The static friction force, F_s, may be expressed in terms of the static friction coefficient μ_s and P^*, the normal force comprised of both the applied load and the normal component of any adhesive forces at the

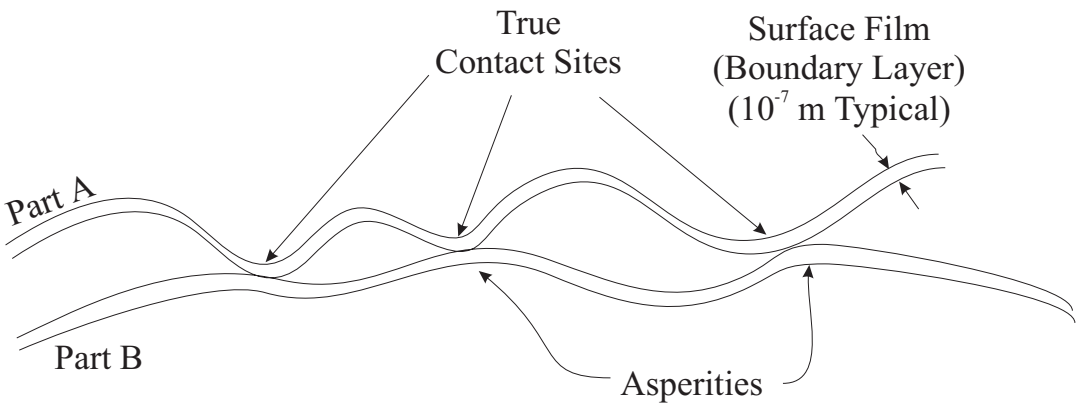

Figure 2-1. Part-to-part contact occurs at surface asperities. Adapted from Armstrong et al. (1994)

interface (Blau 1996). It can also be expressed as the product of the junction shear strength, τ_m and the actual area of contact, A.

$$F_s = \mu_s P^* = \tau_m A \tag{2.1}$$

Alternatively, the static friction coefficient may be expressed as a function of τ_m, A, and P^*,

$$\mu_s = \frac{\tau_m}{P^*} A \tag{2.2}$$

From a macroscopic perspective, friction is independent of the apparent area of contact. At closer inspection, however, we see that the actual area of contact indeed does affect the friction. As the load holding two surfaces together increases the asperities deform thereby increasing the actual area of contact, and increasing the static friction force.

If the applied tangential load is large enough, the asperities begin to break contact. Subsequent motion is referred to as microslip, or pre-sliding displacement. As the surfaces yield “break-away” occurs and larger scale motions follow. After break-away, the friction interfaces enter a regime referred to as boundary lubrication.

2.3.2. Boundary lubrication

Oxide films and other contaminants create a thin boundary layer on the surfaces of solids. These boundary layers typically have lower shear strength than the bulk material on which they form. If the shear strength of boundary layer junctions is less than the shear strength of the parent material junctions then the coefficient of kinetic friction, μ_k, will be lower than the static coefficient, μ_s.

2.3.3. Lubrication effects

In many mechanisms, lubrication is present to reduce friction and wear. For mechanisms employing hydrostatic lubrication, a layer of lubrication is always maintained between the solid surfaces. No direct solid to solid contact occurs; only fluid friction is present. With hydrodynamic lubrication, the moving surfaces are initially in contact with one another. As they begin to move relative to one another, lubricant is forced between the surfaces. More lubricant fills the space between the moving surfaces as the relative velocity increases. Above some critical velocity full fluid lubrication takes place. Under full fluid lubrication, the viscosity of the fluid determines the frictional resistance. A simple and commonly used model for friction in this regime is to multiply the relative velocity, v, by a viscous damping coefficient b.

$$F = bv \tag{2.3}$$

The transition from solid-to-solid friction to full fluid lubrication is explained with two regimes. As fluid fills the region between the solids, the friction force initially decreases. The friction begins to increase at higher velocities due to the viscosity parameters of the fluid. This phenomenon of decreasing friction with increasing velocity at low velocities is called the Stribeck effect after the german engineer Richard Stribeck. For more details on the friction in lubricated mechanisms, the interested reader is referred to Armstrong-Helouvry (1991).

2.3.4. Stick-Slip Vibration and Relaxation Oscillations

Stick-slip is the term coined by Bowden and Leben (Bhushan 1999; Blau 1996) to describe the vibratory phenomenon that is sometimes observed at frictional interfaces. Another commonly used term for the phenomenon is relaxation oscillations. Blau (1996) gives examples of stick-slip that include the squealing of a door hinge, the skipping motion of a wiper blade on a partially wet windshield, or the sound generated when a bow glides over a violin string. Stick-slip can ensue when the static coefficient of friction is greater than the dynamic coefficient of friction. When two objects are stuck together, if a force is applied to one, the friction ramps up to the static friction limit and break-away can occur. After break-away the object can begin sliding, but under stick-slip, the object slips a small amount and then sticks again. The friction versus time curve for stick slip typically looks somewhat like a sawtooth. Some tribologists attribute the phenomenon to adhesive bonds being made and broken at the frictional interface. In order for a model to represent stick slip, it must allow for higher values of friction at lower speeds, and a decreased friction at slightly higher speeds.

2.4. Macroscopic Models

2.4.1. Basic Coulomb models

Aside from the simple viscous damping approximation of friction (Figure 2-2a), the most common representation of dry friction found in engineering is simply referred to as Coulomb friction. With the standard Coulomb friction model, the friction force is represented with a signum function and expressed as

$$F_f = F\,\mathrm{sgn}(v) \tag{2.4}$$

Where F is the value of the Coulomb friction and v is the relative velocity between the mating surfaces. Taking the strict definition of the signum function, the friction is zero at zero velocity. Figure 2-2b shows the standard Coulomb friction model. Occasionally, the Coulomb model and the viscous damping are added. The result is shown in Figure 2-2c.

To represent stiction, a condition where the static friction, F_s, is greater than the dynamic or kinetic friction, F_d, a piece-wise definition of Coulomb friction is sometimes used. Shown in Figure 2-2d, this model is multi-valued at zero velocity. This model has several drawbacks. First, it does not provide a physically realistic representation of the behavior of friction near zero velocity. Second, the hard non-linearity at zero velocity makes efficient computer simulation of friction with this model difficulty. In digital computer simulations, calculation of a velocity of exactly zero is unlikely. Simulations using the standard Coulomb model are prone to oscillate around zero velocity.

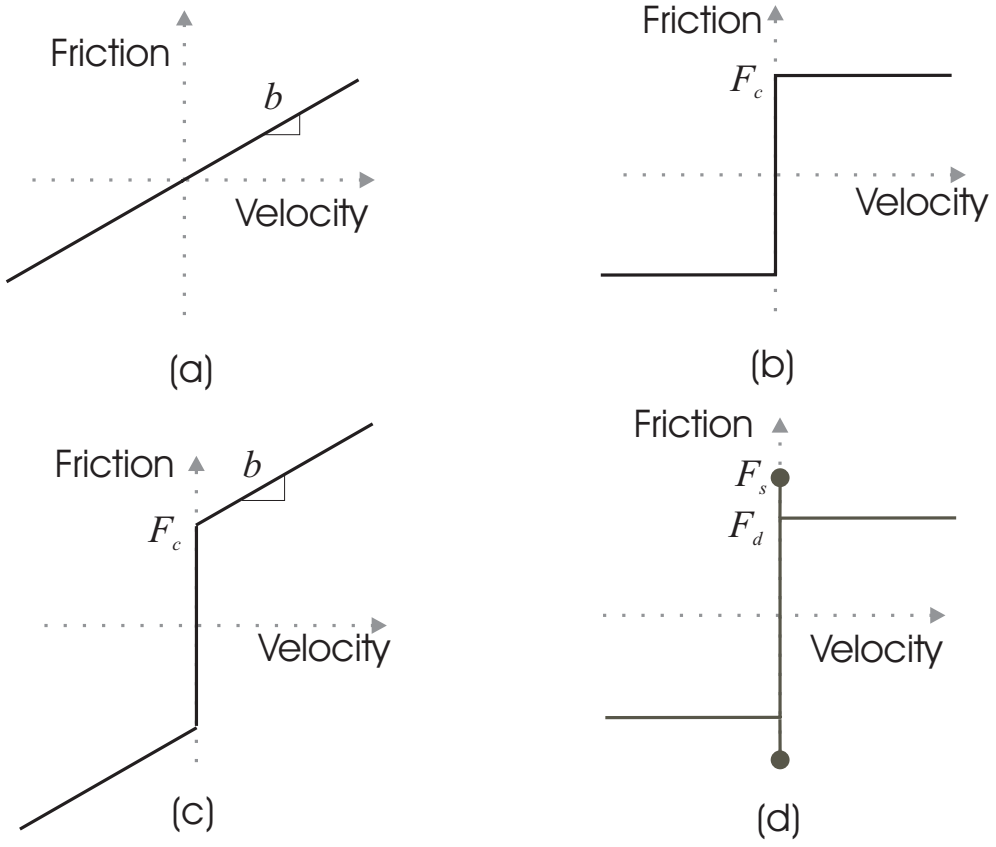

Figure 2-2. Various representations of friction. a) Viscous damping, b) the Coulomb model, c) Coulomb plus viscous, d) Coulomb with stiction.

2.4.2. The "Classic" Model

One attempt to ameliorate the negative effects of the stiffness problems associated with the basic Coulomb model is the so-called classic friction model (Haessig and Friedland 1991). The classic model replaces the steep non-linearity with a relatively steep linear function near zero. The main issue with this model is that is allows a body to accelerate even though the applied force is less than the static friction value. Steeper slopes at zero reduce this effect, but for steep slopes, the classic model has the same drawbacks of the original coulomb model. Figure 2-3 shows the classical stick-slip friction function.

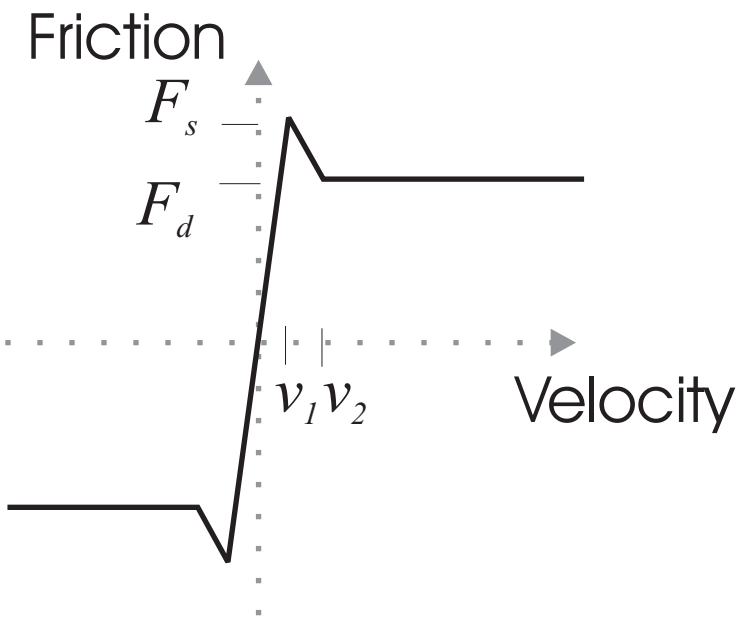

Figure 2-3. The "classic" stick-slip friction model.

2.4.3. Karnopp

As a means of handling the numerical difficulties in simulating the standard highly nonlinear model of Coulomb friction, Karnopp (1985) introduced a method for representing stick-slip friction "without the introduction of numerical stiffness problems." Like the standard Coulomb model, in Karnopp's model friction is ultimately a function of velocity. When the velocity of the system approaches zero, the velocity is considered to be exactly

zero. Inside this band around zero velocity the friction force is calculated to be either a) the value needed to keep the system at zero velocity, or b) the break-away friction force level. The value of (a) or (b) with the smallest magnitude is the one used. A graphical representation of the Karnopp model can be seen in Figure 2-4

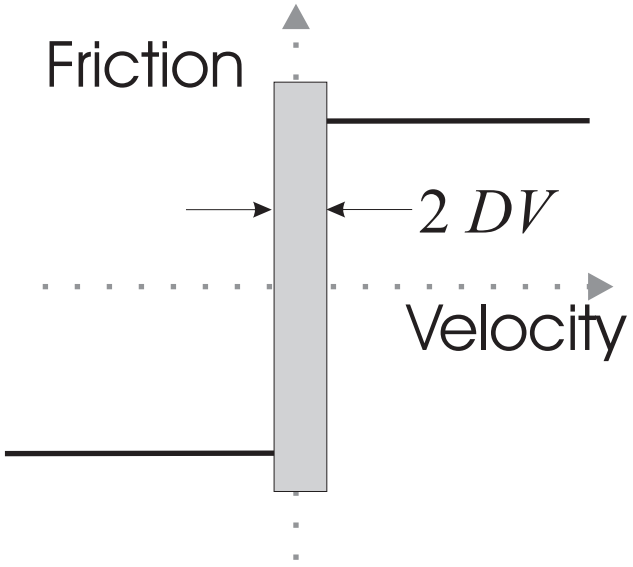

Figure 2-4. The Karnopp friction model

2.4.4. Bristle

In the bristle model, the friction between two surfaces is represented by a set of rigid and pliable bristles. Rigid bristles are attached to one surface and pliable bristles to the other. The bristles bond to one another and it is this bonding that represents the friction. As the surfaces move relative to each other, the bristles deflect and the strain in each bond increases. When the deflection of a particular bristle exceeds a certain level, its bond breaks and it attaches itself to a new bristle with a lower level of strain. (See Figure 2-5.)

The bristle model is based on the physical interaction of the microscopic asperities that are the cause of real friction. The model does not, however, attempt to create a one-to-one correspondence between the actual number of bonds interaction between two surfaces and the number of bristles used in the model. Haessig et al. report that 50 bristles is sufficient

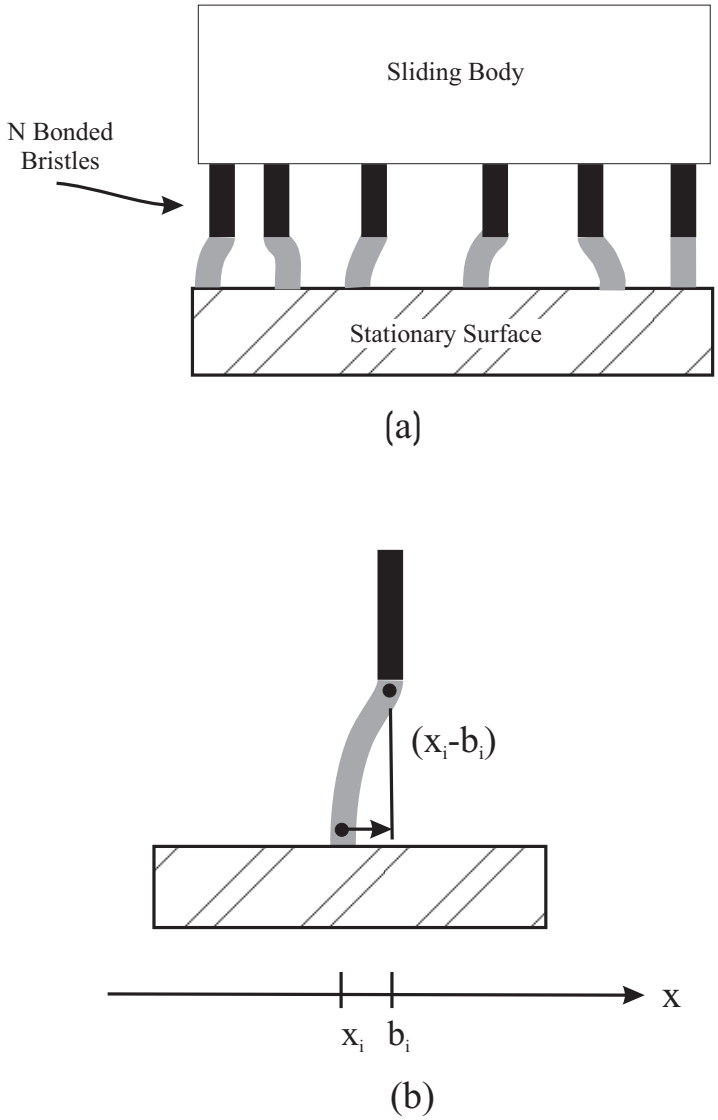

Figure 2-5. Bristle Model, (a) N randomly located bristle bonds, (b) a single bond. Adapted from Haessig and Friedland (1990).

to adequately represent surface friction. For a simulation with n bonds, each bond represents 1/nth of the bonding that occurs on the actual contacting surface.

The spacing between the bristles is random. The force applied by the bonding of a rigid and pliable bristle is

$$F = K(x_i - b_i) \tag{2.5}$$

Where K is the stiffness of the pliable bristle, x_i is the location of the pliable bristle, and b_i is the location of the rigid bond.

The total friction force between the two surfaces is the sum of the forces between each pair of bonded bristles. When the deflection of a pliable bristle exceeds Δ, the bond's snapping point, the bond breaks. The rigid bristle forms a new bond with a different pliable bristle. The location of the new bristle is random. The location of the new bond is defined as

$$b_i = b_i + \text{uniform}(\Delta)\,\text{sgn}(x_i - b_i) \tag{2.6}$$

The "uniform" function places the bristles at random, uniformly distributed distances ranging from 0 to Δ. The friction load can be made a function of velocity by varying the number of bristles as a function of velocity.

2.4.5. Dahl

Dahl (1976), presents a model "to describe friction primarily as a function of displacement." The model states that the rate of change of friction with respect to time is equal to the rate of change of the friction with respect to position multiplied by the relative velocity of the two moving bodies:

$$\frac{dF(x)}{dt} = \frac{dF(x)}{dx}\frac{dx}{dt} \tag{2.7}$$

The hysteretic behavior of friction is captured if $dF(x)/dt$ is of the form:

$$\frac{dF(x)}{dx} = \sigma\left|1 - \frac{F}{F_c}\,\text{sgn}\dot{x}\right|^i \text{sgn}\left(1 - \frac{F}{F_c}\,\text{sgn}\dot{x}\right) \tag{2.8}$$

Where σ is the slope of the friction curve at F=0, and F_c is the Coulomb friction force. 'i' is an empirically determined parameter that adjusts the shape of the friction slope function. This model has been successful in simulating the frictional properties of ball bearings, and is used by the author to model the "solid friction damping" of a pendulum. Figure 2-6 shows a sample of the shape of Dahl friction plotted against displacement.

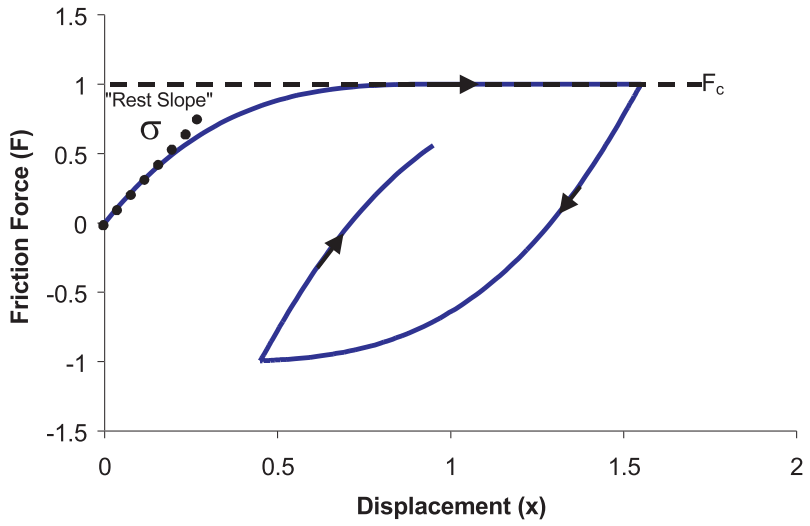

Figure 2-6. Parameters and shape of the Dahl model.

2.4.6. Armstrong's integrated model

Armstrong et al. (1994), is one of the most extensive surveys of friction models and analysis tools. This paper deals with friction as it applies to the automatic control of machines. It is therefore focused primarily on friction in lubricated metal on metal contacts; nevertheless the information included is quite valuable. Some of the key points elicited from Armstrong et al. (1994) are that (a) friction is a function of the true area of contact between two mating surfaces and (b) friction is a function of velocity in four different regimes:

- Static friction (pre-sliding displacement),
- Boundary lubrication,
- Partial fluid lubrication
- Full fluid lubrication.

There is discussion of the Stribeck effect, which says that at velocity near zero, friction decreases as velocity increases. The phenomenon of stick–slip friction is also introduced. The two temporal phenomena of friction that cause stick slip being are listed as (a) dwell time and (b) friction memory. Dwell time refers to the length of time that two contacts are

held together at zero velocity. Frictional memory is the term used to describe the time lag between a change in the velocity of two contacts and the resulting change in friction.

Armstrong et al. (1994) then present a seven parameter integrated friction model that encompasses all of the phenomena discussed above. Parameters in the model include:

- Instantaneous friction force
- Coulomb friction force
- Viscous friction force
- Magnitude of the Stribeck friction
- Magnitude of the Stribeck friction at the end of the previous sliding period
- Magnitude of the Stribeck friction after a long time at rest
- Tangential stiffness of the static contact
- Characteristic velocity of the Stribeck friction
- Time constant of the frictional memory
- Temporal parameters of the rising static friction
- Dwell time

2.4.7. Exponential Models

Majd and Simaan (1995) present a continuous friction model that works in both low and high velocity regimes. Their paper discusses some of the friction models mentioned above and how each deals with friction at low velocities. The authors review the Coulomb friction model and note that the model's discontinuity at zero is not observed in physical systems. They then address a friction model developed by Hess and Soom (1990), and a model by Bo and Pavelescu (1982). Both models more accurately address the friction force at low velocity, i.e. both account for the Stribeck effect, but neither accounts for the pre-sliding displacement observed by Walrath (1984), and discussed by Armstrong et al. (1994). The reason being that both models still have discontinuities at the origin. It is conceded that the Dahl model can account for this pre-sliding displacement, but it "does not include the viscous friction and break away torques and is formulated only for slow motion without considering stiction." The new model that is proposed accounts for the pre-sliding

effects observed in experiments, and also is continuous about the origin. The form is given as:

$$F(\omega) = f_\omega \omega + \left[f_c + \sigma e^{-\left|\frac{\omega}{\omega_c}\right|} - (\sigma + f_c) e^{-\left|n\frac{\omega}{\omega_c}\right|} \right] \mathrm{sgn}(\omega) \qquad (2.9)$$

'ω' is used here because the objects discussed move with angular velocities rather than translational velocities. 'f_ω' is the slope of friction after the Stribeck effect and is the same as the viscous damping coefficient. 'σ' is a real number that chosen so that the above expression has a maximum value of f_s, the static friction of the system. 'n' determines the steepness of the friction-velocity curve at zero velocity. 'ω_c' is known as the critical angular velocity. It is used to demark the transition from the Stribeck friction, where the friction force falls as velocity increases to standard viscous friction when the friction force increases with increasing velocity

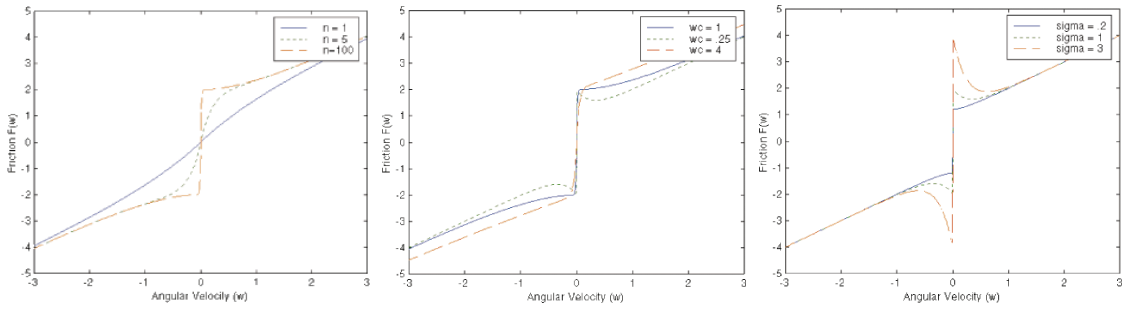

(a) (b) (c)

Figure 2-7. The effect of various model parameters on the Majd and Simaan model. a) The effect of 'n'. b) The effect of ω_c. c) The effect of σ.

2.5. Models for Haptic Friction

Of the models presented here, the Karnopp and Dahl models are most attractive for use in haptics. Haptic interfaces have difficulty sensing velocity. Typically haptic interfaces

rely on digital encoders for position sensing. Velocity is estimated by differentiating the position signal. Discrete-time differentiation of a quantized position signal leads to poor velocity resolution. Using a first-difference, fixed-time, differentiation scheme, the velocity resolution, δv, can be expressed as

$$\delta v = \frac{\delta x}{T} \tag{2.10}$$

Where δx is the encoder's resolution and T is the sample rate. From Equation 2.10 we see that shorter sample rates result in poorer velocity resolution[1].

Most other models, due to the hard nonlinearity, or steep slope near zero velocity, would require very small velocity resolution to be successfully used for haptics. The Dahl model and its derivatives, because they are position based, do not have the same stringent velocity resolution requirements. The Dahl model is somewhat complicated however, because it requires the integration of a differential equation in order to calculate friction force.

The Karnopp model circumvents the low velocity resolution issue with the introduction of the velocity threshold, *DV*. Karnopp's model is also attractive because, although it is relatively simple, it can capture an important feature of friction: higher values of static friction than dynamic friction. For this reason, the Karnopp model is the model of choice for this work.

1. As discussed in 3.4, an alternative is to estimate velocity by measuring the time interval between encoder ticks. Even so, velocity resolution and accuracy at low speeds are problematic.

Chapter 3

Friction Identification

This chapter evaluates approaches by which a haptic interface can be used to identify and model friction present in an environment or device. It begins with a review of previous work in robot and haptic environment identification. Next, it outlines a procedure for identifying the amount of friction present between two surfaces, and the inertia of the moving element. After a presentation of some experimental results, the chapter concludes with a discussion of the procedure's effectiveness and a comparison between the Karnopp and Dahl models as they apply to friction identification.

3.1. Introduction

The challenge of creating realistic, high fidelity representations of physical devices or mechanisms has received much attention by haptics researchers and haptic system developers. Objects such as switches and springs, with impedance characteristics dominated by stiffness, inertia, and damping, have been successfully modeled and subsequently rendered with the same haptic interface. Here, we extend the realm of haptic identification and display to include objects with substantial friction. Friction is present at some level in all sliding objects and mechanisms with sliding parts. Knowledge of an environment's friction is essential to understanding and modeling the system dynamics. Nevertheless, because it is highly nonlinear, friction is rarely fully included in haptic renderings. Friction is often sim-

plified and represented as a constant plus linear damping term, even when the details of the friction can be valuable for distinguishing among different materials.

The problem of identifying friction is complicated when the environment's inertia is also unknown. Unlike stiffness, which can be measured statically, friction identification involves dynamic measurements, which are invariably affected by mass and damping as well. It is possible to include damping in a general friction model, but inertial forces must be isolated. In some cases, it is possible to disassemble a mechanism or otherwise operate on it so that the mass can be evaluated independent of friction. In the most general case, however, the mass and friction must be estimated simultaneously.

3.2. Previous Work

In both the robotics and haptics literature, one can find examples of researches actively probing environments with forces to learn about the environment's dynamics. In certain instances, the robot itself is the environment under investigation as programmers attempt to quantify parameters such as the robot's inertial and frictional properties. In the following sections, we will review active force probing as it has been applied to general environment identification, and more specifically to the problem of measuring friction.

3.2.1. Environment and Device Identification

There are several examples of haptic interfaces used for system identification in the literature. Shulteis et al. (1996) demonstrated that a haptic system used for teleoperation can extract quantities such as an object's dimensions, weight and coefficient of friction. Dupont et al. (1997) showed that the same system can be used to identify the kinematic constraints of an object being manipulated. MacLean (1996) used a haptic interface equipped with a force sensor as a force probe to characterize the nonlinear stiffness properties of a momentary switch. The characterization was done by first recording the force response of the switch over a range of displacements. Next, the nonlinear force versus displacement profile was divided into piece-wise linear segments. The obtained stiffness model was used to sim-

ulate the switch using the same interface that characterized it. Miller and Colgate (1998) used a wavelet network (a nonlinear system identification technique) to identify the impedance characteristic of a spring attached to a wall. The wavelet technique, like MacLean's method, uses force/displacement data collected from a real system. However, the wavelet analysis is done in the spatial frequency domain.

3.2.2. Friction Identification

Johnson and Lorenz (1992) present a novel method for identifying a system's friction by measuring state feedback errors. They begin by building a feed-forward controller that includes relevant dynamic properties of the system such as its mass and viscous damping. The controller does not include compensation for Coulomb friction. Once the feed-forward gains for inertia and viscous damping are properly tuned, the state feedback error signal will contain only errors caused by friction and other unmodeled effects. The unmodeled effects are then minimized with a signal processing technique called Synchronous Spatial Averaging, SSA. SSA averages velocity signals in the spatial velocity domain rather than in the time domain. Averaging in this manner filters noise signals that are uncorrelated to spatial velocity.

Kim et al.(1996) use a numerical optimization scheme to find the unknown parameters of their chosen friction model. Seeking to characterize the friction in an x-y plotter, the authors operate the system by applying a specified force input. The plotter displacement is then recorded. Starting with initial estimates for the friction model parameters, their optimization scheme adjusts the parameters until optimal values are found. The optimal set of parameters minimizes the square of the error between the recorded displacement and the displacement predicted by the model.

Armstrong-Helouvry (1991) used two main schemes to measure the friction present in robotic joints. In the first method, a known torque trajectory was applied to the system while the acceleration was recorded. Because the system's inertia was known, the friction could be calculated as the difference between the known input torque and the calculated

inertial torque. The second method estimated static friction by measuring the minimum input torque necessary to initiate motion.

Kim et al. (1997) began by selecting an exponential friction model. They used least squares regression in the frequency domain and solved for the parameters of their model.

In each of these cases, the first step in friction identification was the selection of the model to be used. The second step was to determine the values for the parameters of the model.

3.3. Model Selection

Though we have an assortment of models to choose from, the model of choice for friction identification here is the Karnopp model. The driving factors behind the choice of the Karnopp model are its simplicity and the fact that it does not require extremely accurate measurements of velocity at low speeds. All of the model parameters can be expressed as linear coefficients of the independent variables velocity and acceleration. This fact will be exploited later to facilitate estimates of the parameter values. Despite its simplicity, the model accurately describes the resistive force present for the materials tested at velocities away from zero. Karnopp's model was also chosen for its flexibility. It is readily adjusted to allow for asymmetric frictional properties in different directions. Viscous damping is easily included and it allows the static and dynamic friction to take on different values. Different static and dynamic friction values are necessary to model the occurrence of stick-slip. Karnopp's model does have some problems, however. The model's behavior around zero velocity is not based on the microscopic interaction of the material asperities. It cannot predict hysteresis even if hysteresis is present in the collected data. For these reasons the Dahl model was also considered.

The Dahl model is best described as a position dependent friction model rather than a velocity dependent model like Karnopp. As stated by Armstrong et al. (1994) "If very small displacements are to be accurately simulated,...position-dependent models could be

more accurate than a velocity-dependent model." The Dahl model is more accurate in describing friction in the low velocity regimes, but it is not without its problems. The model is described by a differential equation. As such, its parameters cannot be expressed as linear coefficients of the independent variables meaning that numerical schemes such as nonlinear least squares or other methods are required to estimate the parameter values. Such methods are more complicated and computationally expensive than linear least squares. The Dahl model does not allow for stiction, or "stick-slip-slide" friction without being modified. Furthermore, it can be subject to numerical instabilities. To be useful for identification purposes, both models need to be modified slightly as explained in the following sections.

3.3.1. Modified Karnopp Model

The modified version of the Karnopp used can be seen in Figure 3-1. It includes both Coulomb and viscous friction and allows for asymmetric friction values for positive and negative velocities. It is expressed as:

$$F_{\text{friction}}(\dot{x}, F_a) = \begin{cases} C_n \operatorname{sgn}(\dot{x}) + b_n \dot{x} & \text{for } \dot{x} < -\Delta v \\ max(D_n, F_a) & \text{for } -\Delta v < \dot{x} < 0 \\ min(D_p, F_a) & \text{for } 0 < \dot{x} < \Delta v \\ C_p \operatorname{sgn}(\dot{x}) + b_p \dot{x} & \text{for } \dot{x} > \Delta v \end{cases} \tag{3.1}$$

where C_p and C_n are the positive and negative values of the dynamic friction, b_p and b_n are the positive and negative values of the viscous friction, $\dot{x}$ is the relative velocity between the mating surfaces, D_p and D_n are the positive and negative values of the static friction, Δv is the value below which the velocity is considered to be zero, and F_a is the sum of non-frictional forces being applied to the system.

Although this model cannot replicate subtle friction features such as the Stribeck effect, it does model the basic stick-slip property. By allowing the friction force to be asymmetric,

this model better matches data observed here and in other friction identification papers (Armstrong-Helouvry 1991; Johnson and Lorenz 1992)

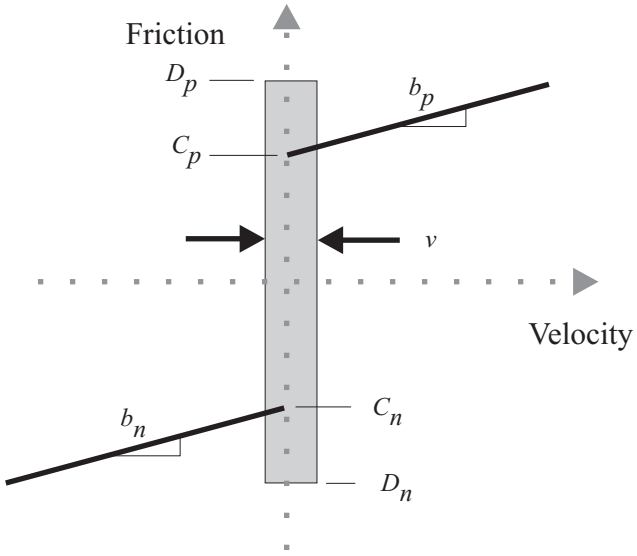

Figure 3-1. Parameters of the modified Karnopp model

3.3.2. Modified Dahl Model

The modified Dahl model is quite similar to the original Dahl model. For the purposes of experimental friction identification, we define the model in a piecewise fashion. This allows the friction force to be different for different directions of motion, a common observance in friction identification. The modified Dahl model also contains a viscous damping term. The model is presented in Equations 3.2 and 3.3.

$$\frac{dF_{friction}}{dx} = \begin{cases} \sigma\left|1 - \frac{F}{D_p}\operatorname{sgn}(\dot{x})\right|^i \operatorname{sgn}\left(1 - \frac{F}{D_p}\operatorname{sgn}(\dot{x})\right) & \text{for } \dot{x} > 0 \\ \sigma\left|1 - \frac{F}{D_n}\operatorname{sgn}(\dot{x})\right|^i \operatorname{sgn}\left(1 - \frac{F}{D_n}\operatorname{sgn}(\dot{x})\right) & \text{for } \dot{x} < 0 \end{cases} \tag{3.2}$$

$$F_{friction} = \int\left(\frac{dF_{friction}}{dx}\frac{dx}{dt}\right)dt + b\frac{dx}{dt} \tag{3.3}$$

Where F is the friction force predicted, D_p and D_n are the friction limits in the positive and negative directions respectively, and b is the viscous damping term. For simplicity only a single viscous damping term is used in this model.

3.4. Experimental Apparatus

A one degree of freedom linear motion haptic interface was constructed in order to conduct friction identification experiments (See Figure3-2). The setup includes a low friction, low inertia, dc motor (Maxon RE025-055) as the actuator. A 2048 line quadrature encoder is used for position sensing. Velocity is estimated with the aid of an I/O Card from Immersion Inc. This card calculates velocity values by measuring the time between encoder pulses rather than counting the number of encoder pulses that occur during a specified time.

Rotary motion from the motor is converted to linear motion/force using a low friction linear stage and a transmission consisting of a steel cable wound several times around the motor pulley. A 10 lbf. (44.8 N) capacity load cell (Sensotec31/1426-04) gives force measurements and a +/-50g accelerometer (Sensotec 60-3629-02) provides acceleration measurements. Estimates of key characteristics, including noise levels, of the apparatus are listed in Table 3-1.

Table 3-1. Experimental Apparatus Parameters

System Equivalent Inertia (motor and slide)	0.692 kg
Force output to commanded voltage	23.315 N/V
Maximum Force (continuous)	9.48 N
Range of Motion	3.2 cm
Position Resolution	2.57×10^{-6} m
Voltage output to measured force	8.896 N/V
Static Friction (motor and slide)	
Forward Motion	1.04 N
Reverse Motion	0.69 N

The force sensor for the apparatus is located downstream of the motor and slide inertia so that it only measures the force applied to the object or system under test. The system being tested and the experimental apparatus are connected by a coupling that is compliant

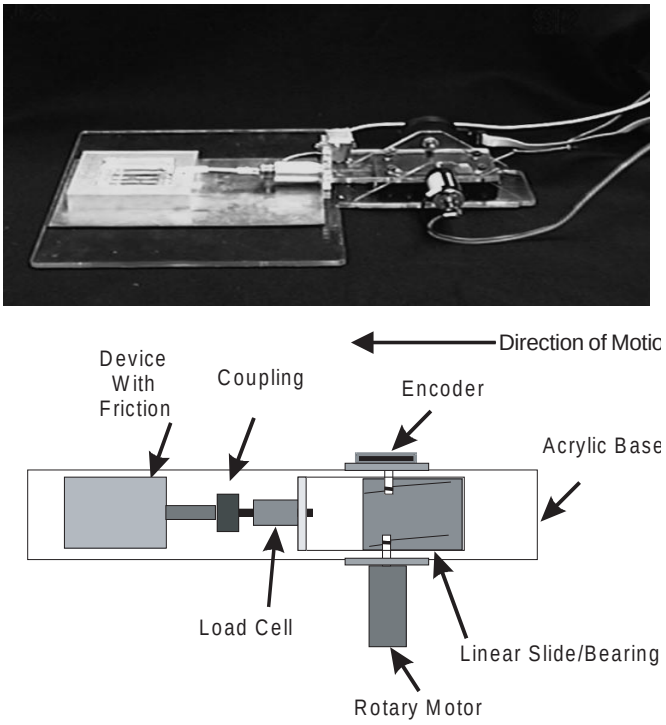

Figure 3-2. Experimental Apparatus for Identification

in the radial direction but stiff in the axial direction. The apparatus was used to identify sliding friction between an aluminum block and sheets of brass, Teflon and rubber.

3.5. Identification Procedure

The procedure for friction identification can be summarized as follows:

- Model the force/motion interaction of the system
- Move system over a range of velocities of interest
- Record force/motion variables included in the model
- Solve for unknown parameters of the system model

These steps are detailed below.

3.5.1. Modeling the force/motion interaction

For our experimental system the force/motion interaction can be described as

$$F_{\text{applied}} = m\ddot{x} + F_{friction} + F_{other} \tag{3.4}$$

where $F_{applied}$ is the force applied to the aluminum block, m is the mass of the aluminum block, $\ddot{x}$ is the acceleration of the aluminum block, $F_{friction}$ is the modified friction model described by either Equation 3.1 or 3.3, and F_{other} includes any effects not included in the inertia term or in the friction model.

Terms in F_{other} can include things such as off-axis force sensor loading, forces caused by elastic deformations, and an inertial force out of line with the primary direction of motion.

3.5.2. Move the system over the range of velocities of interest

For each friction measurement experiment the aluminum block was connected to the apparatus and the apparatus was commanded to move with a periodic trajectory. Various periodic trajectories having frequencies ranging between of 0.5-3 Hz were explored. The sample trajectories presented here are sinusoids with a frequency of 2 Hz and an amplitude of 0.01 meters. The system was driven using a proportional-derivative or PD controller. The PD gains were tuned before the apparatus was connected to a system with friction. They were empirically set to the highest values that gave smooth sinusoidal responses without friction. For additional smoothing, the command output was digitally filtered with a second order low-pass filter with a cut-off frequency of 100Hz. The frequency and amplitude of the command trajectory were selected to stay within the 0.030 meter range of motion of the interface and to match the approximate range of motions that humans use when sliding their fingertips in an exploratory fashion. The sample rate for motion commands and data collection was 1 kHz.

3.5.3. Record force/motion variables included in the model

The system was allowed to warm-up for 10 seconds prior to collecting data for each experiment. During the warm-up, the aluminum block was moved with the same sinusoidal trajectory that was used during data collection. The warm-up served two functions. First, it eliminated the phenomenon of rising static friction because the system was not allowed to dwell at zero velocity for a significant period. Second, it allowed the motion of the system to reach steady state. After the 10 second warm-up was complete, the force applied to the aluminum block was recorded, along with the block's position, velocity and acceleration. Data were collected for 2 seconds, corresponding to four cycles and seven velocity reversals. Figure 3-3 shows typical velocity, acceleration and force data.

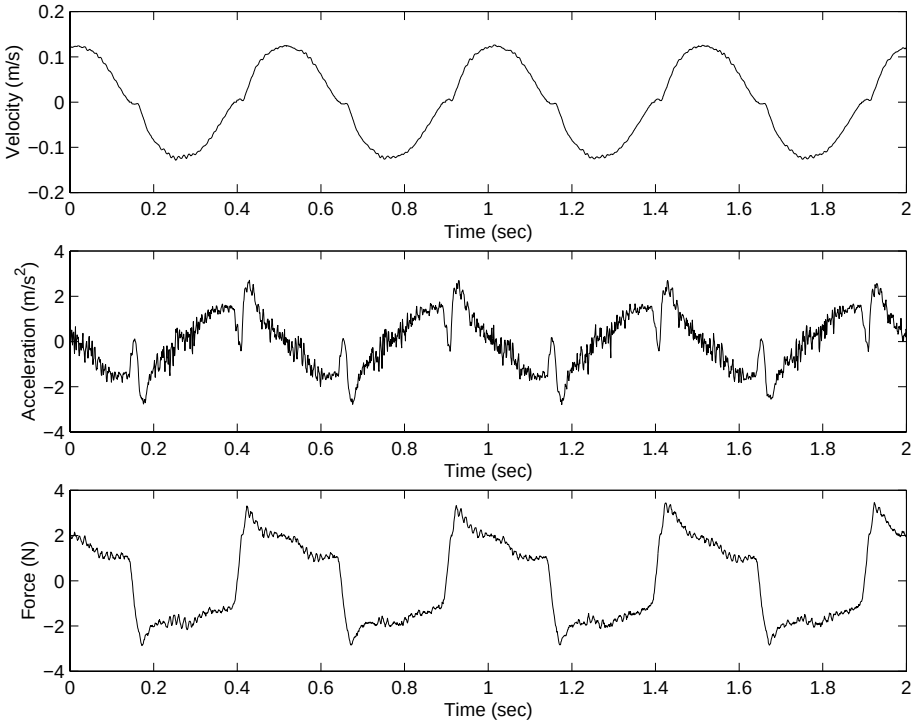

Figure 3-3. Typical velocity, acceleration, and force data

Due to the digital nature of the encoder, position and velocity estimates were obtained with a relatively small measurement error. Force and acceleration estimates, however, had

larger uncertainties arising primarily from noise introduced in signal amplification and analog to digital conversion (See Table3-2).

Table 3-2. Standard Deviations of the Measurement Errors

Measurement Error	**Standar Deviation**	**Units**
position	5.76×10^{-5}	meters
velocity	3.18 x 10-3	meters/second
acceleration	0.2379	meters/second^2
force	0.062	Newtons

The uncertainty estimates are the standard deviations of the difference between the measured trajectories and ideal trajectories. These are conservative estimates since a portion of the difference can be attributed to errors in the control.

To help reduce the errors caused by the drift and temperature sensitivity in the accelerometer, the acceleration signal was scaled and offset for each experimental run. The scale factor and offset were selected to minimize the difference between the accelerometer measurement and a differentiated velocity signal. The differentiated velocity signal was obtained by four-point central differences. The resulting adjusted acceleration signal contains less noise than the differentiated velocity signal and is more accurate than the original accelerometer measurement.

3.5.4. Solve for unknown parameters

With the modeling and data collection complete we can now estimate the parameters of the friction model. We will first fit the parameters of the Karnopp model to the data using linear least squares regression. Next, we will find the parameters of the Dahl model using nonlinear least squares regression.

3.5.4.1. Fitting the Karnopp model to the data

One advantage of the Karnopp model is that its parameters can be expressed as linear coefficients of the input variables. By expressing the parameters as linear coefficients of our inputs the parameters can be estimated using linear least square regression (LLS). As a first

step in expressing the model parameters in a linear fashion, we separate the data into two bins. One bin contains data for velocities of magnitude less than Δv. The second bin holds the remaining data. Δv is selected as the smallest velocity range that fully encompasses the transition from static to dynamic friction. After the data points corresponding to low velocities are removed, the recorded velocity vector is split into two new velocity vectors. The velocity vector vel_p is equal to the original vector *vel* except that negative velocity values are replaced with zeros. The velocity vector vel_n contains the negative portion of the original velocity vector and has zeros where there are positive values in *vel* (See Figure 3-4).

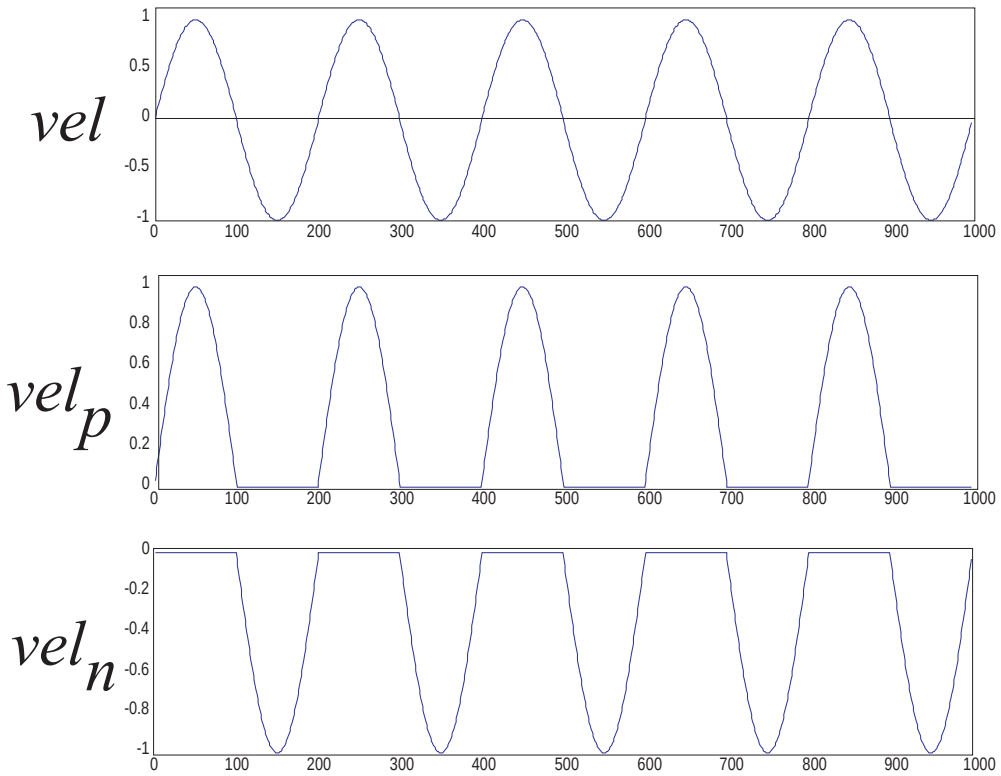

Figure 3-4. Example of how velocity is split into positive and negative components

Now, the measured force can be expressed as the sum of the inertia force, and the friction by

$$\boldsymbol{F_m} = m\mathbf{a} + C_p \operatorname{sgn}(\mathbf{vel_p}) + b_p \mathbf{vel_p} + C_n \operatorname{sgn}(\mathbf{vel_n}) + b_n \mathbf{vel_n} + \varepsilon \tag{3.5}$$

or, in matrix form as

$$\begin{bmatrix} F_{m1} \\ \dots \\ F_{mN} \end{bmatrix} = \begin{bmatrix} \mathrm{a}_1 & \operatorname{sgn}(\mathrm{vel}_{p1}) & \mathrm{vel}_{p1} & \operatorname{sgn}(\mathrm{vel}_{n1}) & \mathrm{vel}_{n1} \\ \dots & \dots & \dots & \dots & \dots \\ \mathrm{a}_N & \operatorname{sgn}(\mathrm{vel}_{pN}) & \mathrm{vel}_{pN} & \operatorname{sgn}(\mathrm{vel}_{nN}) & \mathrm{vel}_{n1N} \end{bmatrix} \begin{bmatrix} m \\ C_p \\ b_p \\ C_n \\ b_n \end{bmatrix} + \begin{bmatrix} \varepsilon_1 \\ \dots \\ \varepsilon_N \end{bmatrix} \tag{3.6}$$

$$\boldsymbol{F_m} = \boldsymbol{X}\beta + \varepsilon \tag{3.7}$$

where $\boldsymbol{F_m}$ is the measured force, **a** is the measured acceleration and ε is the measurement error.

The LLS estimate for β has been shown to be

$$\hat{\beta} = (\boldsymbol{X}^T\boldsymbol{X})^{-1}(\boldsymbol{X}^T\boldsymbol{F}_m) \tag{3.8}$$

Implicit in this estimate for β is the assumption that the variables in $\boldsymbol{X}$, and *vel* in our case, are free of measurement error. Fuller (1987) shows that β's estimated using Equation 3.8 will contain a bias if measurement error is present. Given the fact that measurement errors exist in both *a* and *vel*, we consider an alternate estimator for β. Fuller goes on to present several alternate estimators that account for errors in the input variables and provide unbiased estimates of β. Assuming that the errors in each of our measured variables are independent of each other, our alternate estimate for β is

$$\tilde{\beta} = (N^{-1}\boldsymbol{X}^T\boldsymbol{X} - \ddot{S}_{uu})^{-1}(N^{-1}\boldsymbol{X}^T\boldsymbol{F}_m) \tag{3.9}$$

where N is the number of samples, $\ddot{S}_{uu} = \operatorname{diag}(\mathrm{s}_{\delta a}, 0, \mathrm{s}_{\delta vel}, 0, \mathrm{s}_{\delta vel})$, $\mathrm{s}_{\delta a}$ is the estimated variance of the acceleration, and $\mathrm{s}_{\delta vel}$ is the estimated variance of the velocity.

3.5.4.2. Fitting the Dahl model to the data

The Dahl model is expressed as a differential equation. Because its parameters cannot be expressed as linear coefficients of the input, a numerical optimization scheme such as an unconstrained minimization technique, or nonlinear least squares (NLS) must be used to obtain parameter estimates. For the nonlinear least squares approach, the goal is to minimize the square of the error between our model predicted values and the values obtained via experiment. Mathematically stated, the goal is to minimize a function *f*, subject to the parameters β.

$$\min_{\beta \in \Re^n} \quad f(\beta) = \sum_{j=1}^{l} \left(F_{model}(\beta, t_j) - F_{measured}(t_j)\right)^2 \tag{3.10}$$

The elements in β here are similar to the β parameters found about in the Karnopp model. For the Dahl representation of friction β includes the *m*, the mass of the sliding block, *Dp*, the positive friction limit, D_n, the negative friction limit, and a single viscous damping coefficient *b*. The value for the Dahl stiffness, σ, is not included in the automatic parameter estimation. The magnitude of σ is generally quite large in comparison to the other model parameters. The parameter, σ, proved to limit the efficiency of numerical optimization schemes so it was set and adjusted by hand achieve a good match between the experimental data and the model. The Dahl model is quite sensitive to the parameter σ. If the value of σ is too large, the Dahl model will exhibit numerical instabilities.

To estimate values for β, we employ an iterative nonlinear least squares estimator. The estimator used, `lsqcurvefit,` is implemented in the MATLAB® optimization toolbox. The Levenberg-Marquardt method was used to set search direction for parameter estimation. The interested reader is referred to the MATLAB® Optimization Toolbox Reference Manual (Coleman et al. 1999) for the details of the implementation.

3.6. Results

Here we present results obtained by using the method outlined in the previous section to identify the friction and mass of an aluminum block sliding on brass, Teflon and rubber. The mass of the block was presumed unknown for each experiment; however, for verification purposes the block was weighed and found to be 0.419 keg. Figures 3-5(a), 3-6(a), and 3-7(a) show typical raw force data plotted against velocity for our three material combinations. The effects of some stick-slip vibration are evident in the plots. Figures 3-5(b), 3-6(b), and 3-7(b) show the raw force adjusted for the estimated mass. The solid lines in Figures 3-5(b), 3-6(b), and 3-7(b) represent the predicted friction for each case using the parameters in the Karnopp Model, Equation 3.6. The rectangular box shows Δv, D_n and D_p from Equation 3.1. Figures 3-5(c), 3-6(c), and 3-7(c) show the Dahl models plotted over the measured data adjusted for mass.

Table 3-3 lists estimates of the Karnopp model parameters and their standard deviations. The values for D_n are negative due to the definition for static friction given in Equation 3.1. The viscous damping coefficient, b, for brass is sometimes negative. This indicates that the friction is decreasing with increasing velocity. Decreasing friction with increasing velocity is not uncommon for dry metal on metal contract. For information about calculating the standard deviations of the parameter estimates obtained by Equation 3.9, the reader is referred to Fuller (1987). Two experimental runs are presented for each material combination to give a sense of the friction model parameter repeatability from setup to setup. The use of Equation 3.9 rather than Equation 3.8 had the most profound effect on the mass estimates. Mass estimates are 3.8% larger for brass and rubber and 5% larger for Teflon For comparison purposes, Table 3-4 lists the Dahl model parameter estimates for a single experimental run.

The goodness of the Karnopp model's fit can be seen in Figure3-8 which is a plot of the measured force and the model predicted force for aluminum on rubber. Both measured

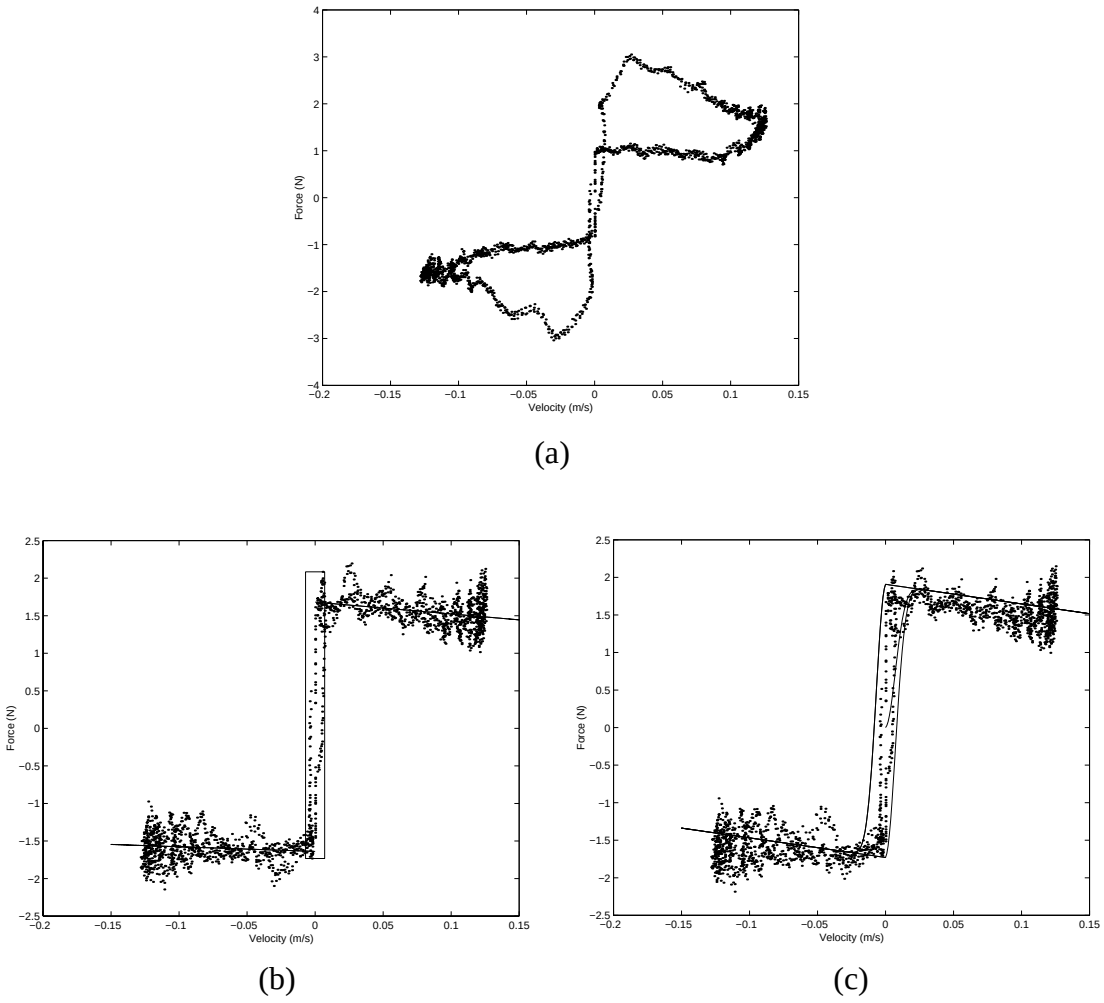

Figure 3-5. Aluminum sliding on brass. a) Measured force versus velocity. b) Force adjusted by inertia with Karnopp fit overlaid. c) Force adjusted by inertia with Dahl fit overlaid.

force and model predicted force are plotted against velocity. A similar plot for the Dahl model is presented in Figure3-9.

The reader will note that second and third columns and the fourth and fifth columns in the matrix ***X,*** defined in Equations 3.6 and 3.7, are related through signum function. For velocity values that are strictly positive, the linear correlation between vel_p and sgn(vel_p)

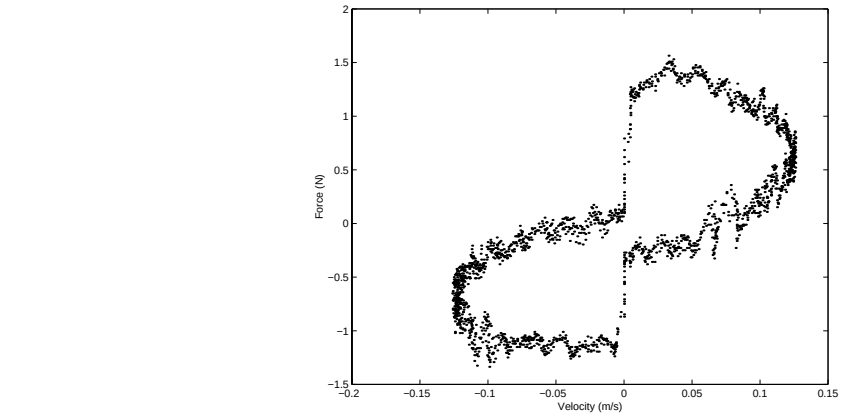

(a)

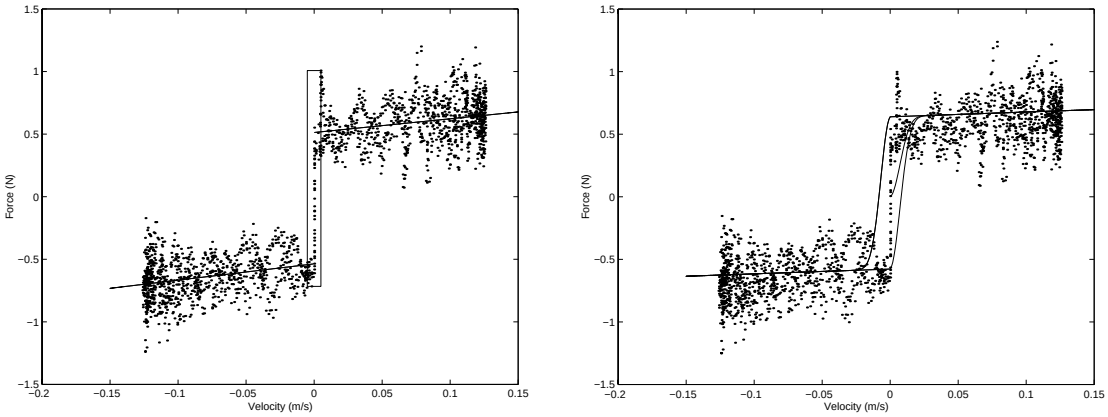

(b) (c)

Figure 3-6. Aluminum sliding on Teflon. a) Measured force versus velocity. b) Force adjusted by inertia with Karnopp fit overlaid. c) Force adjusted by inertia with Dahl fit overlaid.

is undefined. Similarly, when the velocity is strictly negative, there is no linear correlation between vel_n and sgn(vel_n). However, because both vel_p and vel_n contain zeros, there is a quantifiable linear correlation between columns 2 and 3 and between columns 4 and 5. The relationship between the independent variables causes the matrix $\boldsymbol{X}$ to exhibit some multi-collinearity. Multicollinearity leads to a poorly conditioned $\boldsymbol{X}^{\mathrm{T}}\boldsymbol{X}$ matrix, and subsequently poor parameter estimates. For the data presented in this paper the $\boldsymbol{X}^{\mathrm{T}}\boldsymbol{X}$ matrices for all

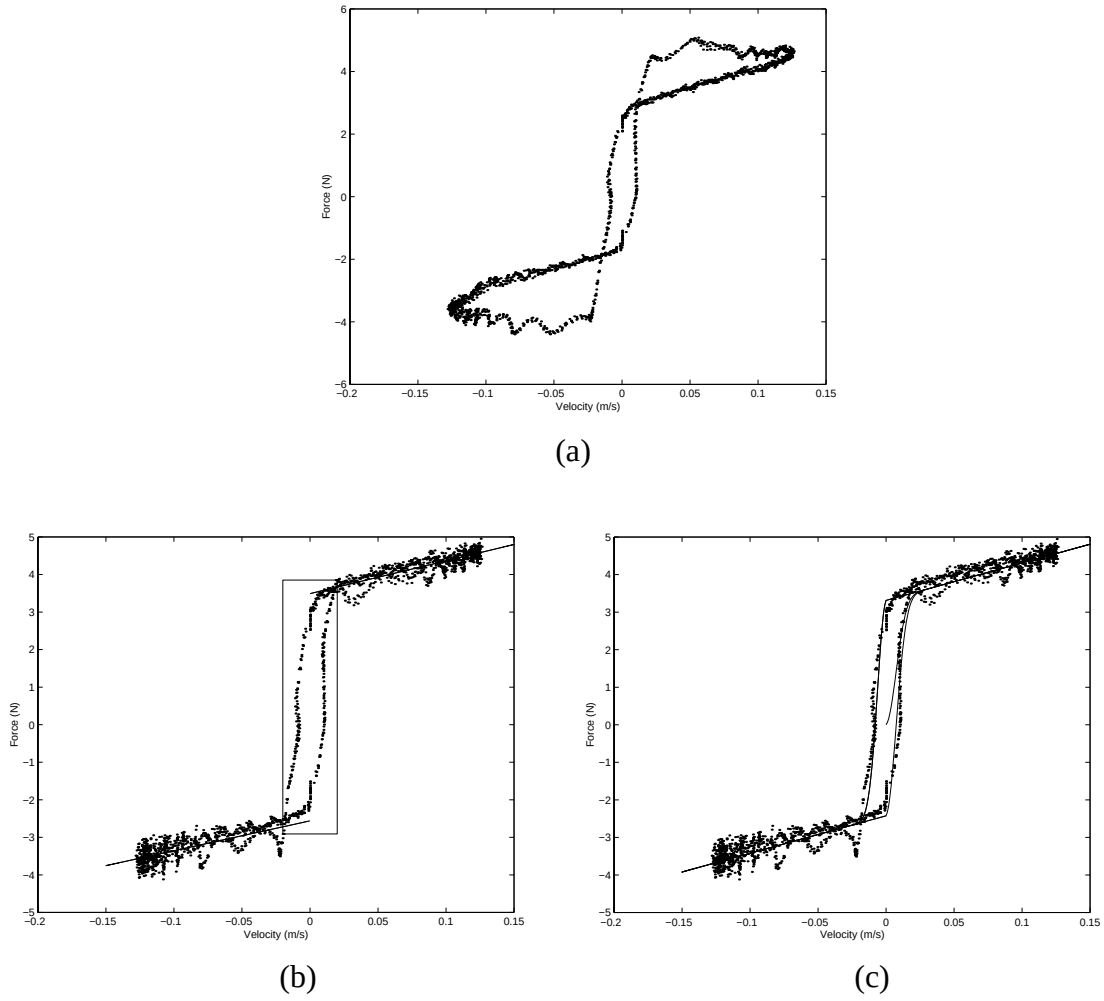

Figure 3-7. Aluminum sliding on rubber. a) Measured force versus velocity. b) Force adjusted by inertia with Karnopp fit overlaid. c) Force adjusted by inertia with Dahl fit overlaid.

materials have condition numbers on the order of 10^{-4}. Matrices with condition numbers on this order are readily invertible with numerical software packages such as MATLAB®.

Table 3-3. Friction estimates for aluminum sliding on brass, Teflon and rubber using Fuller's method (Equation 3.6). The parameters correspond to the modified version of Karnopp's model (Equation 3.1).

	Brass1		Teflon1		Rubber1	
Parameter	Estimate	Std Dev	Estimate	Std Dev	Estimate	Std Dev
m	0.4033	0.0051	0.4436	0.0038	0.3886	0.0045
Cp	1.7714	0.023	0.513	0.0136	3.4901	0.0334
bp	0.457	0.248	1.0957	0.1519	8.7338	0.3621
Cn	1.729	0.0229	0.5365	0.0133	2.5611	0.0298
bn	0.6196	0.2504	1.3038	0.15	7.9521	0.3225
Dp	2.1302		1.0078		3.8513	
Dn	-1.8623		-0.7167		-2.9099	
Δv	0.007		0.005		0.02	
	Brass2		Teflon2		Rubber2	
Parameter	Estimate	Std Dev	Estimate	Std Dev	Estimate	Std Dev
m	0.4117	0.0039	0.4555	0.0037	0.3737	0.0047
Cp	1.6814	0.0173	0.4808	0.0132	3.7244	0.0353
bp	-1.5778	0.1884	1.6554	0.1476	9.6733	0.3853
Cn	1.6384	0.0174	0.5233	0.0127	2.7269	0.0296
bn	-0.618	0.1894	1.5635	0.1434	8.0322	0.3213
Dp	2.0842		0.9319		4.0179	
Dn	-1.7328		-0.6553		-2.7733	
Δv	0.007		0.005		0.02	

Table 3-4. Friction estimates for aluminum sliding on brass, Teflon and rubber using nonlinear least squares regression. The parameter σ is tuned manually. The parameters correspond to the modified version of Dahl's model (Figure3.2).

	Brass	Teflon	Rubber
Parameter	Estimate	Estimate	Estimate
m	0.4489	0.4633	0.3820
b	-2.6071	0.3838	9.9812
Dp	1.9078	0.6389	3.3122
Dn	1.7296	0.5774	2.4238
σ (manually)	30000	10000	50000

3.7. Discussion and Conclusions

This chapter has presented a method for using a haptic interface to estimate the friction and inertia of a real device or system. Sample results were presented for the friction force and

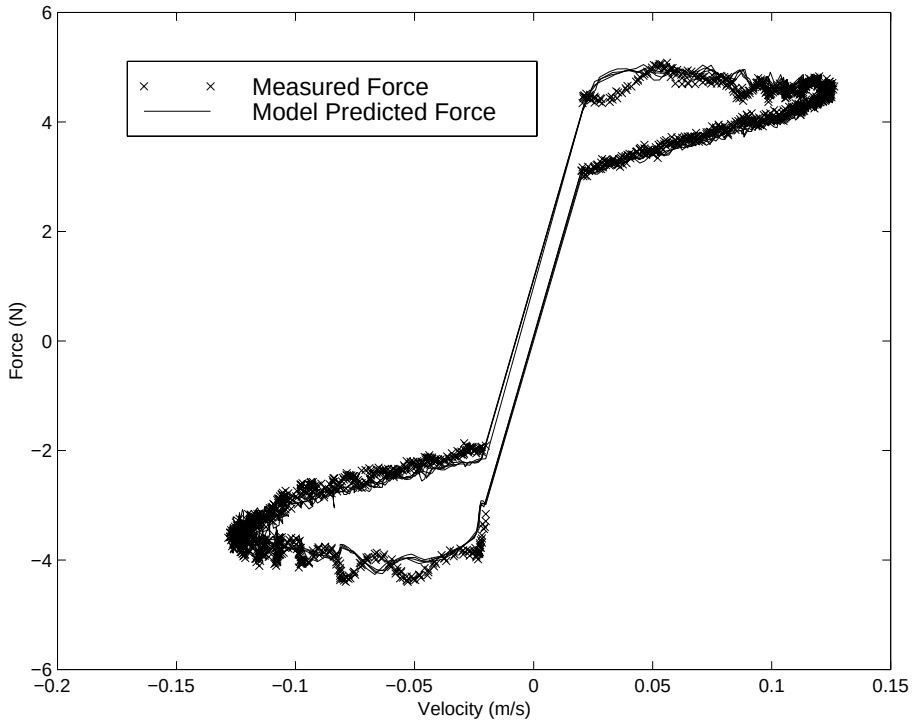

Figure 3-8. Typical measured force and Karnopp model predicted force versus velocity (aluminum on rubber) over four cycles of motion.

mass estimate of an aluminum block sliding on brass, teflon and rubber. Unlike other friction identification techniques, it does not require the experimenter to carefully tune a feedforward controller. Identification via the Karnopp model is not susceptible to the convergence problems experienced when identification is done via the Dahl model or some other numerically based techniques. For identification via the Dahl model, careful selection of the σ parameter was necessary in order for the numerical optimization to converge. It was difficult to obtain an adequately large value for σ when the dynamic value for friction was relatively low. This can be seen for brass and especially Teflon (see Figures 3-5 and 3-6). Ideally, since very little hysteresis is observed for brass and Teflon, σ would take on a relative large value. However, if values larger than those presented in the table are used, numerical difficulties arise. These results indicate that the Dahl model works well in cases where there is a significant amount of dynamic friction and a significant amount of presliding displacement as in the case of rubber.

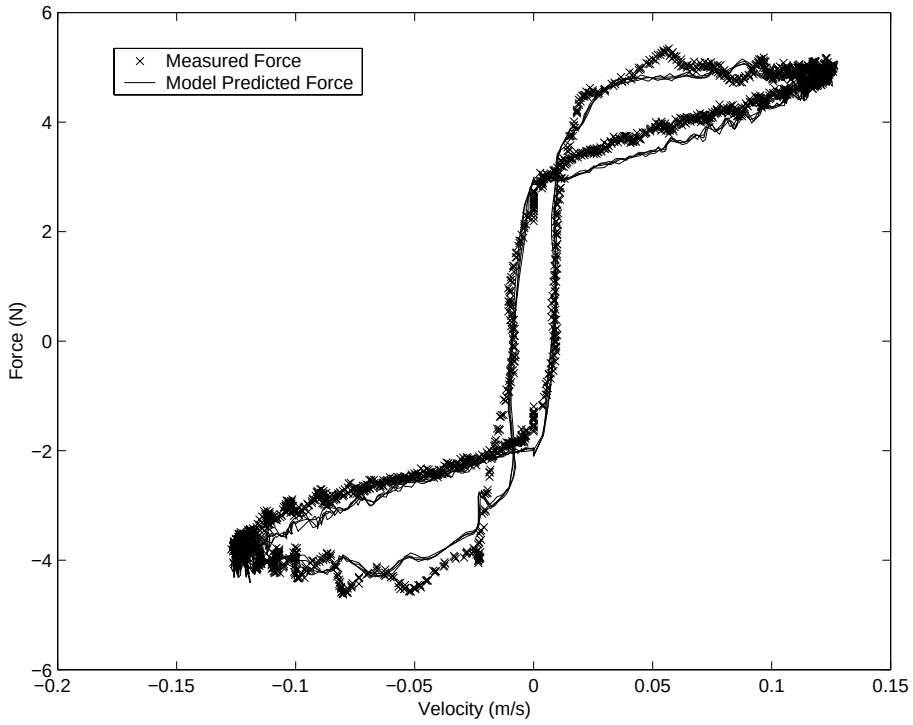

Figure 3-9. Typical measured force and Dahl model predicted force versus velocity (aluminum on rubber) over four cycles of motion.

As is often the case with control or identification strategies, accurate measurements of velocity and acceleration are the key to accurate friction and mass estimates using the method presented here. Much of the spread in the data adjusted for mass ((b) and (c) of Figures 3-5, 3-6, and 3-7) can be attributed to noise in the accelerometer. The effect appears to be less drastic for aluminum on rubber, but this is due to the larger magnitude of the friction force for rubber. The larger the relative magnitudes of the mass and viscous damping for the system being identified, the more acceleration and velocity errors will affect one's estimate. In general, the effect of acceleration and velocity errors will be less profound on estimates of the dynamic friction parameters C_p and C_n.

In addition to measurement accuracy, the selection of the excitation trajectory is important. While it seems that virtually any input trajectory should suffice for friction and mass estimates, the best results were obtained when smooth sinusoidal closed-loop position trajectories were used. The frequency of the input trajectory is limited on the low end by the

signal-to-noise properties of the accelerometer. At low frequencies, the system's acceleration is low and acceleration measurements will be dominated by noise. The frequency of the input trajectory is limited on the high end by the bandwidth of the apparatus. Open-loop force input trajectories did not provide good results. Finding the appropriate amplitude and frequency for an open-loop force input proved to be difficult. If the input force amplitude was made too small, the system would sit at rest, unable to overcome static friction. If the input amplitude was slightly larger, the system would crash into the hard stops delimiting its range of motion. Even if an appropriate open loop force trajectory was found for a given environment, that same trajectory would in all likelihood be inappropriate for a system with different inertia or friction properties.

We have elected to include the observed asymmetry in the friction data in the friction model. Since the force sensor is located between the haptic device and the system with friction, effects like cable drag, D/A calibration offsets, and motor amplifier offsets should not result in asymmetric friction identification. Asymmetry in the force sensor, or in the force sensors amplifier can however lead to an asymmetric response. For this reason, great care should be taken when calibrating the force sensor. Whether or not the asymmetry in the measured force derives from friction or another physical source, it will be experienced by the user of the haptic device and should therefore be included in the haptic rendering.

Our selection of a modified version of Karnopp's friction appears to be a good choice for the range of materials presented here. The model allows for reasonable estimates of static and dynamic friction as well as viscous damping terms. It should be noted, however, that Karnopp's model is not necessarily the best representation of friction from a tribological point of view. Models that are based on the interaction of microscopic surface asperities, or on pre-sliding displacement are better able to capture subtle features of friction. The Karnopp model is preferred to Dahl not because it provides a better quantitative fit to the data, but rather because it provides an adequate representation of the data and it is simple to implement.

The hysteresis that is evident in the force versus velocity plots is most likely due surface elasticity and/or some compliance in the system. This elasticity is, strictly speaking, not part of the friction, and therefore is not included in the model. The true test of the model's adequacy will come from psychophysical user testing.

Chapter 4

Haptic Friction Rendering

This chapter explores the haptic rendering of friction. After reviewing some of the previous work on applying friction models to haptics, we step though a haptic rendering of friction based on the Karnopp model. Karnopp's model is selected because it is numerically simple and therefore implementation of a haptic rendering is rather straightforward. We examine how the Karnopp model parameters effect the overall system response. We will examine both the attributes and limitations of the implementation by focusing on three regimes of the friction model: 1) pre-sliding, 2) stick-slip and sliding, and 3) free motion, or the transition from sliding to zero velocity. Finally, we extend the utility of the model with the addition of a virtual coupling. We show how to choose the virtual coupling's parameters to keep our haptic friction rendering from entering the classic "velocity-reversal" limit cycle that can occur in some friction simulations.

4.1. Introduction

As with any haptic rendering, the challenge of rendering friction is to provide a realistic virtual reproduction of reality: to produce with hardware and software a replica of the natural world around us. Because an exact replica of reality is unachievable, due to limitations of the hardware such as sensor resolution and actuator power, a haptic friction rendering should, at the very least, provide an experience for its user that is of high perceptual fidelity even if it is not physically exact. Sustained oscillations, termed limit cycles, or other insta-

bilities common in haptic renderings not only detract from the realism of a haptic rendering, but can prove to be dangerous to the operator.

4.2. Previous Approaches

4.2.1. The Bristle Model

Chen et al.(1997) sought to simulate not only friction, but compliance and adhesion on surfaces using a haptic interface. They model the interaction of a virtual stylus sliding over a virtual surface. The frictional portion of their model is quite similar to the bristle model developed by Haessig et al. (1991); however, the model of Chen et al. treats the simulated stylus as a single bristle. The details of the bristle model can be found in Chapter 2.

Using the notation of Chen et al., the normal force, F_N, between the stylus and the surface is estimated by giving the simulated surface a stiffness, K_N, in the normal direction and multiplying by the stylus' penetration depth *y*.

$$F_N = K_N y \tag{4.1}$$

The lateral force, F_L, between the stylus and the surface is estimated by giving the stylus a stiffness, K_L, in the lateral direction and multiplying by the stylus' lateral displacement, *x*, from the point where it was previously attached to the surface.

$$F_L = K_L x \tag{4.2}$$

The frictional force, F_F, is defined to be proportional to the normal force. The two are related by a coefficient of friction, C_F, which can represent either static or kinetic friction depending on how long the stylus has been in contact with the current point.

$$F_F = C_F F_N \tag{4.3}$$

When the stylus first comes in to contact with a point, the kinetic coefficient of friction is used. If the stylus remains in contact with the same point for a specified amount of the

time, the static coefficient is used. As long as the as the stylus is in contact with the surface, the user will experience a force that is equal to the lesser of the frictional force or the lateral force. For more details on the bristle model, the reader is referred to Chapter 2.

4.2.2. The Dahl Model

Hayward and Armstrong (Hayward and Armstrong 2000) developed a computational model of friction for haptic rendering that is based upon the Dahl model (Dahl 1976). In Chapter 3 we learned that the Dahl model is well suited for modeling frictional interfaces with significant pre-sliding displacement such as aluminum sliding on rubber. Hayward and Armstrong begin by modeling the frictional interaction between a stationary surface and a sliding object with a virtual spring. The position of the sliding object is denoted x, the length of the spring is z, and the point of attachment between the spring and the stationary surface is w. The force in the spring as it tenses and relaxes represents the friction. They define the change in the spring's length with respect to the sliding objects position as

$$\frac{dz}{dx} = 1 - \alpha(z)\,\mathrm{sgn}(dx)z \tag{4.4}$$

where $\alpha(z)$ is a function defined by the designer.

Integrating over an interval h of arbitrary length, z is found to be

$$z = x - \int_h \alpha(z)z\,dx = x - w \tag{4.5}$$

The initial stretching of the spring models static friction. When the spring is at its maximum length, z_{max}, the model allows the contact point, w to move with x to maintain a constant friction force. In this state, the model emulates sliding or kinetic friction. Most interesting is the model's ability exhibit behaviors such as "stick-slip" at the transition between static and kinetic friction. This transition is governed by $\alpha(z)$. As previous mentioned $\alpha(z)$ is defined by the designer of the haptic rendering. Hayward and Armstrong provide three examples of choices for $\alpha(z)$. The simplest, referred to as *stick-slide*, models

simple dry friction where the static and kinetic values of friction are the same. It is expressed as

$$\alpha(z) = \begin{cases} 0, & |z| \le z_{max}; \\ 1/z_{max}, & \text{otherwise.} \end{cases} \tag{4.6}$$

The second form, referred to as stick-slip-slide allows the static coefficient of friction to be larger than the kinetic value. This is accomplished by introducing a variable z_{stick} and setting its value to be greater than z_{max}. It is expressed as

$$\alpha(z) = \begin{cases} 0, & |z| \le z_{stick}; \\ 1/z_{max}, & \text{otherwise.} \end{cases} \tag{4.7}$$

Last, a form denoted *stick-creep-slip-slide* allows the system to creep slowly if x is increasing slowly. If x increases more rapidly, the system behaves in a manner similar to *stick-slip-slide*. In this form, an example of an appropriate $\alpha(z)$ can be expressed as

$$\alpha(z) = \frac{1}{z_{max}} \frac{z^8}{z_{stick}^8 + z^8} \tag{4.8}$$

4.2.3. The Karnopp Model

Salcudean and Vlaar (1994), Berkelman (1999), and Nahvi et al. (1998) created haptic renderings of friction based on the Karnopp model. In all of these renderings, the sliding object takes on one of two possible states: STUCK or SLIDING. Recall that in the Karnopp model, an object in the STUCK state does not move. Rather, the force due to static friction perfectly balances any external applied force up to the static friction limit. In a haptic rendering of the STUCK state, a proportional position controller similar to Equation4.9 is used to keep the sliding object stationary.

$$f = k_p(x - x_{\text{STUCK}}) \tag{4.9}$$

In Equation4.9, f is an estimate of the force being applied to the sliding object, ik_p the stiffness of the proportional controller, x_{STUCK} is the point where there the object was initially stuck and *x* is the object's current position. Clearly this implementation is not a true representation of the Karnopp friction model because absent an infinite stiffness, k_p the object must move by some measurable amount before any counteracting friction can be applied. What is interesting, however, is that by implementing the STUCK state of Karnopp friction with a virtual spring, we are in fact allowing some pre-sliding displacement. This effect is similar to the pre-sliding displacement that is inherent in the Dahl model. In some implementations (e.g. Nahvi et al.), the stiffness is a function of the normal force vector **n** such that such that $k_p(\mathbf{n}) = k_p\|\mathbf{n}\|$.

If f, the force applied to the object, exceeds the static friction the model transitions from the STUCK state to the SLIDING state. In the SLIDING state, the force experienced by the user can be a velocity dependent viscous friction, a velocity independent kinetic Coulomb friction, or some combination of the two.

Salcudean and Vlaar as well as Berkelman elect to represent only viscous friction in the sliding state. The frictional force exerted on the user is this case is

$$f = k_v\dot{x} \tag{4.10}$$

where k_v is the viscous damping coefficient and $\dot{x}$ is the relative velocity between the sliding object and the surface.

Nahvi et al., however, model the kinetic Coulomb friction. In vector form they express the frictional force in the sliding state as:

$$\mathbf{f} = \mu_k\|\mathbf{n}\|\frac{\dot{\mathbf{x}}}{\|\dot{\mathbf{x}}\|} \tag{4.11}$$

where μ_k is the kinetic coefficient of friction.

In the strict sense of the Karnopp model, the transition from the SLIDING state to the STUCK state occurs when the relative velocity, , falls below a small threshold velocity Δv. A non-backdrivable haptic interface equipped with force sensing however allows a force threshold to determine the sliding to stuck transition. Such a force threshold was used by Berkelman.

4.2.4. Other methods

Ruspini et al.(1997) model static, dynamic and viscous friction with the aid of a virtual proxy. In a virtual environment, a virtual proxy represents the human finger or probe. The motion of the virtual proxy is constrained by the geometry and resistive forces in the virtual environment. The finger and the virtual proxy are connected via a virtual spring of stiffness k_p. (The virtual spring connecting the proxy and the finger is similar to the virtual coupling that will be discussed in Section 4.6.) The force exerted on the virtual proxy is then estimated to be $\vec{f} = k_p(\vec{x} - \vec{p})$, where $\vec{x}$ is the position of the proxy and is $\vec{p}$ the position of finger.

When static friction is present on a virtual surface, the position of the proxy will be static if the magnitude of the force tangential to the surface, f_t, is less than or equal to the magnitude of force normal to the surface, f_n, times the coefficient of static friction $\|f_t\| \leq \mu_s \|f_n\|$.

If the force on the proxy exceeds the limit set by static friction, the proxy begins to slide; the friction becomes kinetic and the equation of motion governing the proxy's motion is given in scalar form as:

$$f_t - \mu_k f_n = m\ddot{x} + b\dot{x} \tag{4.12}$$

where b is the viscous damping term and μ_k is the coefficient of kinetic friction. Setting the mass of the proxy to zero, the velocity of the proxy is found to be

$$\dot{x} = \frac{f_t - \mu_k f_n}{b} \tag{4.13}$$

Equation 4.13 is used by Ruspini et al. to set a velocity bound for the virtual proxy. For each clock cycle in their digital implementation of friction, the motion of the proxy is limited by the velocity bound.

4.3. System description

The system used for friction display consists of three components. Shown in Figure4-1 the components include the human operator, the haptic device, and the virtual environment. In our case, we treat the human operator as a force generating component with an impedance causality. By impedance causality we mean that the force supplied by the human is a function of the input velocity. The term "haptic device" refers to the physical hardware (motors, sensors, structural material, etc.) with which the human interacts. We have chosen to represent the haptic device with admittance causality meaning it takes force as input and moves with an appropriate velocity. The force from the human summed with the force from the virtual environment cause motion of the haptic device. This motion is experienced directly by the human. It is also sensed by the haptic device and relayed back to the virtual environment. The virtual environment in this case is a frictional surface, but in general, it can be represented as any system with impedance causality.

4.3.1. Algorithm for implementing Karnopp Friction

In the original description of the Karnopp model, (Karnopp 1985), the friction model changes depending on the state of the system, STUCK or SLIDING. Recall that according to the Karnopp model, while the system is STUCK, the frictional force takes on whatever magnitude is necessary, up to the static friction limit, to keep the system at zero velocity. While sliding at a velocity greater than *DV* or Δv, the velocity threshold below which the velocity is taken to be zero, the friction force is equal to the level of Coulomb friction plus any viscous damping. From an implementation point-of-view, in the SLIDING state, the friction is a function of the velocity, but, in the STUCK, the friction is a function of the applied force.

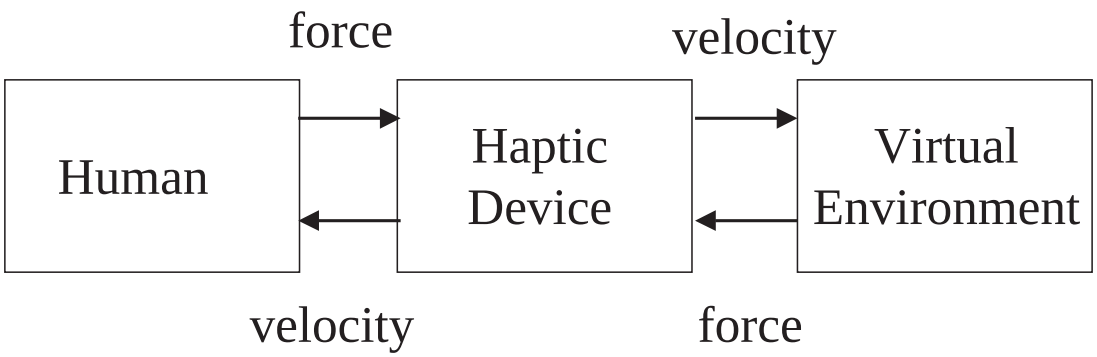

Figure 4-1. Block Diagram of the Haptic System

We however wish to implement friction without direct knowledge of the applied force. In order for our representation of the friction to have impedance causality we must base the friction force only on the motion. This is accomplished by using a virtual spring to convert the input motion to an input force. A small motion of the system away from its stuck position will generate a force proportion to the motion as $F_a \approx -K_p(x - x_{\text{stuck}})$. An algorithm for implementing friction is provided in Table4-1 in pseudocode form.

In the pseudocode, the variable `state` represents the stuck or sliding state of the system. `friction` is the value for the frictional resistance force applied to the haptic device. `ffold` is the friction force applied during the previous execution of the algorithm. `Kp` is the frictional stiffness, `x` and `v` are respectively the position and velocity of the haptic device, `x_stuck` is the position assigned to represent where the system entered the stuck state. `DV` is a velocity threshold set by the designer. `F_static`, `F_dynamic`, and `B` are the static friction level, the kinetic friction level and the level of viscous damping at the frictional interface.

The entire scheme for friction display is implemented on a digital computer. The computer runs a segment of code every T milliseconds. During each of these loops or time steps, the following operations are performed:

```
{
if state = STUCK
   friction = -Kp*(x – x_stuck);
   if abs(friction) > F_static
      state = SLIDING;
      friction = -sign(x - x_stuck)*F_dynamcic –B*v;
   endif
else
   if abs(v)< DV
      state = STUCK;
      x_stuck = x + sign(ff_old)*(F_static/Kp);
      ff = -Kp*(x – x_stuck);
   else
      ff = -sign(v)*F_dynamic – B*v;
   endif
endif
ff_old = friction;
}
```

Table 4-1. Algorithm for rendering Karnopp Friction.

- The position sensor of the haptic device is read
- The system velocity is estimated
- The appropriate amount of friction is calculated
- The friction force is output to the device through its actuators.

To simulate the action of the entire system, human, haptic device, and a virtual environment with Karnopp friction, we much include the force supplied by the human, and the dynamics of the haptic device. A computation program such as MATLAB® is helpful for such simulations.

4.4. Computer simulation of friction rendering

A computer simulation is useful in helping understand the details of our haptic friction rendering. The simulation allows us to examine how the system will respond under specific and repeatable simulated human inputs and responses. The steps of our simulation are listed below:

Create an array representing the time steps for the simulation

Generate an array of applied forces representing the human's input force trajectory

Initialize system parameters including: initial position, velocity, state, friction, etc.

For each time step in the time array:

Calculate the motion of the haptic device based on applied force and friction

Quantize the position and estimate the velocity to simulate the device's sensors

Calculate the new friction based on quantized position and velocity.

The details of each step will now be explained.

4.4.1. Simulating the human

As previously mentioned, the human can be modeled as a force-producing element with impedance causality. For the purposes of the simulation, however, the human is treated as a pure force source. The difference being that a force source supplies a force regardless of the input motion. The force supplied to the haptic device by the human is considered to be independent of the motion of the device. The human is therefore represented in our simulation as a predefined force trajectory. Furthermore in our simulation the force applied by the human is assumed to be constant between time steps. This is equivalent to placing a zero-order hold between the human and the haptic device.

To help reduce some of the effects of quantized velocity, in our physical apparatus, we use a digital encoder I/O card with special velocity sensing characteristics. Rather than using the standard fixed time scheme to estimate velocity, where the number of encoder pulses that occur during a fixed time intervalis measured, our card uses a fixed pulse scheme. In the fixed pulse scheme, one records the amount of time that has lapsed between consecutive encoder pulses. With a fixed pulse scheme, better velocity resolution, especially at low speeds, can be achieved by using a timer with a large number of bits. Because

the fixed time scheme is so prevalent and the analysis more straightforward, we have used a fixed time scheme for our simulation.

4.4.2. Simulating the Haptic Device Motion

The details of the experimental apparatus used for our haptic friction rendering will be described in Chapter 5. The apparatus is essentially a single degree-of-freedom translational device. For the purposes of simulation it is modeled as sliding mass, m, with a small amount of viscous damping b. The small amount of coulomb friction in the apparatus is neglected in the model as are other small effects. The equation of motion governing the apparatus is

$$m\ddot{x} + b\dot{x} = F_a - F_f = F_n \tag{4.14}$$

Where m is the mass of the translating portion of the haptic device, b is the viscous damping coefficient, F_a is the force applied by the human, F_f is the friction force supplied by the virtual environment, and F_n is net force applied to the mass. Equation4.14 can be solved for both velocity, $\dot{x}$, and position, x, for all time. For a specified time step T, the solutions for $\dot{x}$ and x are:

$$\begin{aligned} \dot{x} &= \frac{F_n}{b} + \left(\dot{x}_0 - \frac{F_n}{b}\right)e^{-\frac{T}{\tau}} \\ x &= \frac{F_n}{b}T - \tau\left(\dot{x}_0 - \frac{F_n}{b}\right)\left(e^{-\frac{T}{\tau}} - 1\right) + x_0 \end{aligned} \tag{4.15}$$

Equations 4.15 describe the motion of the haptic device for a given applied force and friction over a given time step T. 'τ' is the time constant of the haptic device. It is defined as $\tau = \frac{m}{b}$.

4.4.3. Simulating the Haptic Device Sensors

Because the haptic device uses a digital encoder for position sensing, the position values sensed and fed to the virtual environment are not only discrete in time, but are quantized by the encoder's resolution. The quantized position measurements of the encoder result in quantized velocity estimates as well. In our simulation of Karnopp friction, the position is only allowed to change by integer multiples of the encoder resolution. The velocity may only change by integer multiples of the encoder resolution divided by the sample rate T. This implies that faster sampling rates degrade the velocity resolution if velocity is estimated based on a fixed time differentiation of a digital encoder.

4.4.4. Determining the friction

The friction force at each time step is determined using the algorithm given in Table4-1. In our simulation of the Karnopp model, quantized versions of position and velocity are used so that the results will better match those from experiment. To assess the behavior of our rendering and to determine how certain parameters affect the system response, a simulation is quite useful. We are interested in both the stability of the system, and the accuracy with which it represents the friction that we desire to emulate. There are three regimes of dry friction that we wish to examine. They are: 1) pre-sliding displacement, 2) stick-slip and sliding and 3) free motion.

4.5. Effects of model parameters in three regimes

The three regimes of interest for looking at the effects of changing model parameters on our haptic rendering are: 1) pre-sliding displacement, 2) stick-slip and sliding and 3) free motion. We will now discuss each of theses regimes individually.

4.5.1. Pre-sliding displacement

Pre-sliding displacement is the term used to describe microscopic motion at a frictional interface before true sliding begins. In many friction models, before macroscopic motion occurs pre-sliding displacement is modeled as a spring. Our rendering of Karnopp friction

uses a virtual spring to estimate the force applied at the interface when the system in the in stuck state. Small displacements result in a restoring force that is proportional to the amount of displacement. In this configuration, the rendering can be viewed as a regulator keeping the system at a specified position subject to a disturbance force F_a. Such a regulator with proportional gain K_p is shown in Figure4-2.

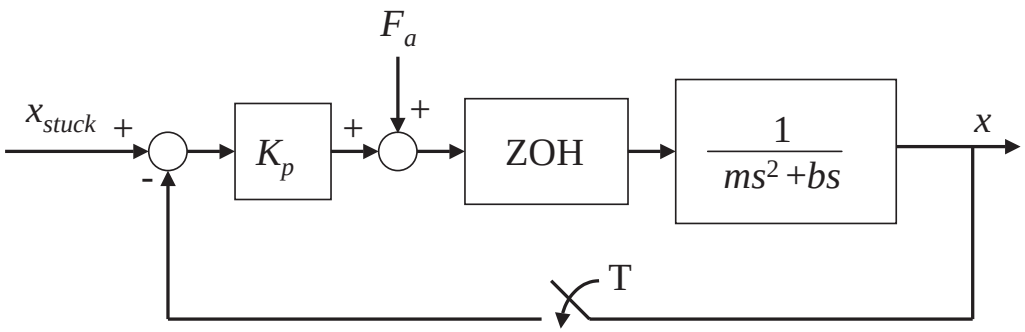

Figure 4-2. Block diagram of a digital regulator

4.5.1.1. Upper limit on K_p

A large value for K_p seems ideal in many respects. In the stuck state, it is desirable for the velocity to remain low. If K_p were infinite, for example, there would be no sliding at the frictional interface and therefore zero velocity. Also, the larger the value of K_p, the higher the system's natural frequency. A system with a high natural frequency can respond more quickly to changes in the applied force. Since we are using K_p to estimate the force being applied to our system, it is important that K_p be large enough that our estimated applied force doesn't lag too far behind the actual applied force. Larger values of K_p will reduce the lag between the actual applied force and our estimated applied force. All of this seems to suggest a very large value should be used for K_p. There is, however, a limit on the maximum value of K_p. Because our system is implemented with digital control, if K_p is too

large, the system will become unstable. A small disturbance will result in a growing oscillation. To find the upper limit on K_p, we must look at the poles of our closed-loop system.

To analyze the stability of the regulator, we begin by expressing Equation4.15 in state-space form. By recognizing that the force F, can be expressed as $F(k) = -K_p(x(k) - x_{\text{stuck}}) = -K_p x(k)$ when $x_{\text{stuck}} = 0$, the state-space equation for the closed-loop system can be written as

$$\mathbf{x}(k+1) = \mathbf{\Phi}\,\mathbf{x}(k) \tag{4.16}$$

Where $\mathbf{x}(k) = \begin{bmatrix} x(k) \\ v(k) \end{bmatrix}$, and

$$\mathbf{\Phi} = \begin{bmatrix} 1 - \dfrac{K_p(T - \tau + \tau e^{(-T/\tau)})}{b} & \tau - \tau e^{(-T/\tau)} \\ -\dfrac{K_p(1 - e^{(-T/\tau)})}{b} & e^{(-T/\tau)} \end{bmatrix}, \tag{4.17}$$

The stability of the system is determined by finding the eigenvalues of $\mathbf{\Phi}$. Taking the determinant of $\lambda(\mathbf{I} - \mathbf{\Phi}) = 0$, the characteristic equation of the closed-loop system is found to be

$$\lambda^2 - \lambda\left(1 + e^{(-T/\tau)} - \frac{K_p T}{b} + \frac{K_p \tau}{b} - \frac{K_p \tau e^{(-T/\tau)}}{b}\right) + \left(e^{(-T/\tau)} - \frac{K_p T e^{(-T/\tau)}}{b} + \frac{K_p \tau}{b} - \frac{K_p \tau e^{(-T/\tau)}}{b}\right) = 0 \tag{4.18}$$

Finally, solving for λ, the poles of the closed loop system are found to be

$$\lambda = \frac{b(1 + e^{(-T/\tau)}) - K_p(T + \tau(e^{(-T/\tau)} + 1)) \pm \sqrt{\left(b(1 + e^{(-T/\tau)}) - K_p(T + \tau(e^{(-T/\tau)} + 1))\right)^2 + 4b\left(-be^{(-T/\tau)} + K_p((T + \tau)e^{(-T/\tau)} - \tau)\right)}}{2b} \tag{4.19}$$

Assuming an haptic device with mass, m = 1kg, damping, b = 10Ns/m and a sample period, T of 0.001 secs, we find that a K_p of about 20,000, results in λ values of magnitude

1. Larger values of $K_p$will result in an unstable system. For all of the computer simulation results in this chapter m will equal 1, b will be 10 Ns/m and T will be 1 ms.

4.5.1.2. System Damping

Most haptic devices have very small amounts of friction and damping by design. While this light damping is beneficial in many respects, it has a negative effect on the stability of haptic rendering control systems. As we saw earlier, the stability limit for K_p is a function of b, the damping in the haptic device. As K_p gets larger, the effective damping of the system decreases. This effect can be seen by examining the equation for the damping ratio or a continuous, linear, second-order system, $\zeta = \frac{b}{2\sqrt{mK_p}}$. As the damping decreases, the result is a system that oscillates more as it settles to its final value. Figure4-3 shows simulation results for a step response with various levels for K_p. Note how the system responds more quickly at higher gains, but the oscillations take longer to settle.

Adding some virtual damping in parallel with the virtual spring seems like a viable method to reduce these oscillations. With virtual damping, the estimate of the friction force in the stuck state becomes $F_f = K_p(x - x_{\text{stuck}}) + K_d\dot{x}$.
damping, K_d, will only be effective if good velocity estimates are available. At low velocities, a quantized velocity signal is quite noisy. Adding a damping term will cause the generated friction signal to be noisy as well. Figure4-4 illustrates the effect of adding damping when using quantized velocity (again assuming fixed time position differentiation). Figure 4-5 shows a quantized and nonquantized velocity signal for comparison purposes.

Given this situation the designer of a haptic rendering is left with two alternatives a) obtain better velocity sensing, or b) select a value of K_p that offers a compromise between natural frequency and oscillation amplitude.

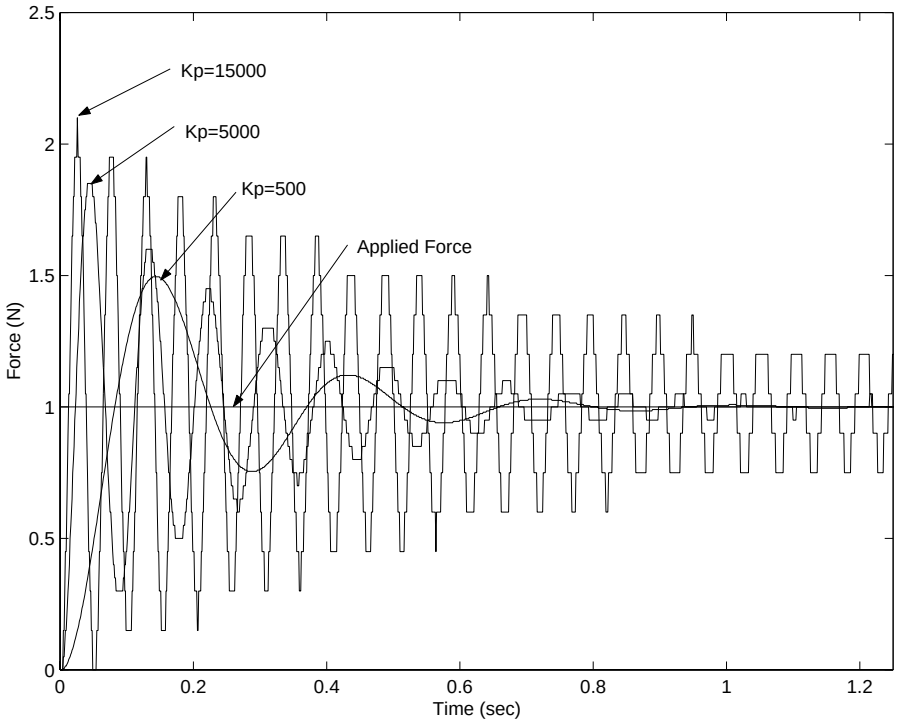

Figure 4-3. Step responses for various gains K_p

4.5.1.3. Lower Limit on K_p

As mentioned previous, K_p should be fairly large. If K_p is too small, the frictional force cannot respond quickly enough to match applied force, and the fidelity of the friction rendering suffers. This lower limit is really one of system bandwidth. A small K_p results in a system with a low natural frequency. As a rule of thumb, the system's natural frequency should be at least 20 times larger than the expected dominant frequency of the applied force. Figures 4-6 and 4-7 show how a low value for K_p leads to a lagging friction force estimate. Figure4-7 especially shows how with low K_p the velocity in the STUCK state exceeds *DV*. The result is an undesirable friction versus velocity curve. Figure4-6 also exhibits stick slip friction, the subject of the next section.

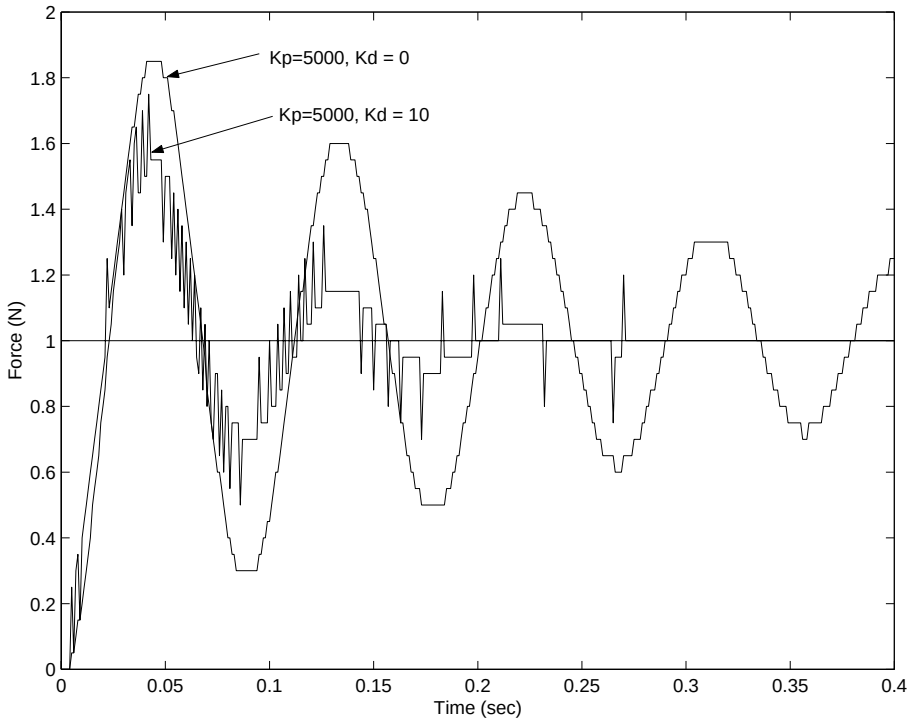

Figure 4-4. Effect of virtual damping, K_d, on system response

4.5.2. Stick-slip and sliding

"Stick-slip" is the term used by Bowden and Tabor (1956) to describe the regime in which a frictional interface is transitioning between being stuck and sliding. Stick-slip is characterized by the friction force oscillating between its static value and a lower kinetic value. As described by Bhushan (1999), "During the stick phase, the friction force builds up to a certain value, and once a large enough force has been applied to overcome the static friction force, slip occurs at the interface."

The stick-slip effect is simulated in our rendering by exploiting the fact that the transition from STUCK to SLIDING depends on force, but the transition from SLIDING back to STUCK depends on velocity (These switching criteria are implemented with '`if`' statements as shown in Table4-1, " Algorithm for rendering Karnopp Friction.," on page 54). There are two factors that affect the stick-slip behavior in our friction rendering. The first is the static friction limit, F_s. Stick-slip will not occur unless the static friction value,F_s, is

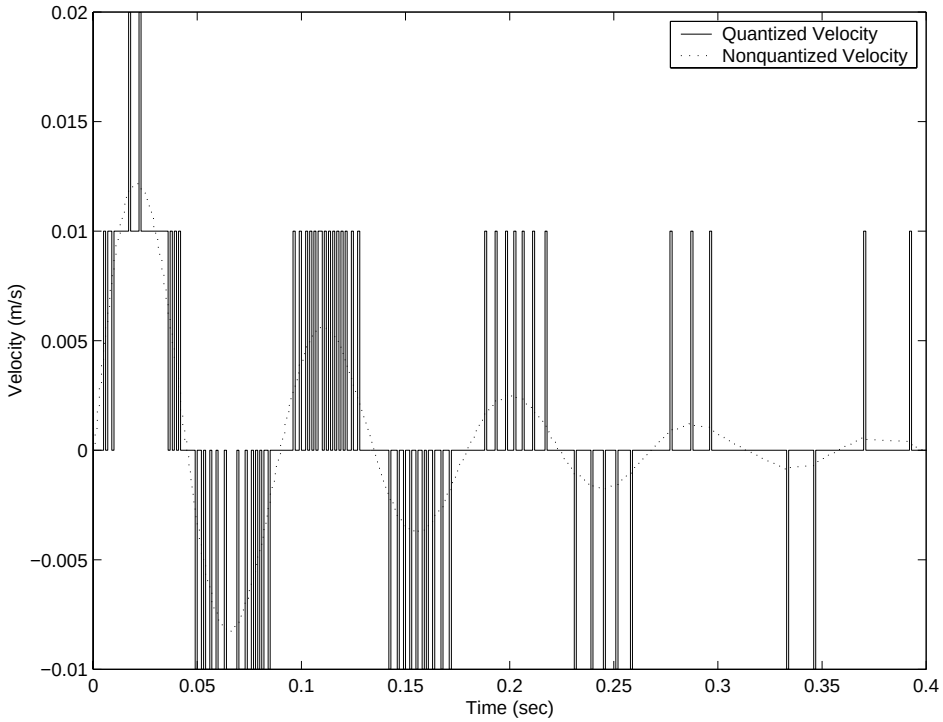

Figure 4-5. Examples of quantized and nonquantized velocity signal.

greater than the dynamic friction value, F_d. The larger the difference between F_s and F_d, the larger the amplitude of the stick-slip cycle. The stick-slip cycle continues as long as the applied force is greater than F_s, and the velocity is less than DV. Recall that DV is a velocity threshold below which the system is considered to be in the stuck state. DV is the second factor that affects stick-slip behavior. A larger value of DV means that stick-slip will occur over a large range of velocities. Once the system velocity is greater than DV, the system enters the sliding state. Figure4-8 shows how changes in DV affect the duration of the stick-slip regime, and Figure4-9 provides a magnified view of the stick-slip regime. Initially, as applied force is increased, the friction force matches the applied force. Once the applied force reaches F_s, the static friction limit, break-away occurs and the system begins to slide. However, if the velocity is low, (lower than DV) the system will immediately return to the STUCK state. The value of friction will oscillate each time step between F_s and F_d until the system has reached a sufficient velocity for stick-slip to cease. A similar effect

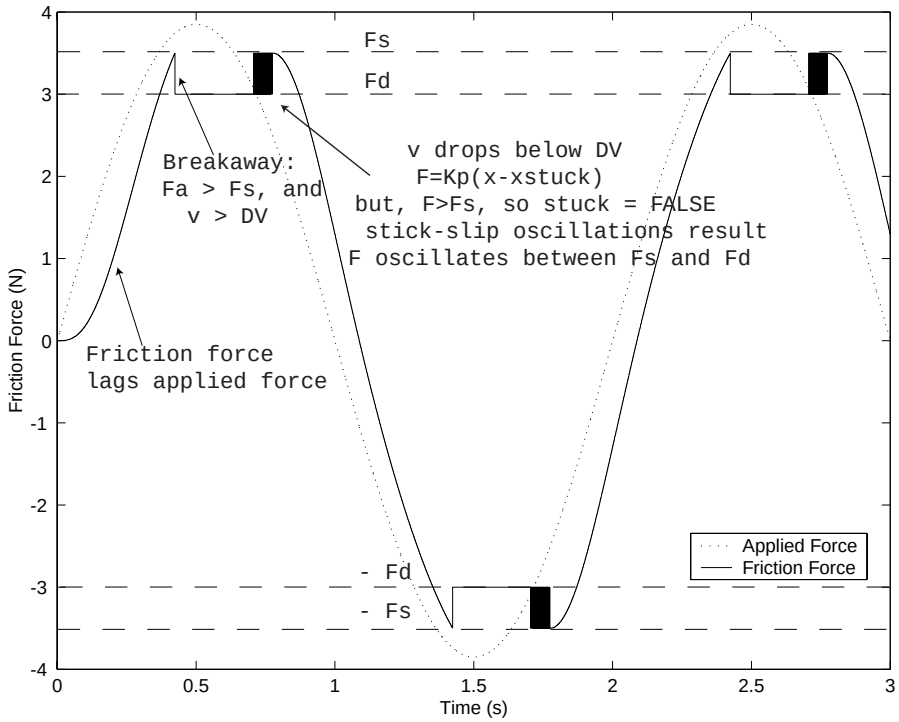

Figure 4-6. Applied Force, F_a, and Friction Force, F_f, plotted against time (K_p = 120).

can occur as the system slows. As the system transitions from SLIDING back to STUCK the friction force will oscillate as it settles to match the new level of applied force.

4.5.3. Free Motion

The third region of interest is free motion. Free motion refers to how the system will behave when the applied force goes to zero. Of particular interest is how the system settles to zero velocity. By selecting K_p to be below the stability limit, we are assured that the system will settle to zero velocity in the STUCK state in the absence of any applied force. We are not sure, however, that the system will even enter the STUCK state if the system was inititally sliding. Consider the case in which the system is traveling at some non-zero velocity that is greater in magnitude than the velocity threshold *DV*. In the absence of any applied force, the friction force will act to reduce the magnitude of the velocity. It is possible in this situation for system's velocity to change sign between sample periods. If this happens, the sign of the friction force will change and the system will be pushed in the

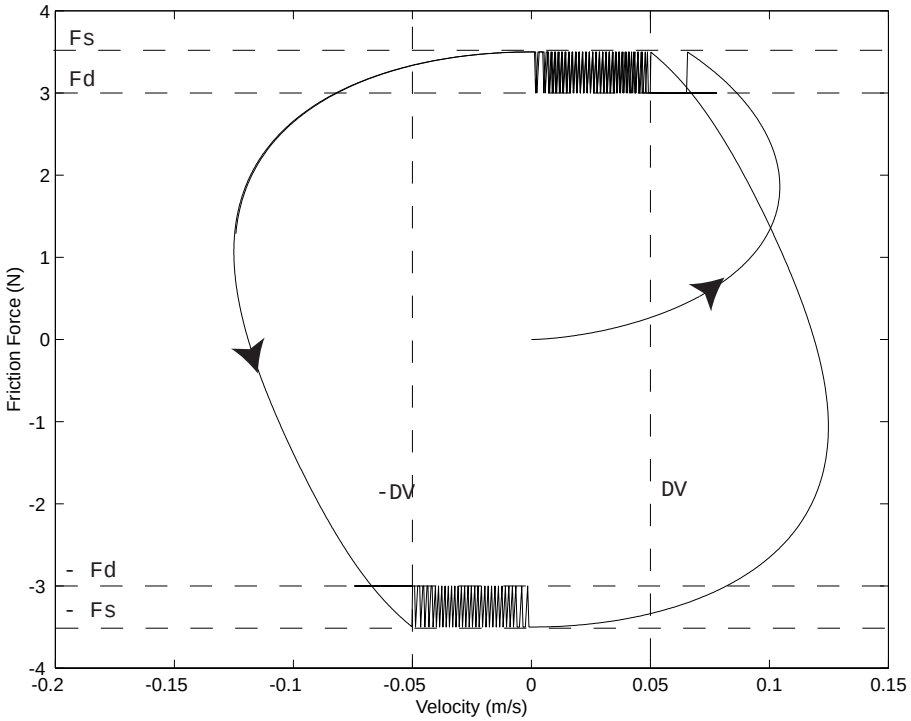

Figure 4-7. Friction force versus velocity (K_p = 120). If K_p is too low, then $v > DV$ even in the STUCK region.

opposition direction. If the magnitude of the new negative velocity is still greater than *DV* the system has entered a limit cycle. The velocity will oscillate between positive and negative values without tending toward zero. The friction force will also oscillate between $\pm F_d$.

One common method used to avoid this limit cycle in friction simulations is to dedicate a routine to detecting "zero-crossings" and then to modify the friction force accordingly. The *DV* parameter in the Karnopp model eliminates the need to detect zero crossings. If *DV* is sufficiently large, then as the system's velocity crosses zero, it will still be within the bounds of *DV* and will therefore enter the STUCK state. If *DV* is too small, the limit cycle can begin. For a given velocity threshold, *DV*, we can calculate the maximum value of dynamic friction that can be simulated. We begin with the equation that defines the system velocity at time step *k*

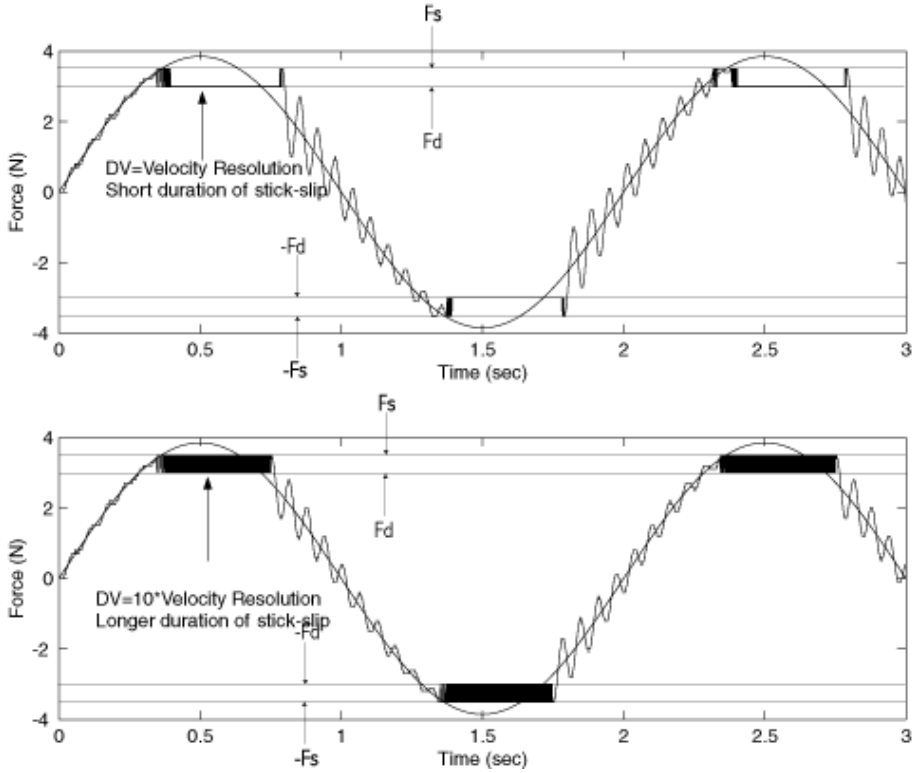

Figure 4-8. Effect of *DV* on the duration of the stick-slip regime.

$$v(k) = \frac{F_n}{b} + \left(v(k-1) - \frac{F_n}{b}\right)e^{(-T/\tau)} \tag{4.20}$$

Note that in free motion there is no applied force so $F_n = F_d$. The only force acting on the system is the dynamic friction force. Next note that for the limit cycle condition to exist *v(k)* must equal *–v(k-1)*. Assuming that the initial velocity, *v(k-1)* is just equal to *DV* and-setting *v(k) = -DV*, we can solve for F_d to obtain

$$F_d = \frac{-bDV(1 + e^{(-T/\tau)})}{(1 - e^{(-T/\tau)})} \tag{4.21}$$

Equation 4.21 is the upper limit on the level of dynamic friction that may be simulated for a given *DV* without the system entering the zero-crossing limit cycle.

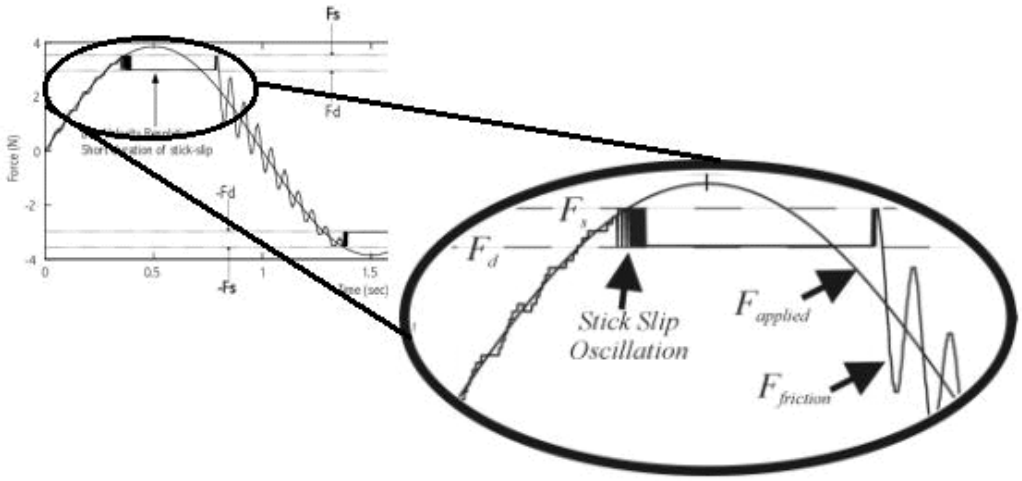

Figure 4-9. Detail of stick-slip regime

4.5.4. Simulation Results

The ultimate goal of the simulation was to find a set of parameters that yields a good representation of the Karnopp friction model when used in conjuction with our haptic interface. To that end, we now present simulation results that show the friction versus velocity curve for a specific set of parameters. The final parameters used to generate Figure4-10 are K_p = 10000 N/m, DV = 0.02m/s = 2*(velocity resolution) = 2*(encoder resolution)/T, F_s= 3.5, and F_d = 3. As can be seen, these parameters allow for a nice representation of the Karnopp model. There is a small region around zero velocity in which the friction force takes on a range of values. The range of possible values is bounded by the static friction limit. The narrowness of the vertical portion of this curve is indicative of the quality with which the fricition force is able to match the applied force. The better the friction force and applied force match, the lower the velocities in the STUCK state. Lower values of K_p, result in poorer matching of the applied force and friction force, and therefore lead to a wider range of velocites in the STUCK state.

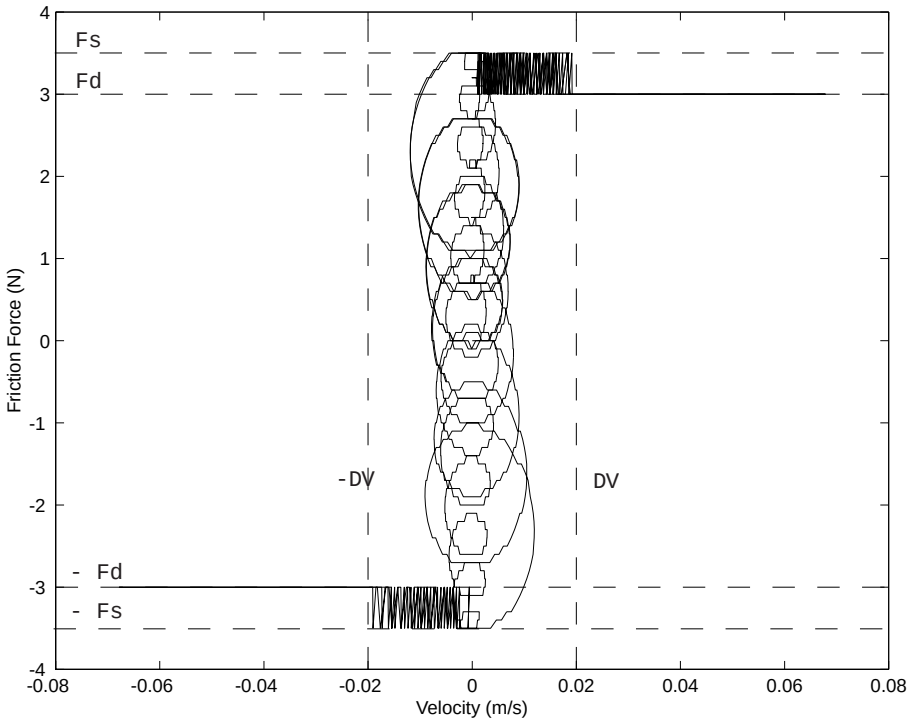

Figure 4-10. A haptic rendering of the Karnopp Model with tuned parameters. The oscillations in the central portion of the figure are due to K_p. (See the upper curve in Figure 4-8)

As the velocity begins the increase, stick-slip is observed. In the stick-slip regime we see the friction fluctuating between F_s and F_d as is expected and desired. Finally at relatively large velocities, the system enters pure sliding and the frictional force is constant.

Thus far we have discussed how to simulate the friction force between two mating surfaces. While discussing friction identification, we found that friction measurements were complicated by inertia. To provide a more realisitc sense of an object sliding across a surface with friction, we must render not only the friction between the object and the surface, but the inertia of the object as well. To add inertial forces, as well as other properties to the virtual environment we are simulating, we will introduce the virtual coupling.

4.6. The Virtual Coupling

In our virtual simulation, we wish to simulate the inertial and frictional forces of a block as it slides. We could choose to simulate the mass of the block with an impedance (where acceleration is the input variable and force is the output variable) or with an admittance (where force is the input variable and acceleration is the output). To simulate the inertia of the block using impedance causality, we would need an estimate of the user's input acceleration. This is unfortunate as accurate acceleration estimates can be difficult to attain. Digital encoders provide reasonable position sensing but introduce errors when the position signal is differentiated to obtain velocity or acceleration estimates. Accelerometers are also prone to errors due to drift and noise. To simulate the inertia of the block using admittance causality, we would need to know the force being applied to the block. While force sensors are often used successfully in control situations, simulation of admittance causality is best suited for haptic interfaces that are not backdrivable.

What then is an effective way of simulating both inertial and frictional forces with a haptic interface? By using a virtual coupling (Adams and Hannaford 1999; Colgate et al. 1995) we are able to effectively simulate both the friction and inertia of the block without estimating either the user's input acceleration or the user's input force. The virtual coupling

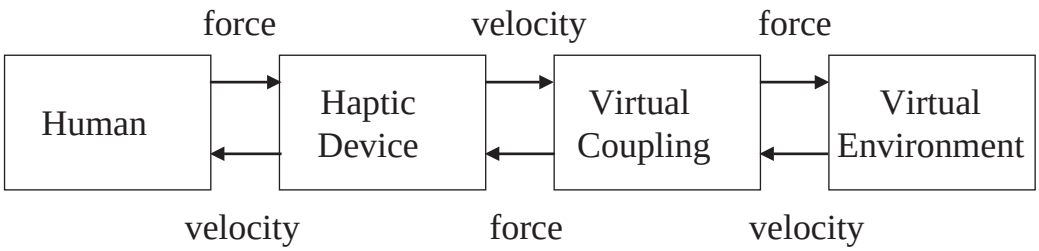

Figure 4-11. The virtual coupling (block diagram adapted from Adams and Hannaford (2000))

is similar to the virtual spring described in section Section4.2.4 that coupled the virtual proxy to the finger.

A block diagram is helpful in explaining the functionality of the virtual coupling (See Figure 4-11). It connects the physical haptic device (which in our case has an impedance causality) to the virtual environment (presented with admittance causality.) For friction rendering, we used a virtual coupling that consisted of a virtual spring and dashpot.

The algorithm for rendering friction and inertia with a virtual coupling is only slightly different than the one explained in Table4-1. Figure4-12 shows the difference between rendering friction with and without the virtual coupling. With the virtual coupling, the stiffness K subsumes the K_p that was needed previously to render the STUCK state.The algo-

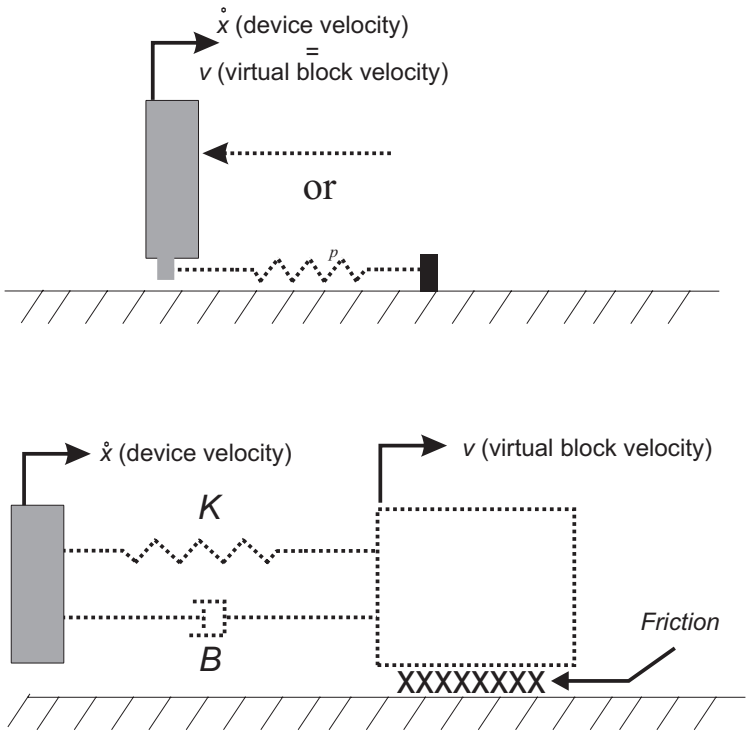

Figure 4-12. Schematic of a sliding block with friction rendered a)without a virtual coupling and b) with a virtual coupling.

rithm for rendering with the virtual coupling proceeds as follows. Once each time step the following actions are taken:

- Obtain position and velocity of the haptic interface.

- Calculate the friction force and state of the block based on previous state and velocity of the block.
- Calculate the net force being applied to the block based on force in the virtual coupling and the frictional force.
- Calculate the block's acceleration based on the applied force and the block's mass, M

$$a = \frac{F_a - F_f}{M} \tag{4.22}$$

- Integrate to find the block's velocity and position

$$\begin{aligned} v &= \int a\,dt + v_0 \\ p &= \int v\,dt + p_0 \end{aligned} \tag{4.23}$$

- Calculate the force in the virtual coupling

$$F_{vc} = K_{vc}(x - p) + B_{vc}(\dot{x} - v) \tag{4.24}$$

  where x is the position of the haptic device, and $\dot{x}$ is the velocity of the haptic device.

- Apply the force in the virtual coupling to the human operator.

There are several advantages to using the virtual coupling. First, because the friction force is depenent on the motion of a virtual block rather than the motion of of the haptic device itself, the position and velocity used to calculate the friction are no longer limited by sensor resolution and sample rate. Similarly, because the motion of the block is virtual, the block velocity can be set to be exactly zero in the STUCK state.

4.6.1. The design of the virtual coupling

Will a system with a virtual coupling enter a limit cycle while settling to zero velocity from free motion? The behavior of our system with a virtual coupling is in many ways quite similar to the system before the coupling was adding. The presence of the coupling provides added stability and facilitates the rendering of environments with richer dynamics than the environment with friction alone. With the virtual coupling, the virtual sliding mass

in our friction simulation is not rigidly connected to the haptic device, but rather is connected to it through a spring and damper. If the human becomes stationary, holding the device velocity to zero, it is possible for the mass to continue to oscillate around zero velocity in an manner similar to the zero crossing oscillation described in the previous section.

From symmetry, it is not difficult to observe that the system will enter a limit cycling condition when the position and velocity at time step *k, t(k)* are equal in magnitude and opposite in sign to the position and velocity at time step *k+1, t(k+1).*

The acceleration of the block, *a*, at any time is found by summing the forces acting upon it.

$$a = \frac{F_f - Kp - Bv}{M} \tag{4.25}$$

where F_f is the dynamic value of the friction, $\text{sgn}(v)F_d$, in this case, K is the virtual coupling stiffness, B is the virtual coupling damping, M is the mass of the sliding block p is the block's position and v is the block's velocity. Recall that x and $\dot{x}$ are zero when the human holds the haptic device stationary.

The block's velocity and position are found by integrating the acceleration with respect to time to obtain:

$$v = v_0 + \int a dt \tag{4.26}$$

$$x = x_0 + \int v dt = x_0 + \int (vo + \int a dt) \tag{4.27}$$

The discrete time value of the accleration at time step k can be expressed as:

$$a(k) = \frac{\text{sgn}(v(k-1))F(k) - Kp(k-1) - Bv(k-1)}{M} \tag{4.28}$$

If a standard digital computer intergation scheme such as Euler's method is employed, the velocity is expressed as:

$$v(k) = v(k-1) + a(k)T \tag{4.29}$$

$$v(k) = v(k-1) + \left(\frac{\text{sgn}(v(k-1))F(k) - Kp(k-1) - Bv(k-1)}{M}\right)T \quad (4.30)$$

and the postion is expressed as

$$p(k) = p(k-1) + v(k)T \quad (4.31)$$

$$p(k) = p(k-1) + \left(v(k-1) + \left(\frac{\text{sgn}(v(k-1))F(k) - Kp(k-1) - Bv(k-1)}{M}\right)T\right)T \quad (4.32)$$

Now applying our limit cycle criteria $v(k) = -v(k-1) = v$, and $p(k) = -p(k-1) = p$, and assuming that sgn($v(n-1)$) = -1 we can simplify Equations 4.30 and 4.32.

$$v = \left(\frac{-F - Kp - Bv}{2M}\right)T \quad (4.33)$$

$$xp = \frac{v - \left(\frac{-F - Kp - Bv}{M}\right)T}{2} \quad (4.34)$$

Solving the set of Equations 4.33 and 4.34 simultaneously we obtain two uncoupled equations for v and p.

$$v = \frac{-2FT}{KT^2 + 2BT - 4M} \quad (4.35)$$

$$p = \frac{-2FT^2}{KT^2 + 2BT - 4M} \quad (4.36)$$

Equation 4.35 gives the amplitude, in terms of velocity, of the zero-crossing limit cycle that can occur when the virtual coupling is used. Similarly, Equation4.36 gives the magnitude of the limit cycle in terms of position. It is worth noting that this analysis does not predict the occurance of a limit cycle if F, the value of the dynamic friction, is zero. Also, no limit cycle will exist for a continuous impleme ntation ($T \to 0$).

4.6.2. Interpretation of the virtual coupling analysis

Equations 4.35 and 4.36 can be quite useful to the designer of a haptic friction simulation. The question that arises for the designer of a haptic simulation is how to avoid exciting the

limit cycle. Alternatively, what parameter values cause the limit cycle to occur? Equations Equations 4.35 and 4.36 help answer these questions. The parameters of the limit cycle amplitude for both velocity and position are the dynamic friction value *F*, the sample period, *T*, the simulated mass, *M* and the virtual coupling stiffness and damping *K* and *B*. If, for example, the designer aims to simulate a mass of .5 kg sliding with a dynamic Coulomb friction value of 4N and is running the simulation with a sample period of .001s, then the virtual coupling parameter *K* and *B* remain to be determined. Once the parameters *F*, *M* and *T* have been selected the amplitude of the limit cyle will be a function of the *K* and *B*. It is possible to plot the surface representing the velocity limit cycle as a function of *K* and *B* (Figure 4-13)

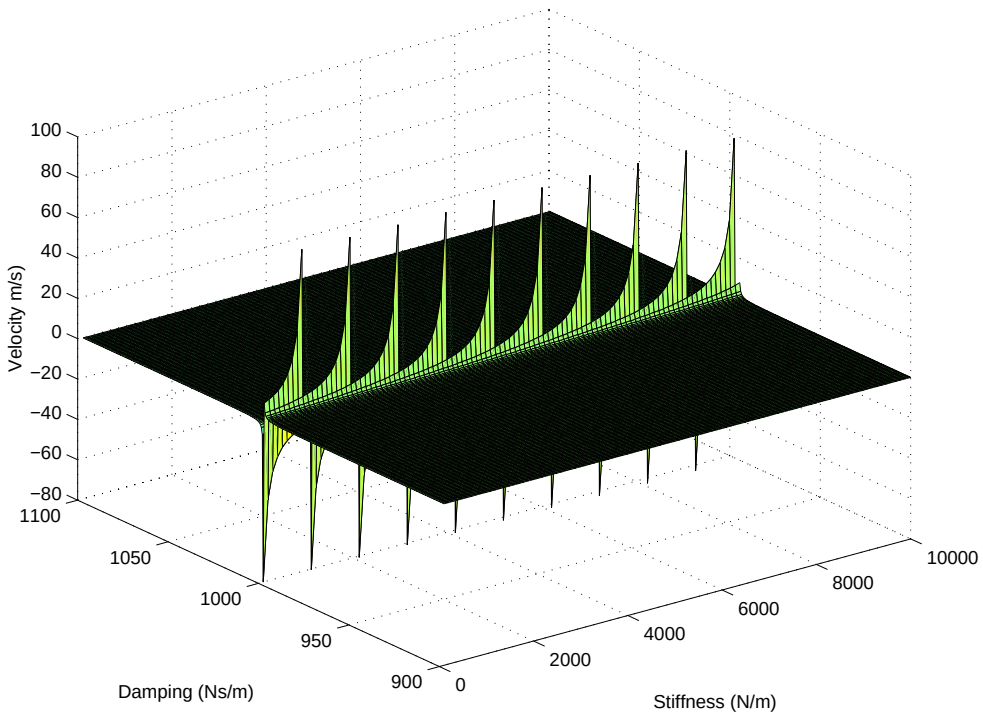

Figure 4-13. Surface representing amplitude (velocity) of the limit cycle as a function of vitural coupling stiffness, K, and damping B.

A similar surface exists for position. From the surface, we see that for some values of *K* and *B*, away from the singularies, the limit cycle amplitude is quite small. There are however values of *K* and *B* that case the denominators of Equations 4.35 and 4.36 to be zero

resulting in the aformentioned singularities. Figure4-14 highlights the singularites. The upper portion of the figure is a cross section of the surface with *K* held constant at 10000N/m. The lower portion of the figure is a cross section of the surface with *B* held at 995 Ns/m.

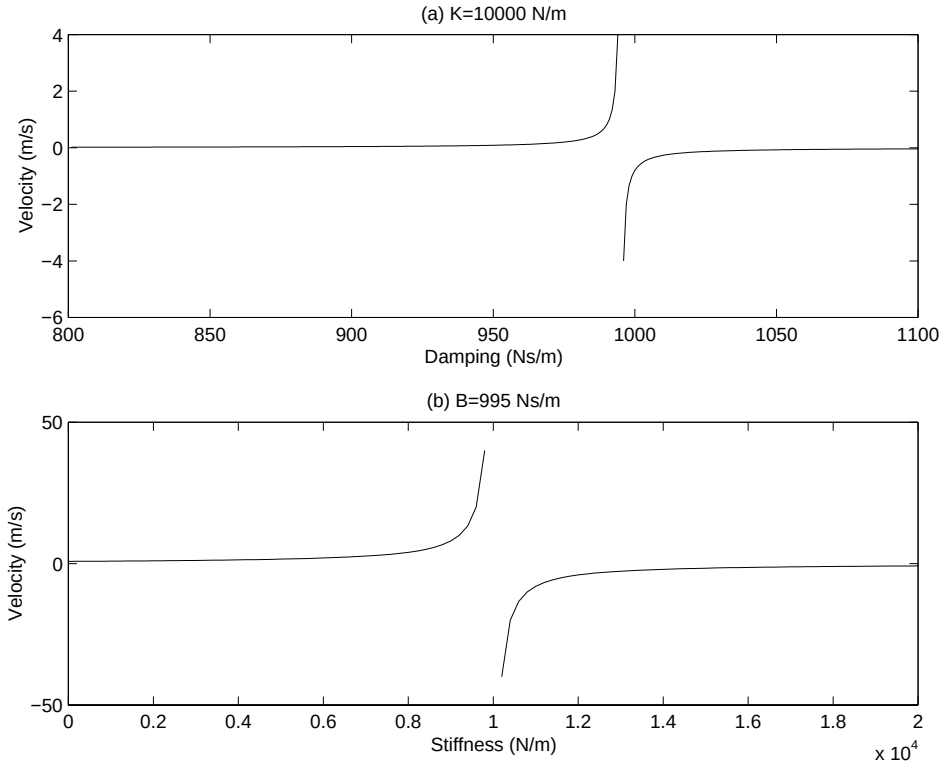

Figure 4-14. Cross section of the limit cycle surface for K=10,000 N/m (upper plot) and B= 995Ns/m (lower plot)

The designer's degree of freedom in the Karnopp model is *DV*. If *DV* is chosen so that it is greater then the critical velocity described by Equation4.35 then no limit cycle will occur. As an example of the effectiveness of the rendering haptic friction with the virtual coupling, Figure4-15 compares simulated friction and inertia against friction and inertia measured for aluminum sliding on Teflon.

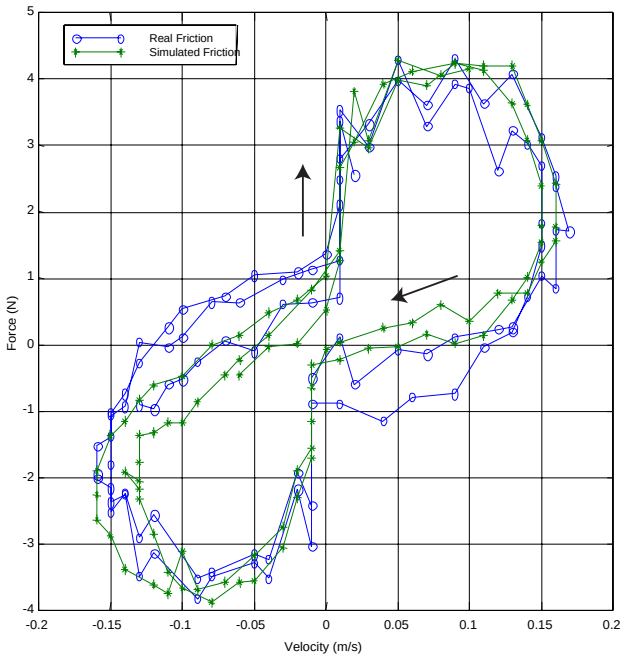

Figure 4-15. Force velocity plots of real fricton and simulated friction. These results are for Aluminum sliding on Teflon. The inertia of the system is 1kg and the friction force is roughly 2N.

4.7. Conclusions

In this chapter we have discussed different strategies for the haptic rendering of friction. We have presented a new implementation of the Karnopp model applied to haptics. Simulation results show that once properly tuned, the Karnopp implentation is capable of representing several desirable feature of a friction model such as presliding displacement, stiction, and stick-slip. The Karnopp based friction rendering was analyzed to show how it behaves in three specific regimes. We have demonstrated that in the STUCK state, the stability of the model depends on the value of a control constant, K_p. If K_p is too large the system will be unstable. Furthermore, we have shown that if K_p is too small an unsatisfactory friction simulation will result.

We have shown how the transition to stick slip depends on F_s, F_d and DV, and that the large the value of DV, the great the opportunity for stick-slip to occur. The zero-crossing

limit cycle, can be avoided by carefully choosing the zero velocity threshold, *DV*, and the maximum level of dynamic friction to be simulated.

Finally we disscussed how the virtual coupling can improve the utility of a friction rendering by allowing other enviroment elements to be rendered in addition to friction. We analyzed the zero-crossing limit cycle with the virtual coupling and showed how it too can be avoided by careful selection of the virtual coupling stiffness, *K*, damping, and the zero velocity threshold *DV*.

Chapter 5

Perception and Psychophysics

This chapter presents the results of humans interacting haptically with real and virtual Coulomb friction. A series of tests explore the effects of various types of friction on human performance in a Fitts-style targeting task. The results indicate that haptically rendered friction affects subject performance in a manner quite similar to that of real physical friction. Furthermore, moderate low-stiction friction tends to improve subject performance both in terms of speed and accuracy. High-stiction friction, however, degrades subjects performance, especially in terms of speed.

Subjects were also tested to determine the level of friction discrimination. The goal of these tests was to estimate the Just Noticeable Difference (JND) for differing levels of kinetic friction and differing levels of static friction.

5.1. Introduction

As mentioned previously, friction is present to some degree in all mechanisms; nevertheless, it is often absent or greatly simplified in virtual simulations of mechanisms. The presence of friction undoubtedly introduces complications into mechanical systems. A mechanism with high friction will require more energy to operate and will therefore be less efficient. Stiction, friction in which the static value is higher than the kinetic value, is often the bane of controls engineers. In servo-systems using integral control, friction can cause the system to “hunt” for its goal position. There are however some benefits associated with

friction. Because friction dissipates energy, it tends to have a stabilizing effect similar to that of viscous damping.

How does the presence or absence of friction in virtual simulations affect the user of a haptic interface? More specifically, how does friction affect human performance in positioning or targeting tasks? Also of interest is a human's ability to distinguish between varying levels of friction. Can humans discriminate between small changes in static or kinetic friction? To answer these questions, we have implemented a haptic rendering of a block sliding along a surface with friction interacting between the two. The design of our apparatus is such that we can easily switch between real and simulated friction. The implementation allows us to change the mass of the sliding block as well as the friction model parameters, such as the level of the static friction, the level of the kinetic friction and a viscous damping coefficient. The friction model used for this work is based on the model developed by Karnopp (1985) and discussed in Chapter 4.

After completing our haptic rendering of friction, we conducted two sets of human subject tests. Designed to examine the effect of friction on subject performance in a targeting task, the first set of tests used a method similar to the one used by Fitts (1954). Subjects moved between targets of various sizes and spaced at various distances. We examined changes in subjects' task completion times, error rates, and average error magnitudes as they moved a cursor through a virtual environment with various types of frictional resistance. We present results of subject performance as they acquired targets in environments with real physical friction, and various types of haptically rendered friction. In the second set of tests, we examined humans' ability to detect small changes in either the level of static friction or the level of both the static and kinetic friction.

5.2. Experimental Apparatus

The apparatus used for this work is the same as the one used by Richard et al.(1999) for friction identification and described in Chapter 3. It is shown in Figure5-1. It was modified by the addition of a mouse shell riding on a low-friction translational bearing. A wrist rest

around the base of the mouse prevented subjects from dragging their fingers along the apparatus structure in order to generate more friction as they performed the task. Because of the wrist rest, subject motion was generated more from the elbow and shoulder than it is on a standard computer mouse.

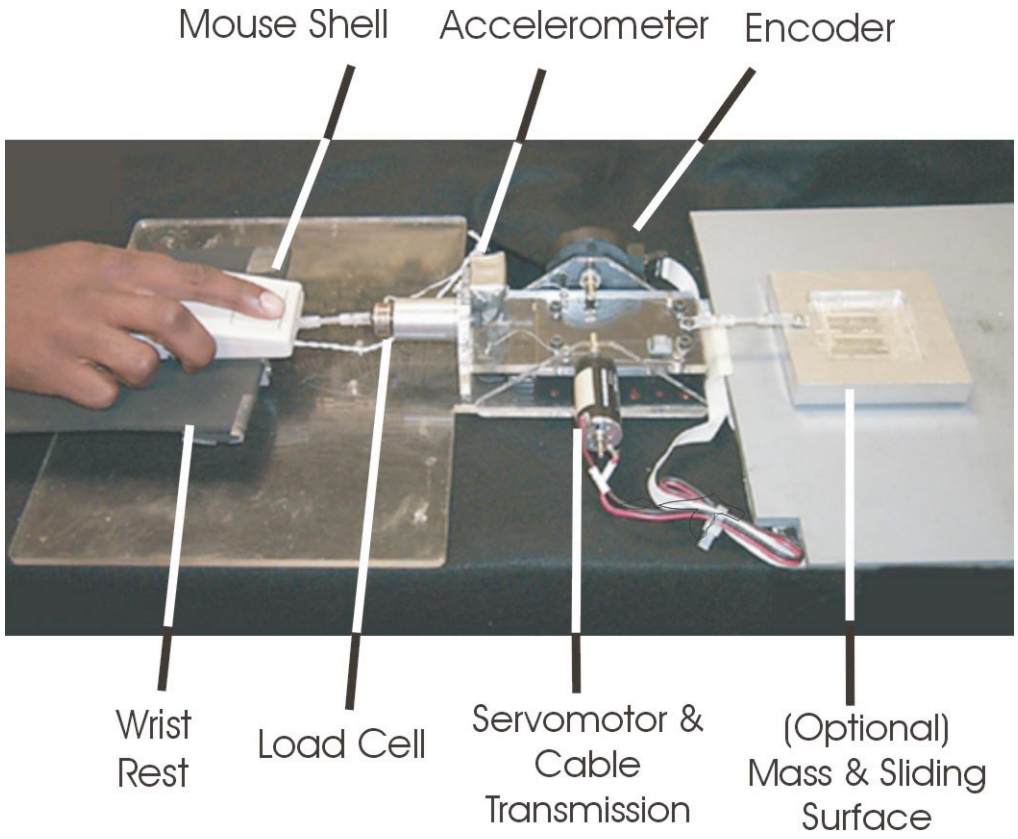

Figure 5-1. Experimental Apparatus for Perception Experiments

5.3. Experiment Descriptions

5.3.1. Fitts-Type Targeting Task

In a targeting task, the user of a haptic interface is required to acquire a target by moving a cursor to the location of the target and pressing a button or pulling a trigger. How does the presence or absence of friction, either in the mechanism itself or in the virtual environment, affect a user's performance in a targeting task? The answer to this question may

depend on many factors. For example, one might expect a moderate amount of friction to be helpful. It may dampen a subject's involuntary hand movements and help him or her acquire a target more quickly. Conversely, the presence of significant friction may actually slow a subject; more work and larger muscle forces are required to move the system when large amounts of friction are present. Finally, if the value of static friction is significantly higher than the dynamic value of friction (a high stiction type of friction), we may expect a subject to have difficulty homing in on the target. High stiction may cause the subject to "hunt" around the target area much like a servo-system hunts around its goal position in the presence of stiction.

A targeting task is useful for comparing the effects of real versus virtual friction. Asking subjects to discriminate between real and virtual friction in a subjective manner (e.g. exploring two environments, one with real friction and one with virtual friction and asking subjects which is which) will nearly always favor the real friction over the virtual friction. It is too stringent a criterion on which to base the value of a haptic simulation. Humans are quite adept at exciting incipient instabilities in haptic simulations and at detecting subtle phenomena caused by sensor resolution and actuator limitations.

Rather than asking subjects to compare a real friction and virtual friction directly, we present them with a targeting task, the idea being that the task at hand will mask any irrelevant shortcomings of the simulation and provide a comparison of the real and virtual phenomena under the context of the task. If the subjects' performance with simulated friction is similar to their performance with real friction, we can infer at a minimum, that the virtual friction similarly affects the user's performance for the task of interest. In fact, subjects did comment that the real and simulated friction were very close.

To determine how the presence of Coulomb friction affects a user's performance in a targeting task, and to compare the effects of real friction and simulated friction in an objective manner, we conducted a series of Fitts-type targeting tasks (Fitts 1954). In a Fitts test, subjects are required move back and forth between two targets in rapid succession. Fitts defines the index difficulty, I_d , for a targeting task as:

$$I_d = -\log_2 \frac{W_s}{2A} \qquad (5.1)$$
$$W_s = W - D$$

where A is the distance between the targets; W is the width of the targets and D is the diameter of the cursor.The concept is that a targeting task becomes more difficult as either the amplitude of the required motion becomes larger (A increases) or as the required accuracy increases (W_s decreases).

For our friction-based Fitts tests, subjects were instructed to move a cursor vertically on the screen by manipulating the computer mouse attached to the experimental apparatus. Their task was to move the cursor back and forth between two colored regions on the screen (See Figure5-2).

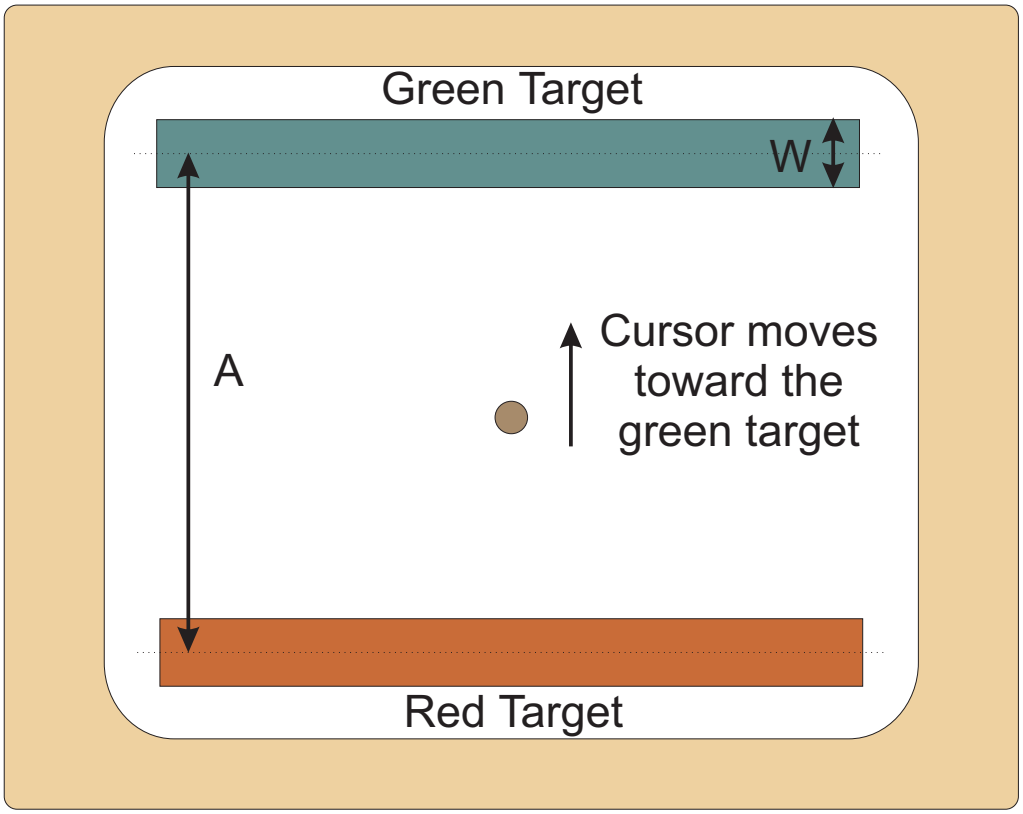

Figure 5-2. Screen seen by subjects during the Fitts test.

They were instructed to click the mouse button once the cursor was completely within the bounds of the green region. If subject clicked the mouse button with the cursor completely within the bounds of the green region, a valid click was registered, the green target would turn red, and the red target would become green. If the subject clicked the mouse button while the cursor was not within the bounds of the green target, an error click was recorded. After making a valid click, the subject would then proceed to the new green target and click the mouse button. Eight valid clicks were required to complete one segment of the Fitts test. Subjects were asked to complete the task as quickly as possible.

Twenty right-handed subjects (10 male and 10 female) participated in this experiment. Each subject completed 45 batches of Fitts tests. The 45 batches included 9 different indices of difficulty (see Table 5-1) and five variations of frictional resistance to the subjects motion (see Table 5-2). Before beginning the experiment subjects practiced the baseline test, and the test with real friction added to the system (an aluminum block sliding on a rubber pad). After practicing, subjects began the experiment by completing nine batches of Fitts tests with the baseline resistance. Subjects completed nine batches of the remaining four resistances (real friction, simulation, high stiction, and viscous damping) in random order. In each case the order of the batches was also presented in random order. After each batch, we recorded the subject's completion time, number of errors, and average error magnitude (in millimeters).

5.3.2. Forced Choice Tests

In addition to our studies of how friction improves or degrades human task performance, we are also interested in learning about human friction perception in general. Perception, in this context, refers to both a human's ability to detect the presence of friction and a human's ability to discern between two frictional stimuli that vary in some subtle way. Recent research has focused on measuring humans ability to discern between various level of virtual haptic stimuli such as force, velocity, compliance and viscosity (Jones and I.W. 1990; Jones and I.W. 1993; Millman and Colgate 1995; Tan et al. 1995). Along a similar vein, Lawrence et al. (98) outlined a procedure for measuring the human perception of

Table 5-1. Indices of difficulty for Fitts test

Batch	*A, pixels(mm)*	W_s *pixels(mm)*	I_d
1	228(342)	12(18)	5.25
2	228(342)	40(60)	3.51
3	228(342)	68(102)	2.75
4	300(450)	12(18)	5.64
5	300(450)	40(60)	3.91
6	300(450)	68(102)	3.14
7	380(570)	12(18)	5.98
8	380(570)	40(60)	4.25
9	380(570)	68(102)	3.48

Table 5-2. Frictional resistances used for the Fitts test

	Resistance	Description
1	Baseline	No frictional resistance is added. Subjects interact only with the friction (approx. 0.8N) and mass (approx. 1.4kg) inherent in the haptic interface
2	Real Friction	A 0.5kg block of aluminum sliding on a rubber pad. (Friction Force is approx 3.5N)
3	Simulated Friction	A simulated level of friction that approximately matches case 2.
4	High Stiction	Similar to case 3 except that the value of static friction is set to a higher value (approx. 7.0N)
5	Viscous Damping	Subjects interact with virtual viscous damping of with a damping coefficient of approx. 35Ns/m and mass of 0.5 kg.

the friction inherent in a haptic interface rather than the friction rendered by a haptic interface.

Lawrence et al.(1998) were concerned with measuring the absolute threshold for human friction perception. Their goal was to develop a haptic system where the impedance of the interface itself (i.e. its inertia, friction and compliance) was transparent to the user. Because true physical transparency is not possible, perceptual transparency becomes the goal. The first step toward perceptual transparency of friction is finding the threshold below which humans can no longer perceive the presence of friction. Second, through care-

ful mechanical design and possibly with the aid of a friction-reducing controller, the interface in constructed so that the friction is below the requisite threshold.

We are interested in the perception of friction for a different reason. Our goal is to include virtual friction to our system in order to better emulate reality and to potentially improve human performance. We are more concerned with adding sufficient friction that the user be able to detect it. Since there will always be some inherent friction in the interface we are most interested in how humans apperceive changes in friction. There are many dimensions in which friction can be changed. To limit the scope of the problem will investigate human perception when static and kinetic friction change together and when static friction changes independent of the kinetic value of friction.

5.3.2.1. Basics of discrimination

Discrimination and detection are two of the four standard paradigms of psychophysics. (the other two, recognition and scaling, deal with a human's ability to organize stimuli into like categories and to assign magnitudes to stimuli respectively). The interested reader is referred to Millman (1995). The detection and discrimination paradigms are quite similar. Detection experiments find the absolute threshold for detectability while discrimination experiments find difference threshold for detectability. For example, a detection experiment may be used to find the minimum volume level necessary for humans to detect a pure tone signal. A discrimination experiment would seek to find the volume level difference necessary for subjects to distinguish tone A from tone B. The difference threshold is often referred to as the just-noticeable-difference, or JND.

5.3.2.2. Weber's Law

For a large number of stimuli, the JND is proportional to the stimulus intensity. A larger difference is necessary for subjects to distinguish between stimuli of larger intensities than for stimuli of smaller intensities. E. H. Weber (Weber 1834) first noted this phenomenon when conducting experiments to find the JND of weights. Weber found that two heavier weights had to have a larger difference in weight than two lighter weights in order

for a subject to perceive one the weights to be heavier than the other. Weber for the ratio of the JND to be linearly related to the stimulus intensity. Weber's law is stated as

$$\phi = c\Delta\phi$$

where ϕ is the stimulus intensity, $\Delta\phi$ is the JND and c is the constant of proportionality known as the Weber fraction. Weber's law has been shown to hold for a wide range of sensory modalities including the discrimination of the intensities of light, sound, pressure on the skin and electric shocks. (Heeger 1999).

5.3.2.3. Standard Methods for Measuring the JND

Because detection experiments are just a special case of discrimination experiments (in a detection experiment the stimulus has an intensity of zero), the procedures for finding both absolute thresholds and difference threshold are fundamentally the same. Essentially, subjects are presented with pairs of stimuli separated by either time or distance. Subjects are then asked to select, for example, the larger of the two stimuli. The difference in intensity of the stimuli is varied so that in some trials subjects will be unable to distinguish between the two while it other cases the distinction will be made quite easily. Several standard procedures exist for finding absolute and difference thresholds. Three of the more popular methods are: the method of limits, the method of adjustment and the method of constant stimuli.

5.3.2.4. Method of limits

The method of limits is perhaps the most popular method for estimating sensory thresholds (Millman 1995). It is popular because it is generally faster than the method of constant stimuli and more accurate than the method of adjustment. To find a difference threshold the experimenter presents the subject with series of stimulus pairs. Each pair includes the reference stimulus and a comparison stimulus. Subjects are asked whether the comparison stimulus is less than, equal to, or greater than the reference stimulus. Initially the comparison stimulus is much greater or much less then the reference stimulus. After the subject

responds, the intensity of the comparison stimulus is increased to decreased to bring it closer to the level of the reference. Eventually the subject will report that the pair of stimuli are equal. With continued adjustment in the same direction, the subject will, at some point, report that the comparison has become greater than or less than the reference. The difference threshold is taken to be the midpoint between the intensity level at which the subject reported a change from "greater than" to "equal to" and the intensity level where the subject reported a change from "equal to" to "less than."

The process is repeated several times. To help limit the effects of habituation (where the subject habitually gives the same report) and expectation (where the subject will response based on the expected arrival of a stimulus) the experimenter must be sure to vary the order (ascending versus descending) in which stimulus intensities are varied.

5.3.2.5. Method of adjustment

When the method of adjustment is used the subjects themselves adjust the intensity of the comparison stimulus until it matches the reference stimulus. Occasionally subjects adjust the comparison stimulus intensity so that is below the reference stimulus. At other times the comparison stimulus intensity is to a value above that of the reference. Typically several trials are conducted and the mean and variance of the subject response are reported as the difference threshold. Although this method can proceed rather quickly, it is not very accurate. Some experimenters like the method claiming that active subject participation helps to reduce boredom and apathy. Others dislike the method stating that it puts undue stress on the subjects.

5.3.2.6. Method of constant stimuli

In the method of constant stimuli, a set of predetermined comparison stimuli is used. Half of the comparison stimuli have intensity greater than the reference stimulus and half have intensity less than the reference. The subject is presented a stimulus pair consisting of the reference stimulus and a comparison stimulus. The subject is then asked to indicate if the comparison stimulus is different than the reference. Each pair is presented to all sub-

jects multiple times. For some stimulus pairs, when the difference between the comparison stimulus and the reference stimulus is very small, subjects will almost never state that the pairs are different. For other stimulus pairs, when the difference between the comparison stimulus and the reference stimulus is relatively large, subjects will detect and report a difference nearly one hundred percent of the time. The JND or difference threshold is defined as the intensity level at which subjects detect a difference in the stimulus pairs fifty percent of the time.

5.3.2.7. Modified method of constant stimuli

For our friction perception experiments, we employed a modified version of the method of constant stimuli. During each trial subjects were presented with three friction renderings, a reference stimulus and two comparison stimuli. One of the comparison stimuli was identical to the reference stimulus. For the other comparison stimulus the static and/or the kinetic value of the friction was different. Subjects first explored the reference level of friction, the Baseline case, by moving the mouse shell forward and backward. When ready, subjects would click the mouse button and then explore the first comparison case, Case A. By clicking a second time, the subject could explore the second comparison case, Case B. Subsequent clicks would cycle the subject through the cases in the order Baseline, Case A, Case B and then back to the Baseline. Once the subjects had explored each case to his or her satisfaction, they were asked to report which case, A or B, was different than the Baseline case. If the subjects could not readily detect a difference, they were asked to make their best guess.

When the difference in the static and/or kinetic friction between Case A and Case B was very small, subjects were essentially guessing as to which one was different than the reference case. The chance of guessing correctly is fifty percent. When the difference between Case A and Case B was rather large, subjects could detect the difference nearly one hundred percent of the time. Between these two extremes, we expected to see subjects correctly discriminate between cases more often as the magnitude of the difference increased. Plotting the percent of correctly discriminated cases versus the difference in

stimulus intensity should result in the classic s-shaped curve observed in detection and discrimination experiments. By convention, the JND is defined as the difference in intensity that corresponds to seventy-five percent of the cases being correctly distinguished. Hypothetical data fit to an s-shaped psychometric function is shown in Figure5-3.

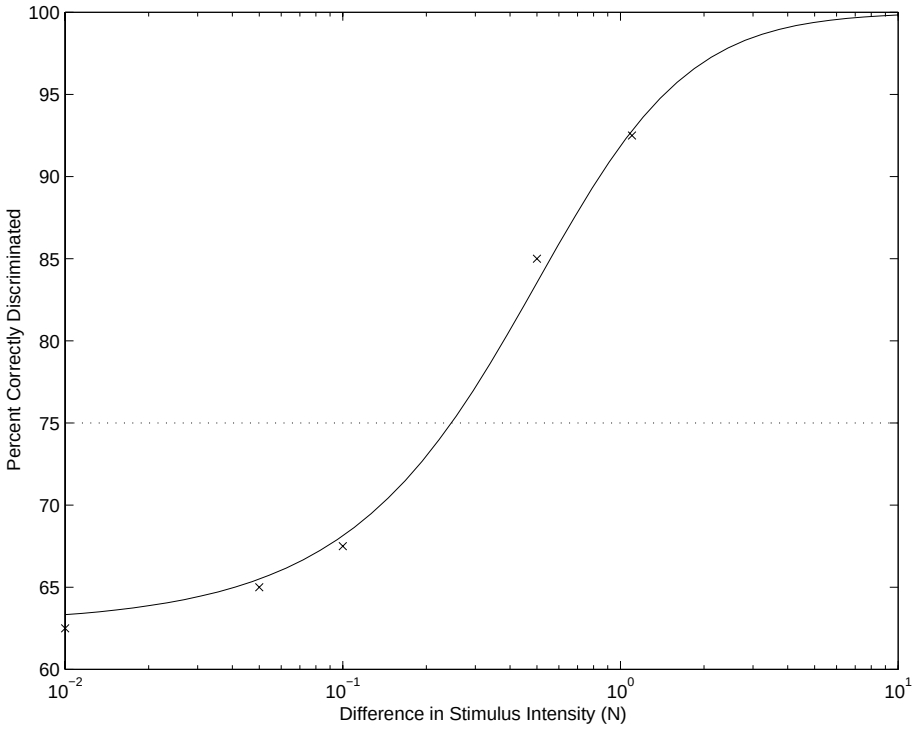

Figure 5-3. Hypothetical results of a difference threshold experiment

All friction rendering was done using the modified Karnopp model as described in Chapter 4. Every subject underwent three batches of experiments. Each batch contained two rounds of five different comparison stimuli for a total of ten experimental trials. The same reference stimuli were used in each trial. The parameters of the friction are listed in Table 5-3. Note that in the Baseline case, there is no stiction: the static friction and the kinetic friction are equal.

Table 5-3. Friction rendering parameters for the reference stimulus

Model Parameter	Value
F_s	2.0 (N)
F_d	2.0 (N)
b	20 (Ns/m)
DV	0.001 (m/s)
m	0.5 (kg)
K_{vc}	25000 (N/m)
B_{vc}	10 (Ns/m)

In experimental batch 1, subjects were asked to discern between the reference and both the static, F_s, and dynamic, F_d, friction parameters varied together. In all cases the friction was higher than in the reference case. Table 5-4 lists the values used for the 5 comparison stimuli.

Table 5-4. Parameter differences for Batch 1

	1	2	3	4	5
F_s	2.03	2.08	2.1	2.5	3.1
F_d	2.03	2.08	2.1	2.5	3.1

In experimental batch 2, subjects were asked to discern the effect of increasing static friction. The dynamic friction value remained the same as the reference case while the stiction increased.Table 5-5 lists the five comparison values used in Batch 2.

Table 5-5. Parameter differences for Batch 2

	1	2	3	4	5
F_s	2.2	2.6	3	3.5	4.0
F_d	2.0	2.0	2.0	2.0	2.0

Batch 3 is similar to batch 1 except in this batch the static and kinetic values are below those of the reference case. Table 5-6 shows the five comparison values used for Batch 3.

Table 5-6. Parameter differences for Batch 3

	1	2	3	4	5
F_s	1.95	1.9	1.8	1.5	1.0
F_d	1.95	1.9	1.8	1.5	1.0

5.4. Results

5.4.1. Forced Choice Test Results

We wish to examine the subjects' results on the Fitts test by comparing their performance on a given test with added friction with their performance on the same test under the baseline condition. For each index of difficulty and for all added resistances, we subtract the subjects' baseline performance on the same index. The results are a subject's time difference, difference in number of errors and difference in average error magnitude.

As is often the case when human subjects are involved, the person to person variability was high. For example, in some cases most of the subjects showed improvement in performance, but a few showed a decrease in performance. Average scores and variations were therefore not particularly instructive. Nonetheless, some clear qualitative trends can be seen in the data. These trends are best illustrated with the scatter plots in Figures 5-4 through 5-7.

Plotting the difference in error (either number of errors or error magnitude) versus the difference in time we obtain a graphical comparison of performance with added friction versus baseline performance. Figure 5-4 shows how one can interpret each quadrant of the error/time plane. Near the origin, the presence of added friction makes little difference in subject performance. In quadrant 1, added friction negatively impacts subject performance. Data in this quadrant indicates that the presence of friction caused subjects to perform more slowly and with less accuracy. Quadrant 3, on the other hand, indicates that the presence of added friction results in performance enhancement. Data in this quadrant indicate that friction helped the subject perform the task more quickly, and with fewer errors.

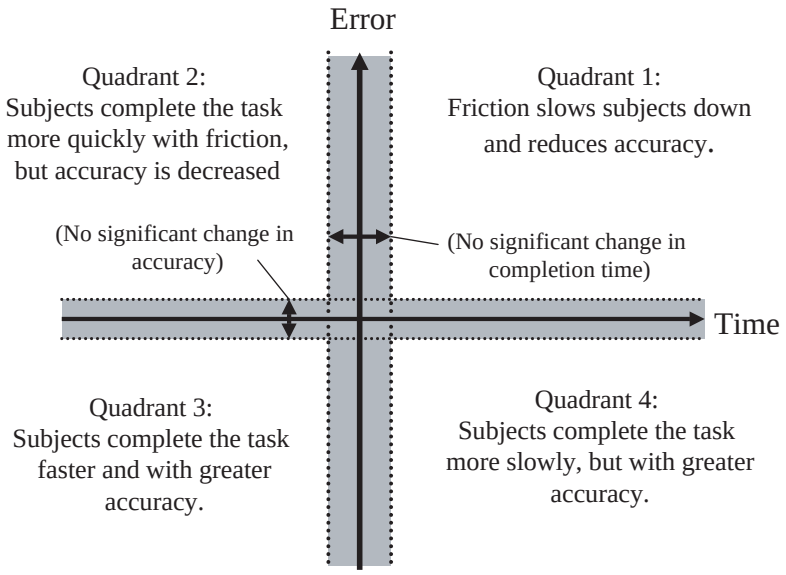

Figure 5-4. Possible effects of friction on subject performance.

Figures 5-5, 5-6, and 5-7 compare subjects' performance for the three most difficult indices of difficulty 1, 4, and 7. For index 1 (Figure5-5) we see a clustering of data points in quadrant 3. This indicates, that for this index, friction generally helps subjects perform the Fitts tests. Completion times were 17% faster for real friction and 23% faster for simulated friction. Subjects committed an average of 1.4 fewer errors for real friction and 2.8 fewer errors for simulated friction. There is however a small cluster of data points in quadrant 1. Most of these data represent high stiction cases.

For index 4 (Figure 5-6) we see more clustering in quadrant 1, and again this clustering is mostly due to the high stiction case. Subjects took 64% longer to complete index 4 and committed 1.35 more errors under the high stiction case.

For index 7 (Figure 5-7) we see most of the data clustered around the origin indicating that the presence or absence of friction has made little difference from a performance

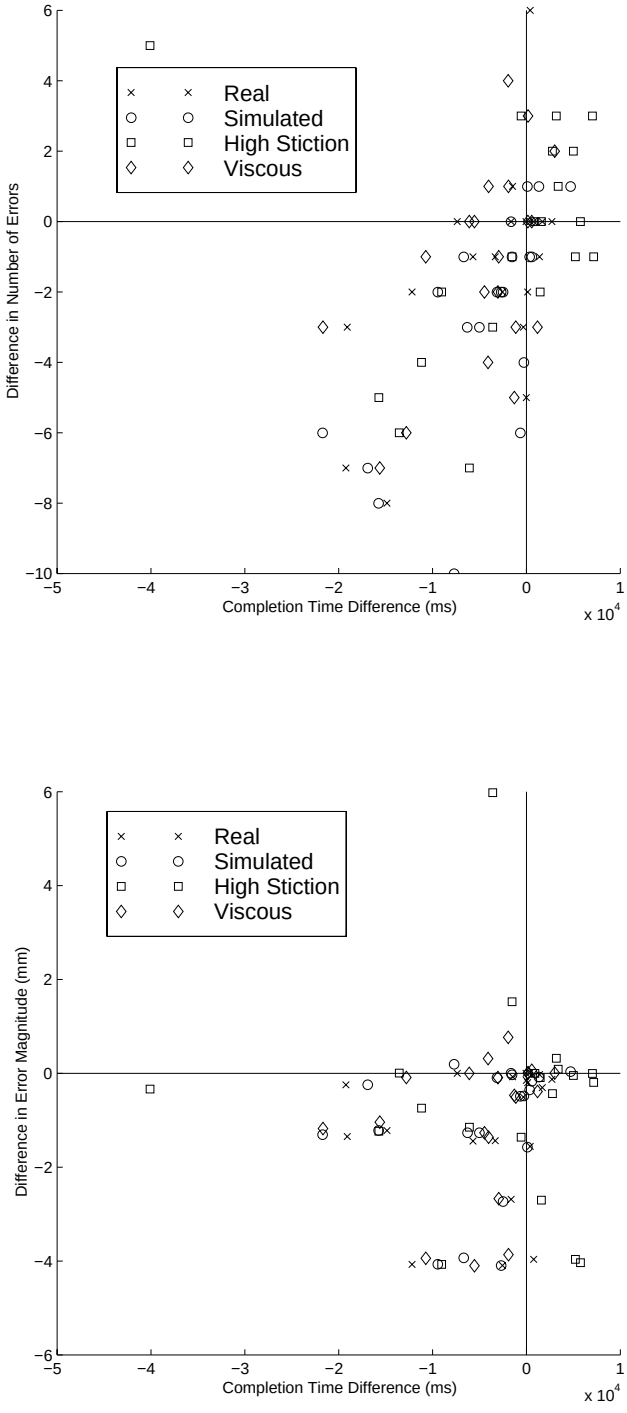

Figure 5-5. Subjects' performance relative to their baseline case for index of difficulty #1 (upper) Number of Errors versus Time (lower) Average Error Magnitude versus Time.

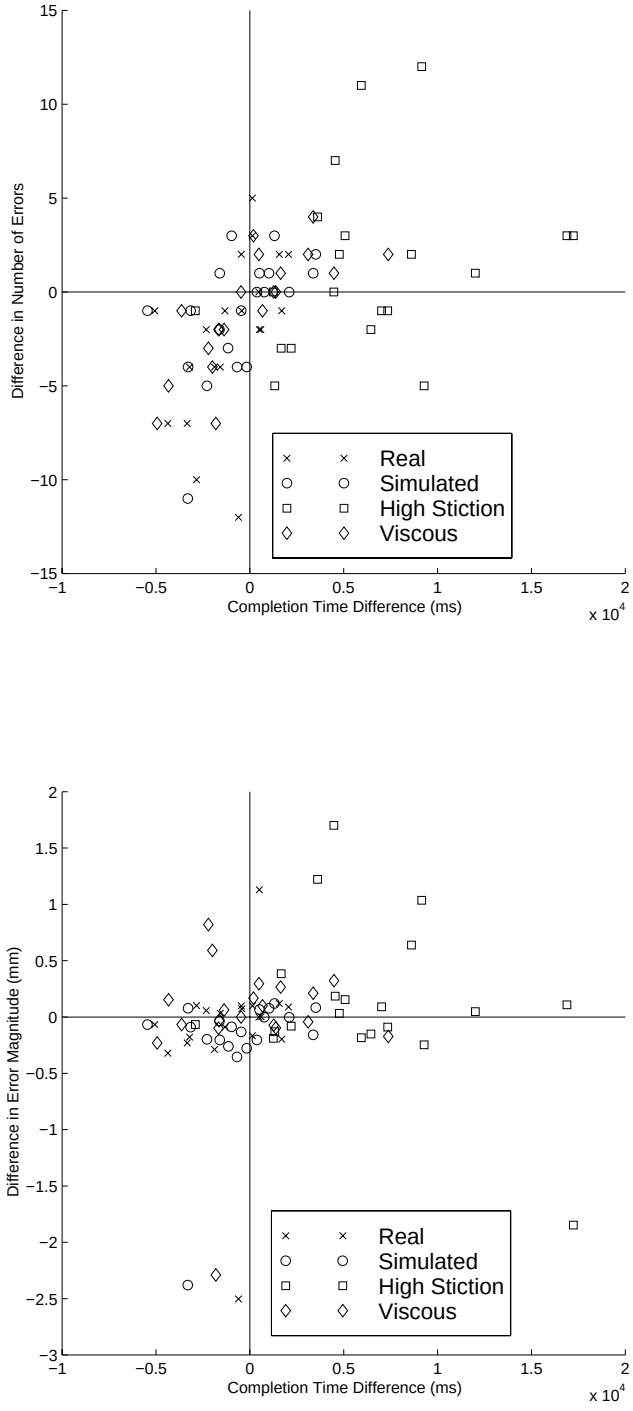

Figure 5-6. Subjects' performance relative to their baseline case for index of difficulty #4 (upper) Number of Errors versus Time (lower) Average Error Magnitude versus Time.

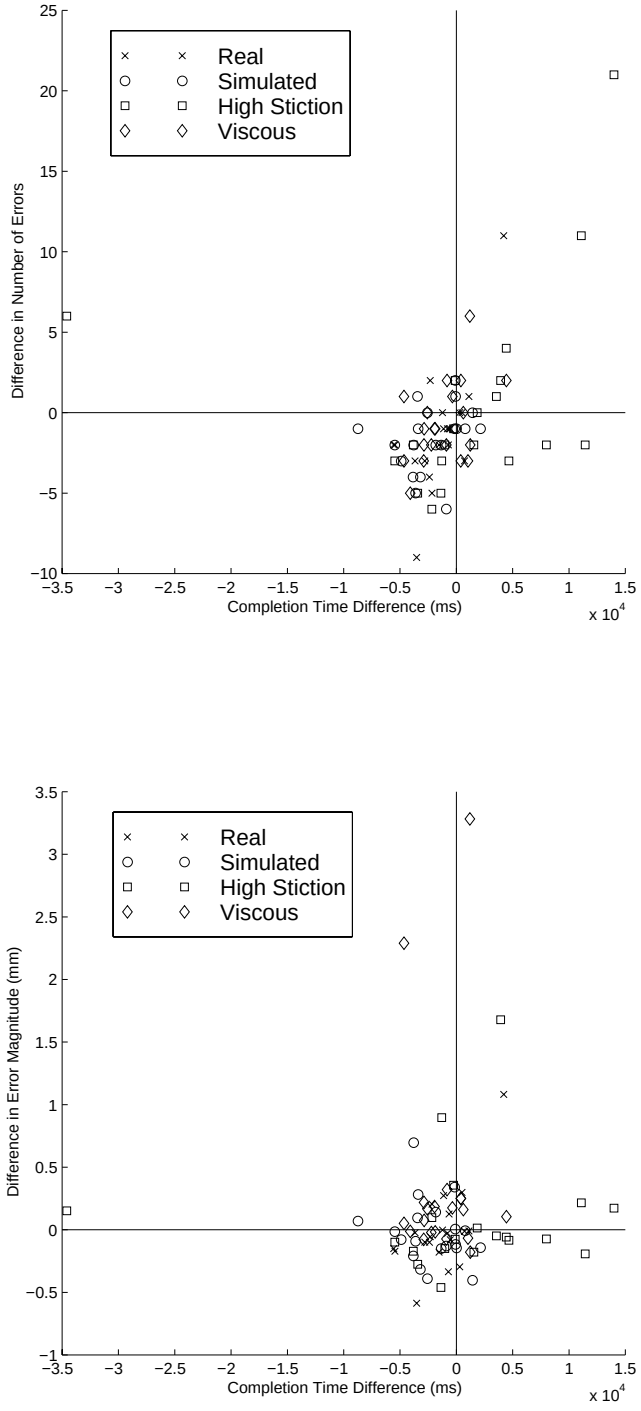

Figure 5-7. Subjects' performance relative to their baseline case for index of difficulty #1 (upper) Number of Errors versus Time (lower) Average Error Magnitude versus Time.

standpoint. We do see, however, some high stiction outliers in quadrant 1 as was the case in indices 1 and 4.

It is not surprising that the high stiction case degrades subjects' performance. As mentioned previously, high stiction can cause a servo-system to "hunt" about its goal position. A similar behavior was observed in several subjects as they attempted to location the cursor within the bounds the of the target. Figures 5-8 and 5-9 show the position trajectory for a subject completing index 4 under baseline conditions and under the high stiction case. In the high stiction case we see the subject repeatedly missing the target by overshooting while trying to adjust to the goal position. Because the static value of the friction is significantly higher than the dynamic value, subjects found that the amount of friction necessary to "break-away" was more than they wanted to accelerate the mass once it was free. Because of this overshooting and undershooting, we see that it takes the subject longer to complete each cycle of motion in the presence of stiction (compare the subject's seven target entries in Figure 5-8 with the three target entries in Figure 5-9 for the same 800 ms of time).

Tables 5-7, 5-8, and 5-9 show the number of subjects that performed better and worse than their base case. Performance improvement or degradation is based on task completion time, number of errors committed, and the average error magnitude. In terms of time, (Table 5-7), subjects were considered to have performed better if there completion time was more than 0.5sec faster than their baseline time. They were marked as performing worse if there time was more that 0.5 sec. slower than their baseline time. We see from the table that real and simulated performed worse in high stiction cases.

In terms of the number of errors committed (Table 5-8), subjects were considered to have improved if they committed at least 1 fewer error than the baseline case. They were marked worse if they committed as least one more error than they did on the baseline case.

For error magnitude (Table 5-9), subjects must have had an average error magnitude at least 1 mm smaller than their base case to register an improvement; if their average mag-

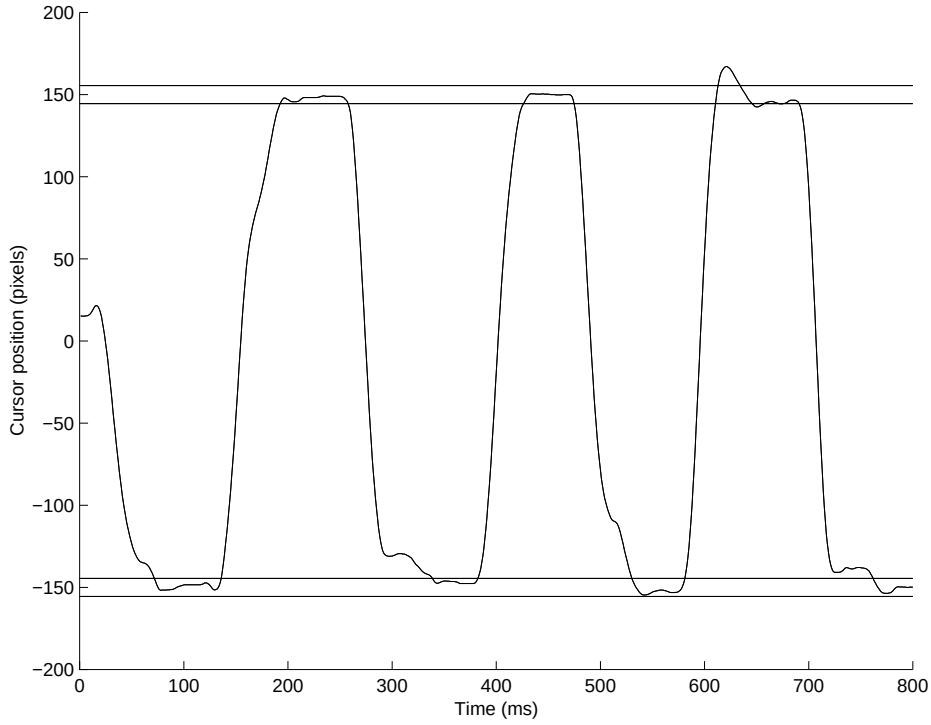

Figure 5-8. Subject's trajectory on a the baseline case. The subject was able to acquire the target 7 times in 800ms.

nitude was greater than 1 mm larger than their base case, their performance was declared worse. (One millimeter was judged to be the minumm significant change based on the repeatability for a single user.)

5.4.2. Forced Choice Test Results

The psychometric curves resulting from nineteen right-handed subjects (10 male 9 female) performing the forced choice test are shown in Figures 5-10, 5-11, and 5-12. Figure 5-10 is for Batch 1. Here we observed that in only one of the five selected values do subjects correctly discern different levels of friction with an accuracy greater than 75%. Ideally at least two or three values would be about the JND. For Batch 1, the estimated just-noticeable-difference is 0.78N.

As is evident from Figure 5-11 subjects had a difficult time with Batch 2. Subjects were never able to distinguish the different cases with an accuracy of greater that 75%. We there-

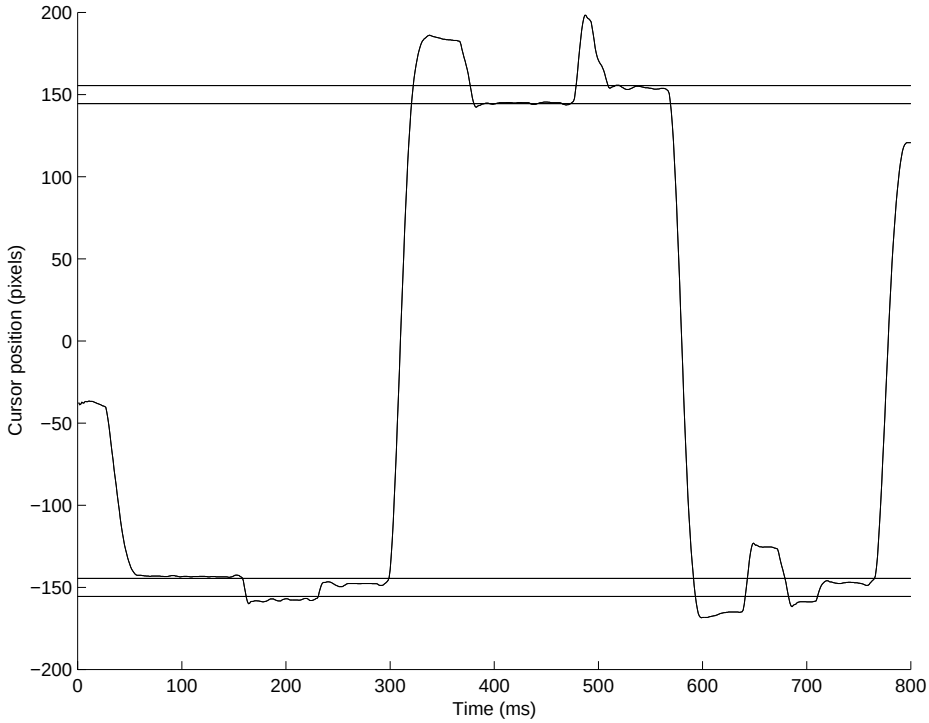

Figure 5-9. Subject's trajectory on a High Stiction case--note the difficulty positioning the cursor within the target bounds.

Table 5-7. Number of subjects (out of 20) that performed better and worse based on task completion time. Tests with highest index of difficulty are highlighted.

Index	*Real*		*Simulated*		*High Stiction*		*Viscous*	
	Better	*Worse*	*Better*	*Worse*	*Better*	*Worse*	*Better*	*Worse*
1	10	4	14	3	9	11	15	3
2	6	10	5	9	3	9	8	7
3	8	4	5	5	5	9	7	4
4	10	5	10	7	1	19	9	8
5	3	8	6	4	3	9	6	5
6	5	6	3	4	3	7	2	5
7	15	3	13	3	8	10	12	5
8	8	6	12	3	8	9	11	3
9	9	4	7	5	8	5	10	4

Table 5-8. Number of subjects that performed better and worse based on the number of errors committed. Tests with highest index of difficulty are highlighted.

Index	*Real*		*Simulated*		*High Stiction*		*Viscous*	
	Better	*Worse*	*Better*	*Worse*	*Better*	*Worse*	*Better*	*Worse*
1	11	2	16	3	10	7	11	5
2	1	8	3	9	5	7	3	7
3	4	5	5	5	3	5	4	5
4	14	5	10	7	8	10	10	7
5	7	2	6	6	5	5	6	6
6	5	2	3	7	3	4	4	5
7	14	3	15	3	12	7	12	6
8	6	7	9	6	6	11	9	4
9	4	5	5	5	5	5	4	9

Table 5-9. Number of subjects (out of 20) that performed better and worse based on average error magnitude. Tests with highest index of difficulty are highlighted.

Index	*Real*		*Simulated*		*High Stiction*		*Viscous*	
	Better	*Worse*	*Better*	*Worse*	*Better*	*Worse*	*Better*	*Worse*
1	17	1	17	2	14	5	13	5
2	4	8	6	7	6	7	6	7
3	5	5	5	5	3	7	4	6
4	9	10	14	5	9	11	9	10
5	10	3	4	10	9	5	8	8
6	5	3	4	8	4	5	4	7
7	15	5	13	7	12	8	7	13
8	10	5	9	7	10	9	7	7
9	6	6	6	5	6	6	6	7

fore had to extrapolate to estimate the JND. From our psychometric curve, the estimated JND for Batch 2 is 3.14N.

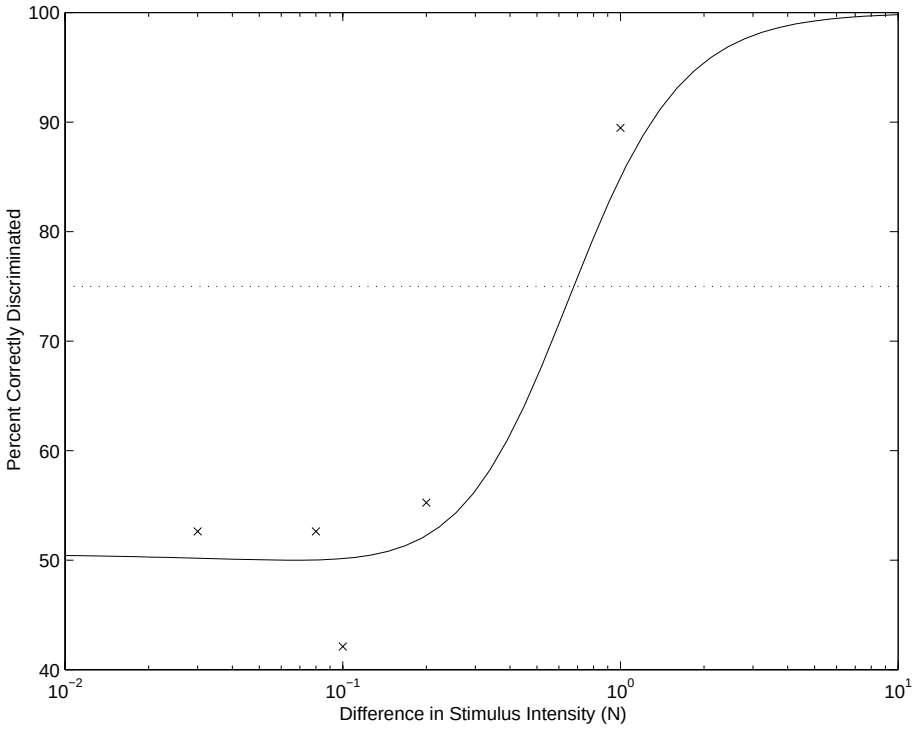

Figure 5-10. Psychometric curve fit to subject responses during Batch 1. Estimated JND = 0.78 N

The best results for the forced choice test were obtained with Batch 3 (Figure5-12). In Batch 3 for two out of the five cases, subjects were able to correctly identify the different friction case more than 75% of the time. The estimated JND for Batch 3 is 0.36N

5.5. Discussion and Conclusions

5.5.1. Friction effects in a targeting task

This chapter presents results obtained with simulated friction in a haptic interface. Using our haptic rendering of friction as well as real physical friction, we have compared the effects of friction on human performance in targeting tasks. Our results indicated that a moderate amount of low-stiction friction can improve human performance in a Fitts type targeting task in terms of both speed and accuracy. This result was observed whether the subjects were experiencing real or virtual friction. Anecdotally, subjects indicated a pref-

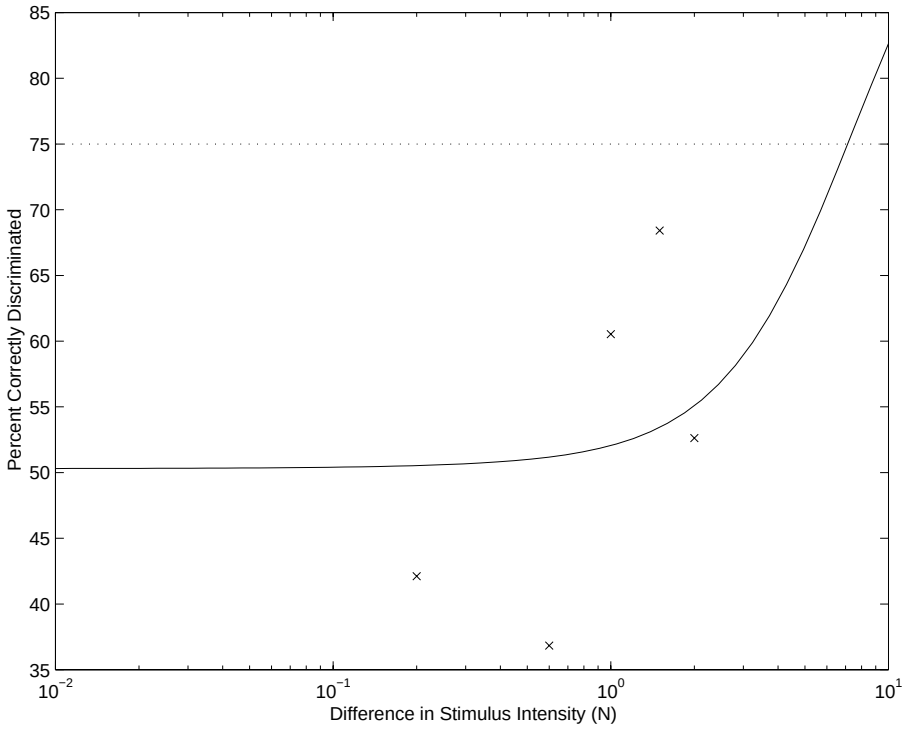

Figure 5-11. Psychometric curve fit to subject responses during Batch 2. Estimated JND = 3.14 N

erence for the frictional cases over the baseline case. Many indicated that the frictional cases “felt better.” Subjects also noted that simulated and real low-stiction cases felt very similar.

Not surprisingly, the results also indicate that high stiction friction negatively impacts subject performance, particularly with regard to task completion time, as subjects had difficulty acquiring narrow targets in a high stiction environment.

5.5.2. Just Noticeable Difference

Making conclusions about the just noticeable difference is more difficult than it was for the targeting task. The greatest difficulty comes for Batch 2. For the range of stimuli tested in batch two, the pool of subjects was never able to correctly identify the different stimulus more than 75% percent of the time. In Batch 1 only the largest difference in stimulus magnitude was identified more than 75% of the time. It appears that the stimuli levels

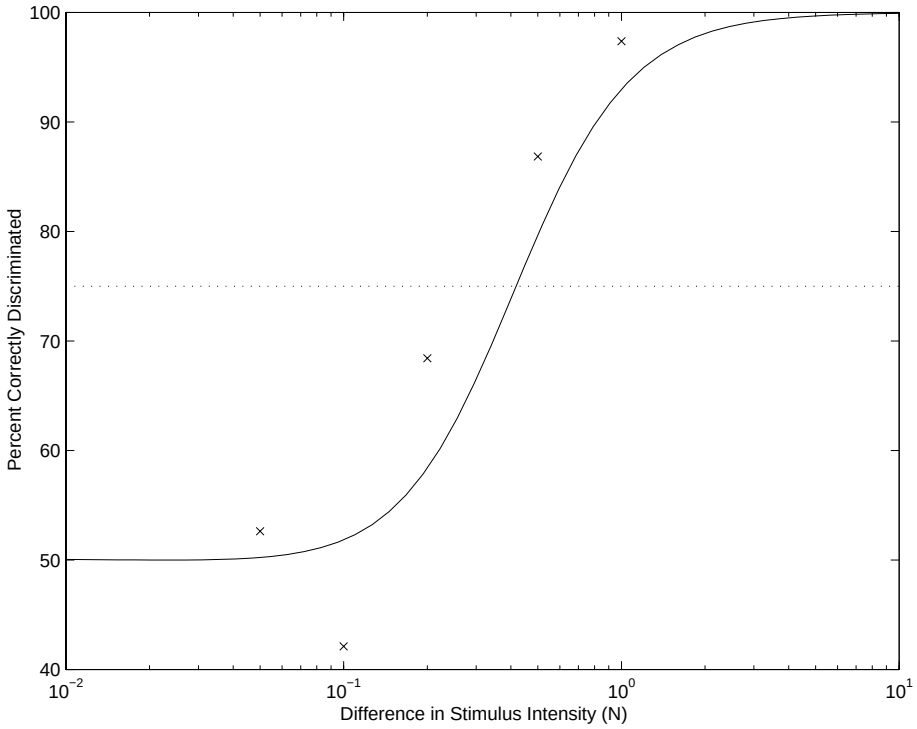

Figure 5-12. Psychometric curve fit to subject responses during Batch 3. Estimated JND = 0.36 N

tested for Batches 1 and 2 are not in the correct range. However during a short pilot study experienced users had little difficulty discriminating between the largest two stimuli in all three batches. It is also evident that a subject's strategy and pattern of motion played a role in their success, particularly during Batch 2. Recall that in Batch 2 the level of static friction differed from the level of dynamic friction. Subjects that employed a pattern of motion with frequent starts and stops performed better in Batch 2. The difference in static friction is really only noticed as the apparatus begins to slide. Perhaps the strongest conclusion to be drawn is that subjects more readily distinguish small changes dynamic friction than changes in static friction

Chapter 6

Conclusions

6.1. Thesis Summary

This thesis presents a study of the resistive force commonly referred to as friction as it applies to haptics. More specifically, it is deals with

- using a haptic interface to model the frictional properties of an environment.
- the development and evaluation of an algorithm to produce realistic haptic simulations or renderings of friction.
- studying how humans perceive computer generated friction.

6.1.1. Friction Modeling and Identification

Although many friction models exist, the two that seem best suited for haptic friction identification and haptic friction renderings are versions of the Dahl model and the Karnopp model. Chapter 2 provided a overview of several models listing some of the strengths and weaknesses of each. Chapter 3 provides details of a procedure for using a haptic interface to identify the frictional and inertial properties of an unknown environment. Experimental results are presented for identification using both the Karnopp and Dahl models. We learned that the Karnopp model provides a simple linear expression that leads to few numerical difficulties. It is also able to accurately capture stiction, but not pre-sliding displacement. The Dahl, on the other hand, is expressed with a differential equation making

optimization (friction identification) difficult. If the initial values for the model parameters are selected improperly, the optimization scheme will either not converge, or converge to unrealistic values. Lastly, we learned that while the Dahl model easily captures pre-sliding displacement for more elastic materials, it does not represent stiction. For these reasons we conclude the Karnopp model provides the simplest entree into haptic friction identification.

6.1.2. Haptic Friction Rendering

In Chapter 4, we showed that the Karnopp models works as well for friction rendering as it did for friction identification. In fact, it was demonstrated that when used for friction rendering, the Karnopp model *is* able to capture the frictional effect of pre-sliding displacement. We learned that varying the parameters of our model affects the quality of the simulation. We set bounds on the proportional gain, and showed how its magnitude affects both the stability and realism of the haptic friction rendering. The effect of *DV*, a velocity threshold set by the designer, can be exploited to produce and change the character of stick-slip oscillations. We also found how the free motion limit cycle is avoided with proper parameter selection. Lastly, we introduced the concept of the virtual coupling into the realm of friction rendering and showed how it helps deal with the causality issues associated with rendering both friction and inertia. We concluded by describing how to select the virtual coupling parameter in such a manner as to avoid the free motion limit cycle.

6.1.3. Human Perception of Friction

Chapter 5 dealt with the human perception of friction. In this chapter we showed how humans perceive simulated versus real friction through the use of a targeting task. We also made estimates of humans ability to distinguish between varying levels of simulated friction.

The results of the targeting task showed that a moderate amount of friction typically results in improved performance for more difficult task levels. The results also indicate that high stiction degrades subjects' performance. From our discrimination tests we learned

that human subjects are able to discern between small differences in friction, however, subjects more readily distinguish small changes in dynamic friction rather than small changes in static friction.

6.2. Recommendations for Future Work

One limitation to the rendering of friction with a velocity based model is the quality of velocity estimation. As mentioned in Chapter 2, velocity in haptic interfaces is often obtained by differentiation of a quantized position signal in discrete time. For our haptic rendering we have obtained a better than standard velocity estimate by using fixed-distance or fixed encoder-pulse differentiation rather than a fixed sample period or fixed time differentiation. Nevertheless, to really model the subtle low velocity phenomena of friction, better velocity sensing will be necessary.

With improved velocity sensing in place, another avenue for future work would be the inclusion other frictional effects such as rising static friction, the phenomenon in which the static level of friction between two mating surfaces increases with time. In our representation of stick-slip oscillation, the frequency of the oscillation is governed by the frequency of the servo-system. Future implementations of haptic friction should allow for variations in the frequency of stick-slip oscillations as a function of the properties of the frictional interface. We have chosen to focus on dry friction. The presence of lubrication adds to the richness of frictional phenomena. One interesting effect of friction in lubricated systems is the Stribeck effect. The Stribeck effect is the name given to the phenomenon of the friction force decreasing with increasing velocity at low velocity. At higher velocities the viscous forces are larger and the friction force will begin to increase.

A final avenue for future work is extending friction rendering to two dimensions. The addition of a second dimension to both friction identification and rendering will add significant challenges for future research. Two dimensional friction allows for more realistic renderings of surfaces which can have different frictional properties in different directions. Such surfaces would greatly improve the realism of today's haptic simulations.

References

Adams, R. J., and Hannaford, B. (1999). "Stable haptic interaction with virtual environments." *IEEE Transactions on Robotics and Automation*, 15(3), 465-474.

Armstrong-Helouvry, B. (1991). *Control of machines with friction*, Kluwer Academic Publishers, Boston.

Armstrong-Helouvry, B., Dupont, P., and Canudas De Wit, C. (1994). "Survey of models, analysis tools and compensation methods for the control of machines with friction." *Automatica*, 30(7), 1083-1138.

Berkelman, P. (1999). "Tool-Based Haptic Interaction with Dynamic Physical Simulations using Lorentz Magnetic Levitation.," Ph.D. Thesis, Carnegie Mellon University, Pittsburgh, PA.

Bhushan, B. (1999). *Principles and applications of tribology*, John Wiley, New York.

Blau, P. J. (1996). *Friction science and technology*, Marcel Dekker, New York.

Bo, L. C., and Pavelescu, D. (1982). "Friction-Speed Relation and Its Influence On the Critical Velocity of Stick-Slip Motion." *Wear*.

Bowden, F. P., and Tabor, D. (1956). *Friction and lubrication [by] F. P. Bowden and D. Tabor*, Methuen;Wiley, London,New York,.

Burdea, G. (1996). *Force and touch feedback for virtual reality*, John Wiley & Sons, New York.

Carpenter, P. S., Brown, R. H., Heinen, J. A., and Schneider, S. C. "On algorithms for velocity estimation using discrete position encoders." *1995 IEEE 21st International Conference on Industrial Electronics, Control, and Instrumentation. Part 2 (of 2)* , Orlando, FL, USA, 844-849.

Chen, J., DiMattia, C., Taylor, R. M., II, Falvo, M., Thiansathaporn, P., and Superfine, R. "Sticking to the point: A friction and adhesion model for simulated surfaces." *1997 ASME International Mechanical Engineering Congress and Exposition*, Dallas, TX, USA, 167-171.

Coleman, T., Branch, M. A., and Grace, A. (1999). *Optimization Toolbox User's Guide*, The MathWorks Inc., Natick, MA.

Colgate, J. E., and Brown, J. M. "Factors affecting the Z-width of a haptic display." *1994 IEEE International Conference on Robotics and Automation*, San Diego, CA, USA, 3205-3210.

Colgate, J. E., Grafing, P. E., Stanley, M. C., and Schenkel, G. "Implementation of stiff virtual walls in force-reflecting interfaces." *1993 IEEE Annual Virtual Reality International Symposium*, Seattle, WA, USA, 202-208.

Colgate, J. E., Stanley, M. C., and Brown, J. M. "Issues in the haptic display of tool use." *1995 IEEE/RSJ International Conference on Intelligent Robots and Systems. Part 3 (of 3)*, Pittsburgh, PA, USA, 140-145.

Dahl, P. R. (1976). "Solid Friction Damping of Mechanical Vibrations." *AIAA Journal.*

Dowson, D. (1998). *History of tribology*, Professional Engineering Publishing, London.

Dupont, P. E., and Dunlap, E. P. (1995). "Friction modeling and PD compensation at very low velocities." *Journal of Dynamic Systems, Measurement and Control, Transactions of the ASME*, 117(1), 8-14.

Dupont, P. E., Schulteis, T. M., and Howe, R. D. “Experimental identification of kinematic constraints.” *1997 IEEE International Conference on Robotics and Automation, ICRA. Part 3 (of 4)*, Albuquerque, NM, USA, 2677-2682.

Fitts, P. M. (1954). “The Information Capacity of the Human Motor System in Controlling the Amplitude of Movement.” *USAF Personnel & Training Research Center Research Bulletin*(54-41), 11.

Friedland, B., and Mentzelopoulou, S. “Estimation of dynamic friction.” *32nd IEEE Conference on Decision and Control. Part 2 (of 4)*, San Antonio, TX, USA, 1919-1924.

Fuller, W. A. (1987). *Measurement error models*, Wiley, New York.

Gillespie, R. B., and Cutkosky, M. R. “Stable user-specific haptic rendering of the virtual wall.” *1996 ASME International Mechanical Engineering Congress and Exposition*, Atlanta, GA, USA, 397-406.

Gillespie, R. B., and Stanford University. Dept. of Mechanical Engineering. (1996). “Haptic display of systems with changing kinematic constraints: the virtual piano action,” Ph.D., Stanford University, Stanford, CA.

Haessig, D. A., Jr., and Friedland, B. (1991). “On the modeling and simulation of friction.” *Journal of Dynamic Systems, Measurement and Control, Transactions of the ASME*

Hasser, C. J., Goldenberg, A. S., Martin, K. M., and Rosenberg, L. B. “User performance in a GUI pointing task with a low-cost force-feedback computer mouse.” *1998 ASME International Mechanical Engineering Congress and Exposition*, Anaheim, CA, USA, 151-155.

Hayward, V., and Armstrong, B. (2000). “ A new computational model of friction applied to haptic rendering.” Experimental Robotics VI, P. Corke and J. Trevelyan, eds., Springer-Verlag, 403-412.

Heeger, D. (1999). "Course Notes for Introduction to Perception, Stanford University couse in psychology." , D. Heeger, Stanford University.

Hess, D. P., and Soom, A. (1990). "Friction at a lubricated line contact operating at oscillating sliding velocities." *Journal of Tribology, Transactions of the ASME*, 112(1), 147-152.

Johnson, C. T., and Lorenz, R. D. (1992). "Experimental identification of friction and its compensation in precise, position controlled mechanisms." *IEEE Transactions on Industry Applications*.

Jones, L. A., and I.W., H. (1990). "A Perceptual Analysis of Stiffness." *Experimental Brain Research*, 79, 150-156.

Jones, L. A., and I.W., H. (1993). "A Perceptual Analysis of Viscosity." *Experimental Brain Research*, 94(2), 343-351.

Karnopp, D. (1985). "Computer Simulation of Stick-Slip Friction in Mechanical Dynamic Systems." *Journal of Dynamic Systems, Measurement and Control, Transactions ASME*.

Kim, J.-H., Chae, H.-K., Jeon, J.-Y., and Lee, S.-W. (1996). "Identification and control of systems with friction using accelerated evolutionary programming." *IEEE Control Systems Magazine*, 16(4), 38-47.

Kim, S. J., Ha, I.-J., Kang, J. H., Kim, C. H., and Lim, S. G. (1997). "New parameter identification method for mechanical systems with friction." *IECON Proceedings (Industrial Electronics Conference)*.

Lawrence, D. A., Pao, L. Y., Dougherty, A. M., Pavlou, Y., Brown, S. W., and Wallace, S. A. "Human perception of friction in haptic interfaces." *1998 ASME International Mechanical Engineering Congress and Exposition*, Anaheim, CA, USA, 287-294.

MacLean, K. E. "'Haptic camera': a technique for characterizing and playing back haptic properties of real environments." *1996 ASME International Mechanical Engineering Congress and Exposition*, Atlanta, GA, USA, 459-467.

Majd, V. J., and Simaan, M. A. "Continuous friction model for servo systems with stiction." *1995 IEEE Conference on Control Applications*, Albany, NY, USA, 296-301.

Miller, B. E., and Colgate, J. E. "Using a wavelet network to characterize real environments for haptic display." *1998 ASME International Mechanical Engineering Congress and Exposition*, Anaheim, CA, USA, 257-264.

Millman, P. A. (1995). "Haptic Perception of Localized Features," Ph.D., Northwestern University, Evanston, IL.

Millman, P. A., and Colgate, J. E. "Effects of non-uniform environment damping on haptic perception and performance of aimed movements." *1995 ASME International Mechanical Engineering Congress and Exposition. Part 2 (of 2)* San Francisco, CA, USA, 703-711.

Minsky, M., Ouh-young, M., Steele, O., Brooks, F. P., Jr., and Behensky, M. (1990). "Feeling and seeing. Issues in force display." *Computer Graphics (ACM)*, 24(2.), 235-243.

Nahvi, A., Hollerbach, J. M., Freier, R., and Nelson, D. D. "Display of friction in virtual environments based on human finger pad characteristics." *1998 ASME International Mechanical Engineering Congress and Exposition*, Anaheim, CA, USA, 179-184.

Richard, C., Cutkosky, M. R., and MacLean, K. E. "Friction Identification for Haptic Display." *1999 ASME International Mechanical Engineering Congress and Exposition*, Nashville, TN USA, 327-334.

Ruspini, D. C., Kolarov, K., and Khatib, O. "Haptic display of complex graphical environments." *1997 Conference on Computer Graphics, SIGGRAPH* , Los Angeles, CA, USA, 345-352.

Salcudean, S. E., and Vlaar, T. D. “On the emulation of stiff walls and static friction with a magnetically levitated input/output device.” *1994 International Mechanical Engineering Congress and Exposition*, Chicago, IL, USA, 303-309.

Schulteis, T. M., Dupont, P. E., Millman, P. A., and Howe, R. D. “Automatic identification of remote environments.” *1996 ASME International Mechanical Engineering Congress and Exposition,* Atlanta, GA, USA, 451-458.

Tan, H. Z., Durlach, N. I., Beauregard, G. L., and Srinivasan, M. A. (1995). “Manual discrimination of compliance using active pinch grasp: The roles of force and work cues.” *Perception & Psychophysics*, 57(4), 495-510.

Taylor, M. M., and Lederman, S. J. (1975). “Tactile roughness of grooved surfaces: A model and the effect of friction.” *Perception & Psychophysics,* 17(1), 23-36.

Walrath, C. D. (1984). “Adaptive Bearing Friction Compensation Based On Recent Knowledge of Dynamic Friction.” *Automatica*.

Weber, E. H. (1834).*De pulsu, resorpitione auditu et tactu: Annotationes anantomicae et physiologicae*,, Koehlor, Leipzig.